Effects of the environment on the dynamics of driven open quantum systems

Thesis submitted for the degree of
"Doctor of Philosophy"

By

Morag Am-Shallem

Submitted to the Senate of the Hebrew University of Jerusalem

December 2015

This work was carried out under the supervision of:

Prof. Ronnie Kosloff

תודות

אני מודה לרוני קוזלוב על הייעוץ והיחס החם לאורך כל העבודה המשותפת.

אני מודה גם לחברי הקבוצה של רוני לאורך השנים, ובפרט לשמשון קלוש, טובה פלדמן, עמיקם לוי ועדו שפר, על אינספור שיחות ודיונים.

מוקדש בהרבה אהבה והערכה למשפחתי, המצומצמת והמורחבת, ובפרט:

- לאשתי שגית, על העידוד והאמונה לאורך כל השנים
- להורי – עמיקם חיים ז״ל וידידה, שלמדו אותי להתבונן ולשאול
- לילדי – ניצן, הראל, עמיחי וישי

Abstract

Open quantum systems are characterized by coupling to an external environment. The dynamics of the system is affected by the coupling, and typically relaxation and dephasing processes emerge. We adopt a framework of a reduced description, treating the primary system explicitly and the environment implicitly. The reduced description of Markovian open quantum systems utilizes the L-GKS quantum master equation, also known as the Lindblad equation, to describe the dynamics.

The interaction of quantum systems with external driving fields is used in many areas of physics and chemistry. Two generic examples are spectroscopy, where the driving field is used to probe the system, and coherent control, which employs an external field to drive the system to a desirable state.

In this thesis we investigated the influence of the environment on the dynamics of systems under the driving of external fields. In particular, we studied two phenomena:

- The scaling of weak field phase-only control in Markovian dynamics;
- Exceptional points in the dynamics of Markovian open quantum systems.

Our work on *the scaling of weak field phase-only control in Markovian dynamics* stems from the field of molecular spectroscopy, and is a noteworthy example for a situation where the influence of the environment on the driven-system dynamics can appear. When a weak radiation field is applied to a molecule, the energy absorbed from this field interrogates the energy levels of the molecule. The basic assumption is that there is a direct link between the energy loss from the field and the energy spectrum of the molecule. This assumption is justified by the time dependent perturbation theory for isolated systems, which states that the phase properties of the weak driving fields do not alter the final state of the system.

A series of experiments and numerical simulations suggested that this assertion does not hold for open systems. Therefore, the effect of the phase properties of driving weak fields has to be analyzed within an open system formalism. To cope with this task, we considered population transfer in open quantum systems described by the L-GKS equation. We used the second order perturbation theory of this equation to analyze the dynamics. We showed that the population transfer depends

on a weak external field only through the field's autocorrelation function which is phase independent. Therefore, for the leading order in the perturbation, this dynamics cannot support the dependence of the population transfer on the phase properties of the weak field. Subsequently, the experiments have to be explained in an alternative formalism.

The analysis was demonstrated by an example of a weak-field phase-dependent population transfer. The field is a Gaussian laser pulse with a chirp, meaning that each spectral component has a different phase. We showed that while the population transfer scales as the square of the field strength, which is the leading order in the perturbation, the chirp effect, which expresses the phase-dependence in such cases, scales as the next order in the perturbation.

Our work on *exceptional points of the L-GKS equation* requires a mathematical foundation: The eigenvalues of the L-GKS generator are complex, reflecting unitary as well as dissipative dynamics. For certain values of parameters defining the generator, non-hermitian degeneracies emerge, known as exceptional points (*EP*). At these points the matrix that represents the generator in not diagonalizable. The resulting dynamics comprises polynomial behaviour. This unique time evolution can be revealed using harmonic inversion methods, and can be used experimentally to locate the *EP* accurately. We suggested to employ this feature to determine the intrinsic system parameters with high accuracy.

We investigated the *EP* of an L-GKS generator that is defined by the parameter space composed from the external field parameters. We found that generally there are continuous lines of *EP* in the parameter space, which merge into cusps of higher order degeneracy. We studied the implications of such points in the open system dynamics of the Bloch equations and the spontaneous emission of laser-driven atoms.

The Bloch equation is the simplest example for the L-GKS equation, and has become the template for dissipative quantum dynamics in many area of physics, from NMR to quantum information and elementary particles. Nevertheless, the *EP* of this equation were not studied before. We calculated the *EP*-curves of this system, and suggested a procedure to determine accurately the system parameters, i.e., the system frequency, the dipole moment and the relaxation coefficient.

The spontaneous emission of excited atoms is properly described by the L-GKS equation. The parameters of such atomic systems are determined by fundamental physical constants, therefore an accurate parameter estimation is advocated. The decoherence associated with the spontaneous emission limits the performance of common measurement techniques. The method of parameter estimation using *EP* turns the disadvantage of the dissipation into an advantage. We demonstrated the method for the atomic spectrum of $S \to P$ transitions of ^{85}Rb and $^{40}Ca^{+}$.

Research papers included in the thesis

This Ph.D. thesis includes the following research papers:

- Morag Am-Shallem and Ronnie Kosloff
  The scaling of weak field phase-only control in Markovian dynamics.
  Published at *The Journal of Chemical Physics*, 141, 044121 (2014)

- Morag Am-Shallem, Ronnie Kosloff and Nimrod Moiseyev
  Exceptional points for parameter estimation in open quantum systems: analysis of the Bloch equations
  Published at *New Journal of Physics*, 17 113036 (2015)

- Morag Am-Shallem, Ronnie Kosloff and Nimrod Moiseyev
  Parameter estimation in atomic spectroscopy using exceptional points.
  Published at *Phys. Rev. A*, 93 032116 (2016)

A Letter of Contribution

All of the work on this PhD thesis was done by Morag Am-Shallem as the main contributor, under the supervision of Prof. Ronnie Kosloff.

In particular, the following holds:

1. The chapter of population transfer induced by weak fields summarizes the study that was done by Morag Am-Shallem, under the supervision of Prof. Ronnie Kosloff.

2. For the chapter of exceptional points in open quantum system we enjoyed the fruitful consultation of Prof. Nimrod Moiseyev from the Technion. Nevertheless, the study was performed by Morag Am-Shallem, under the supervision of Prof. Ronnie Kosloff.

Contents

Preface

Quantum mechanics of isolated systems is a well-established and thoroughly-studied theory. The predictions of the theory were verified by experiments to a very high accuracy.

In practice, any quantum system is coupled to external environments. The coupling of the system to the environments induces essential changes to the nature of the dynamics. Typically, the coupling causes relaxation and dephasing. Many aspects of the dynamics of open quantum systems were studied. However, other effects of the environment on the dynamics of such systems still have to be unravelled.

This work is devoted to the investigation of Markovian open quantum systems that interact with external fields. The interaction of electromagnetic fields with matter, especially with atoms and molecules, is ubiquitous in physics and chemistry. For example:

- In many types of measurements the measured system is driven with external fields and the effects are probed. For example, spectroscopy is based on using a weak probe to unravel pure molecular properties. Specifically, absorption spectroscopy measures the energy absorption from the field.

- In coherent control the goal is to drive a quantum system to a desired state by an external field. In particular, coherent control was suggested to control population transfer in molecular electronic surfaces and chemical reaction channels.

- Light-matter interaction is ubiquitous in natural phenomena. For example, the terrestrial solar spectrum, which has central significance in solar energy applications, is a result of the interaction of the radiation from the sun with the molecules in the atmosphere .

We studied the effects of the environment of the dynamics of such systems. To present coherently the thesis outline, a concise theoretical background is needed. In the following we describe the theoretical framework for this study. Subsequently we present the research subjects and thesis outline.

Chapter 1

Theoretical background: The dynamics of open quantum systems

Built into the dynamics of isolated quantum systems is time reversal, meaning that any time-evolution from an initial state to a final state, can be reverted to the initial state. In quantum mechanics this property is reflected mathematically by employing unitary operators for the description of the evolution. The operator norm of unitary operators is 1. A unitary operator $\hat{\mathbf{U}}$ can be expressed as an exponential of an anti-hermitian operator $i\hat{\mathbf{H}}t$ (where $\hat{\mathbf{H}}$ is a hermitian operator and we use $\hbar = 1$):

$$\hat{\mathbf{U}} = e^{i\hat{\mathbf{H}}t}. \tag{1.1}$$

The eigenvalues of an anti-hermitian operator are always purely imaginary, and therefore the eigenvalues of the unitary operator are of magnitude 1, located on the unit circle of the complex plane.

A Markovian open quantum system interacts with its environment in a non-reversible way. The systems loses information into the environment. This results in a contraction of the available space of states. The evolution is described by contracting operators instead of unitary operators. The norm of a contracting operator is less than 1, and it is expressed as an exponential of a generating operator which is neither hermitian nor anti hermitian. The eigenvalues of this generating operator are complex, with negative real part, and therefore the magnitude of the eigenvalues of the evolution operator is less than 1.

In this work we studied effects of the environment on the dynamics of a driven Markovian open quantum system. Below, we briefly present the necessary theoretical background for such studies. A thorough presentation can be found in many sources, e.g., Refs. [Breuer 2002, Alicki 2002, Alicki 2007, Nielsen 2011].

1.1 Isolated quantum systems

Any real quantum system is coupled and interacts with some environments. Nevertheless, the concept of isolated quantum systems is of great benefit. The dynamics of isolated quantum systems can be described by the unitary dynamics of wave functions, density operators, and expectation values of observable operators. These methods are outlined below.

1.1.1 Wave function description

Wave functions and the Hilbert space. The state of isolated quantum systems is usually described by a wave function $|\psi\rangle$. The wave function is an element in a Hilbert space that includes the possible states of the system. The scalar product in this Hilbert space is expressed using Dirac's bra–ket notation:

$$\Big(|\phi\rangle\,,\,|\psi\rangle\Big) = \langle\phi\,|\,\psi\rangle \tag{1.2}$$

The squared absolute value of the wave function serves as the population probability, therefore the norm satisfies:

$$|\langle\psi|\,\psi\rangle|^2 = 1. \tag{1.3}$$

The description of quantum systems using wave functions in a Hilbert space employs the linear operators that operate on elements in this space. The hermitian adjoint of an operator $\hat{\mathbf{M}}$, denoted $\hat{\mathbf{M}}^\dagger$, is the operator that satisfies

$$\Big\langle \phi \,\Big|\, \hat{\mathbf{M}}\psi \Big\rangle = \Big\langle \hat{\mathbf{M}}^\dagger \phi \Big|\, \psi \Big\rangle \tag{1.4}$$

for any two wave functions $|\phi\rangle$ and $|\psi\rangle$. A hermitian operator is an operator that equals to its adjoint, $\hat{\mathbf{O}}^\dagger = \hat{\mathbf{O}}$.

Dynamics. The dynamics of the wave function is generated by the hermitian Hamiltonian operator $\hat{\mathbf{H}}_S$ and governed by the Schrödinger equation:

$$\frac{\partial}{\partial t}\,|\psi(t)\rangle = -\frac{i}{\hbar}\hat{\mathbf{H}}_S\,|\psi(t)\rangle\,. \tag{1.5}$$

(in the following we use $\hbar = 1$). Starting from an initial state $|\psi(t_0)\rangle$, the resulting evolution for time-independent Hamiltonian is:

$$|\psi(t)\rangle = e^{-i\hat{\mathbf{H}}_S(t-t_0)}\,|\psi(t_0)\rangle\,. \tag{1.6}$$

The dynamics preserves the norm, meaning that the population is conserved.

The evolution can also be described by the propagator $\hat{\mathbf{U}}(t, t_0)$, which is the operator that propagates the state from time t_0 to time t:

$$|\psi(t)\rangle = \hat{\mathbf{U}}(t, t_0) |\psi(t_0)\rangle . \tag{1.7}$$

The differential equation for the propagator is:

$$\frac{\partial}{\partial t}\hat{\mathbf{U}}(t, t_0) = -i\hat{\mathbf{H}}_S\hat{\mathbf{U}}(t, t_0), \tag{1.8}$$

with the condition $\hat{\mathbf{U}}(t, t) = \hat{\mathbf{1}}$ for any time t, where $\hat{\mathbf{1}}$ is the identity operator. The resulting evolution with a time-independent Hamiltonian is:

$$\hat{\mathbf{U}}(t, t_0) = e^{-i\hat{\mathbf{H}}_S(t-t_0)}. \tag{1.9}$$

The dynamics of the wave function, Eq. (1.6), is reproduced with the evolution of the propagator (Eq. (1.9)), along with Eq. (1.7).

Since the Hamiltonian $\hat{\mathbf{H}}_S$ is hermitian, the evolution is an exponential of an anti hermitian operator, and therefore it is unitary. The immediate consequence is that the hermitian conjugate is equal to the inverse:

$$\hat{\mathbf{U}}^{\dagger}(t, t_0) = e^{i\hat{\mathbf{H}}_S(t-t_0)} = \hat{\mathbf{U}}^{-1}(t, t_0). \tag{1.10}$$

Inverting the propagator is equivalent to propagating the system inversely from time t to time t_0. The unitary evolution reflects the reversibility of the dynamics.

The time evolution forms a one-parameter family of maps. This map is closed, associative, includes the identity operator $\hat{\mathbf{U}}(t, t) = \hat{\mathbf{I}}$, and includes the inverse of any element of it as shown above. Therefore this family of maps forms a group.

1.1.2 Density operator description

Density operators. To pave the way to a more general description, and to enable the description of open quantum systems, we describe the state of a quantum system by the density operator $\hat{\boldsymbol{\rho}}$. The counterpart of the isolated-system wave function $|\psi\rangle$ is the pure-state density operator, composed from a single wave function:

$$\hat{\boldsymbol{\rho}}_{pure} = |\psi\rangle \langle\psi| . \tag{1.11}$$

A more general density operator mixes a number of states:

$$\hat{\boldsymbol{\rho}}_{mixed} = \sum_i a_i |\psi_i\rangle \langle\psi_i| , \quad \sum_i a_i = 1, \quad a_i \geq 0 \tag{1.12}$$

The population probability is expressed by the diagonal of the density operator, and therefore the counterpart of Eq. (1.3) is:

$$\mathrm{Tr}\left\{\hat{\boldsymbol{\rho}}\right\} = 1, \tag{1.13}$$

where the trace of a matrix (denoted as $\mathrm{Tr}\{\cdot\}$) is the sum of its diagonal elements. In addition to this constraint, a general density operator has to be hermitian and positive semi-definite.

The mixed states *cannot* be represented by the wave function formalism. We measure the mixing of the density operator by the purity, defined as:

$$P = \mathrm{Tr}\left\{\hat{\boldsymbol{\rho}}^2\right\}, \tag{1.14}$$

The purity alway fulfills $P \leq 1$, where for a pure state we have $P = 1$, while for a mixed state $P < 1$. In both cases, the total population is 1.

Liouville space. The density operator is an element in the Liouville space of operators (this space is also known as the Hilbert-Schmidt space). The Liouville space is a Hilbert space, with the scalar product defined as

$$\left(\hat{\mathbf{X}}_1, \hat{\mathbf{X}}_2\right) \equiv \mathrm{Tr}\left\{\hat{\mathbf{X_1}}^{\dagger}\hat{\mathbf{X_2}}\right\}. \tag{1.15}$$

It is useful to choose the Identity operator and a set of traceless operators as the basis to the Liouville space.

Linear operators that operate on elements in the Liouville space of operators are usually referred to as *super-operators*. Hilbert space definitions and conventions apply also to the Liouville space. In particular, the adjoint of a super-operator $\mathcal{M}$, denoted as $\mathcal{M}^{\dagger}$, is the super-operator that satisfies

$$\left(\hat{\mathbf{A}}, \mathcal{M}\hat{\mathbf{B}}\right) = \left(\mathcal{M}^{\dagger}\hat{\mathbf{A}}, \hat{\mathbf{B}}\right), \tag{1.16}$$

for any two operators $\hat{\mathbf{A}}$ and $\hat{\mathbf{B}}$ in the Liouville space.

Dynamics. The dynamics of the density operator of an isolated system is generated by the von-Neumann equation:

$$\frac{\partial}{\partial t}\hat{\boldsymbol{\rho}} = -i\left[\hat{\mathbf{H}}, \hat{\boldsymbol{\rho}}\right], \tag{1.17}$$

where $\left[\hat{\mathbf{H}}, \hat{\boldsymbol{\rho}}\right]$ denotes the commutator of the Hamiltonian $\hat{\mathbf{H}}$ with the density operator $\hat{\boldsymbol{\rho}}$. We look at the commutator with the Hamiltonian as a super-operator,

denoted by $\left[\hat{\mathbf{H}}, \cdot\right]$. This super-operator is hermitian, as can be derived using the definitions Eqs. (1.16) and (1.15):

$$\begin{aligned}\left(\hat{\mathbf{A}}, \left[\hat{\mathbf{H}}, \cdot\right] \hat{\mathbf{B}}\right) &\equiv \left(\hat{\mathbf{A}}, \left[\hat{\mathbf{H}}, \hat{\mathbf{B}}\right]\right) = \left(\left[\hat{\mathbf{H}}, \hat{\mathbf{A}}\right], \hat{\mathbf{B}}\right) \\ &\equiv \left(\left[\hat{\mathbf{H}}, \cdot\right] \hat{\mathbf{A}}, \hat{\mathbf{B}}\right),\end{aligned} \tag{1.18}$$

and therefore

$$\left(\left[\hat{\mathbf{H}}, \cdot\right]\right)^{\dagger} = \left[\hat{\mathbf{H}}, \cdot\right]. \tag{1.19}$$

The resulting evolution is expressed using the exponential of this super-operator:

$$\hat{\boldsymbol{\rho}}(t) = e^{-i\left[\hat{\mathbf{H}}, \cdot\right](t-t_0)} \hat{\boldsymbol{\rho}}(t_0). \tag{1.20}$$

The evolution can be encapsulated in the propagator, which is the super-operator that propagates the density operator:

$$\mathcal{U}(t, t_0) = e^{-i\left[\hat{\mathbf{H}}, \cdot\right](t-t_0)}. \tag{1.21}$$

The propagator is unitary since the commutator is hermitian. Under unitary evolution the purity is conserved. In particular, for a density operator that originated from a pure wave function as in Eq. (1.11), the dynamics will be the same as of Eq. (1.6):

$$\begin{aligned}\hat{\boldsymbol{\rho}}_{pure}(t) &= e^{-i\left[\hat{\mathbf{H}}, \cdot\right](t-t_0)} \hat{\boldsymbol{\rho}}_{pure}(t_0) \\ &= e^{-i\left[\hat{\mathbf{H}}, \cdot\right](t-t_0)} \left|\psi(t_0)\right\rangle\!\left\langle\psi(t_0)\right| \\ &= e^{-i\hat{\mathbf{H}}(t-t_0)} \left|\psi(t_0)\right\rangle\!\left\langle\psi(t_0)\right| e^{+i\hat{\mathbf{H}}(t-t_0)} \\ &= \left|\psi(t)\right\rangle\!\left\langle\psi(t)\right|.\end{aligned} \tag{1.22}$$

Conceptually, the dynamics of a mixed-state density operator can be decomposed to the dynamics of the mixing wave functions. In a similar manner to Eq. (1.22), the dynamics can be shown to be equivalent to the dynamics generated by the Schrödinger equation, Eq. (1.5).

1.1.3 Observables

Quantum mechanics associates measured quantities to observable operators. The expectation value of such an observable expresses its associated measured quantity. For a pure state $|\psi(t)\rangle$, the expectation value of an observable $\hat{\mathbf{O}}$ is defined using

the wave function $|\psi(t)\rangle$, or the appropriate density operator $\hat{\boldsymbol{\rho}}(t) = |\psi(t)\rangle\langle\psi(t)|$:

$$\begin{aligned}\left\langle \hat{\mathbf{O}}(t) \right\rangle &\equiv \left\langle \psi(t) \left| \hat{\mathbf{O}} \right| \psi(t) \right\rangle \\ &= \mathrm{Tr}\left\{ \hat{\mathbf{O}}\, \hat{\boldsymbol{\rho}}(t) \right\} \\ &\equiv \left(\hat{\mathbf{O}}, \hat{\boldsymbol{\rho}}(t) \right)\end{aligned} \tag{1.23}$$

The hermitian conjugation was omitted since the observables are hermitian operators. The definition $\langle \hat{\mathbf{O}}(t) \rangle = \mathrm{Tr}\{\hat{\mathbf{O}}\, \hat{\boldsymbol{\rho}}(t)\}$ holds also for mixed-state density operators. We use the propagator and its adjoint to assign the dynamics of the expectation value to the operator:

$$\left(\hat{\mathbf{O}}, \hat{\boldsymbol{\rho}}(t) \right) = \left(\hat{\mathbf{O}}, \mathcal{U}(t,t_0)\, \hat{\boldsymbol{\rho}}(t_0) \right) = \left(\mathcal{U}^\dagger(t,t_0)\, \hat{\mathbf{O}}, \hat{\boldsymbol{\rho}}(t_0) \right) \equiv \left(\hat{\mathbf{O}}(t), \hat{\boldsymbol{\rho}} \right). \tag{1.24}$$

The differential equation that generates this dynamics is the Heisenberg equation:

$$\frac{\partial}{\partial t} \hat{\mathbf{O}} = i \left[\hat{\mathbf{H}}, \hat{\mathbf{O}} \right], \tag{1.25}$$

which is the hermitian adjoint of the von-Neumann equation, Eq. (1.17).

1.2 Driven quantum system

In many instances we are interested in the dynamics that result from the driving of an external field. Examples for such driving are: Absorption spectroscopy, which measures the energy absorption from the driving field [Tannor 2007, Chapter 14]; Coherent control of population transfer in molecular electronic surfaces and of chemical reaction channels [Tannor 2007, Chapter 16], [Shapiro 2003, Rice 2000]; the interaction of the radiation from the sun with the atmosphere molecules [Bird 1984, Bird 1983, Riordan 1986]. The driving of the external fields is described by additional terms in the Hamiltonian:

$$\hat{\mathbf{H}}(t) = \hat{\mathbf{H}}_0 + \hat{\mathbf{H}}_f(t) = \hat{\mathbf{H}}_0 + \sum_k f_k(t) \hat{\mathbf{V}}_k, \tag{1.26}$$

where $\hat{\mathbf{V}}_k$ are operators that operate on the Hilbert space, and $f_k(t)$ are time-dependent coefficients. For time-dependent Hamiltonians the propagator involves the time-ordering operator $\mathcal{T}$:

$$\hat{\mathbf{U}}(t,t_0) = \mathcal{T} \exp\left\{ -i \int_{t_0}^{t} \hat{\mathbf{H}}(\tau)\, \mathrm{d}\tau \right\}, \tag{1.27}$$

instead of Eq. (1.6). A similar expression will replace the evolution of the density operator, Eq. (1.20). Nevertheless, the evolution is still unitary, reflecting the reversibility of the dynamics under the proper time-reversal of the external fields.

The dynamics of Eq. (1.27) can be expressed explicitly using the Dyson series or the Magnus expansion [Blanes 2009]. However, in this thesis we limited the evolution to simple scenarios, namely low order time dependent perturbation theory (based on the Dyson series), and the rotating wave Hamiltonian. These frameworks are described below.

1.2.1 Time dependent perturbation theory

Dyson series. The time dependent perturbation theory (TDPT) is based on expressing the propagator as a composition of two operators:

$$\hat{\mathbf{U}}(t,t_0) = \hat{\mathbf{U}}_0(t,t_0)\hat{\mathbf{U}}_I(t,t_0), \tag{1.28}$$

where $\hat{\mathbf{U}}_0(t,t_0) = \exp\{\text{-}i\hat{\mathbf{H}}_0(t-t_0)\}$ is the propagator generated by the time independent part of the Hamiltonian, and $\hat{\mathbf{U}}_I(t,t_0)$ is generated by the *interaction Hamiltonian*,

$$\hat{\mathbf{H}}_I(t) = \hat{\mathbf{U}}_0^{-1}(t,t_0)\hat{\mathbf{H}}_f(t)\hat{\mathbf{U}}(t,t_0). \tag{1.29}$$

The Dyson equation is an integral equation reflecting the Schrödinger equation:

$$\hat{\mathbf{U}}_I(t,t_0) = \hat{\mathbf{1}} + \int_{t_0}^{t} d\tau\, \hat{\mathbf{H}}_I(\tau)\hat{\mathbf{U}}_I(\tau,t_0). \tag{1.30}$$

A recursive substitution of $\hat{\mathbf{U}}_I(t,t_0)$ in this equation leads to the infinite Dyson series. If the interaction Hamiltonian is small, the series can be truncated to give:

$$\hat{\mathbf{U}}_I(t,t_0) = \hat{\mathbf{1}} + \int_{t_0}^{t} d\tau_1\, \hat{\mathbf{H}}_I(\tau_1) + \int_{t_0}^{t} d\tau_1 \int_{t_0}^{\tau_1} d\tau_2\, \hat{\mathbf{H}}_I(\tau_1)\hat{\mathbf{H}}_I(\tau_2) + \cdots . \tag{1.31}$$

A similar practice holds for the approximation of the propagator of the von-Neumann equation.

Expectation values. When we describe the evolution of expectation values it is important to keep track of the relevant orders of the small parameter. Suppose the small parameter is λ. The second-order approximation for the wave function can be expressed as:

$$|\psi(t)\rangle \approx |\psi_0(t)\rangle + \lambda\,|\psi_1(t)\rangle + \lambda^2\,|\psi_2(t)\rangle\,. \tag{1.32}$$

The resulting second-order approximation for the expectation value of the operator $\hat{\mathbf{O}}$ is:

$$\begin{aligned}\left\langle \hat{\mathbf{O}}(t) \right\rangle \approx & \left\langle \psi_0(t) \left| \hat{\mathbf{O}} \right| \psi_0(t) \right\rangle \\ & + \lambda \left(\left\langle \psi_0(t) \left| \hat{\mathbf{O}} \right| \psi_1(t) \right\rangle + c.c \right) \\ & + \lambda^2 \left\langle \psi_1(t) \left| \hat{\mathbf{O}} \right| \psi_1(t) \right\rangle \\ & + \lambda^2 \left(\left\langle \psi_2(t) \left| \hat{\mathbf{O}} \right| \psi_0(t) \right\rangle + c.c \right).\end{aligned} \tag{1.33}$$

We see that the first-order wave function yields also second-order terms for the expectation value. But to obtain the full second-order term we need also $|\psi_2(t)\rangle$ (if $\left\langle \psi_2(t) \left| \hat{\mathbf{O}} \right| \psi_0(t) \right\rangle \neq 0$), therefore the second order TDPT is required. If we use the TDPT for density operator instead, we have

$$\hat{\boldsymbol{\rho}}(t) \approx \hat{\boldsymbol{\rho}}_0(t) + \lambda \hat{\boldsymbol{\rho}}_1(t) + \lambda^2 \hat{\boldsymbol{\rho}}_2(t), \tag{1.34}$$

and the expansion of the expectation value follows order by order with the density operator expansion:

$$\mathrm{Tr}\left\{ \hat{\mathbf{O}}\, \hat{\boldsymbol{\rho}}(t) \right\} \approx \mathrm{Tr}\left\{ \hat{\mathbf{O}}\, \hat{\boldsymbol{\rho}}_0(t) \right\} + \lambda \mathrm{Tr}\left\{ \hat{\mathbf{O}}\, \hat{\boldsymbol{\rho}}_1(t) \right\} + \lambda^2 \mathrm{Tr}\left\{ \hat{\mathbf{O}}\, \hat{\boldsymbol{\rho}}_2(t) \right\}. \tag{1.35}$$

There are situations where $\left\langle \psi_2(t) \left| \hat{\mathbf{O}} \right| \psi_0(t) \right\rangle = 0$, e.g., when the observable measures population transfer that is induced only by the time dependent part of the Hamiltonian, i.e., $\hat{\mathbf{H}}_f(t)$, and is not allowed by $\hat{\mathbf{H}}_0$. On such cases only first-order TDPT is needed for the wave function description, but the equivalent description using the density operator will require the second order approximation.

1.2.2 Rotating frame

Many systems in atomic and molecular physics may be separated into two subsystems. These two manifolds have an energy difference ΔE, and are coupled through an external field. For example, a molecule with two electronic surfaces can be subject to a laser that excites the molecule to the excited surface.

Suppose that the separated subsystems are described by the Hamiltonians $\hat{\mathbf{H}}_1$ and $\hat{\mathbf{H}}_2$. The total free-field Hamiltonian is:

$$\hat{\mathbf{H}}_0 = \begin{pmatrix} \hat{\mathbf{H}}_2 & 0 \\ 0 & \hat{\mathbf{H}}_1 \end{pmatrix}. \tag{1.36}$$

These subsystems are coupled by a time-dependent laser field $f(t)$. The field

operator is described by

$$\hat{\mathbf{H}}_f(t) = \begin{pmatrix} 0 & \hat{\boldsymbol{\mu}} f(t) \\ \hat{\boldsymbol{\mu}}^\dagger f(t)^* & 0 \end{pmatrix}, \tag{1.37}$$

where the operation of the field operator is represented by the linear operator $\hat{\boldsymbol{\mu}}$. The total Hamiltonian is $\hat{\mathbf{H}} = \hat{\mathbf{H}}_0 + \hat{\mathbf{H}}_f$.

If the field is composed from an envelope $\tilde{f}(t)$ and oscillations with the carrier frequency ω_L,

$$f(t) = \tilde{f}(t) e^{i\omega_L t}, \tag{1.38}$$

we can use the rotating frame for a more convenient representation of the problem. We define the rotation operator

$$\hat{\mathbf{R}}(t) = \exp\left\{-i\tfrac{\omega_L}{2}\hat{\mathbf{S}}_z t\right\}, \quad \hat{\mathbf{S}}_z = \begin{pmatrix} \hat{\mathbf{1}} & 0 \\ 0 & -\hat{\mathbf{1}} \end{pmatrix}. \tag{1.39}$$

The rotation operator is used to rotate the wave function

$$\left|\tilde{\psi}(t)\right\rangle = \hat{\mathbf{R}}(t) \left|\psi(t)\right\rangle. \tag{1.40}$$

The Schrödinger equation for the rotated wave function employs the rotating frame Hamiltonian, $\hat{\mathbf{H}}_{RF}$,

$$\frac{\partial}{\partial t}\left|\tilde{\psi}(t)\right\rangle = -i\hat{\mathbf{H}}_{RF}\left|\tilde{\psi}(t)\right\rangle \tag{1.41}$$

with

$$\hat{\mathbf{H}}_{RF} = \hat{\mathbf{R}}(t)\hat{\mathbf{H}}\hat{\mathbf{R}}^\dagger(t) - \frac{\omega_L}{2}\hat{\mathbf{S}}_z = \begin{pmatrix} \hat{\mathbf{H}}_2 - \frac{1}{2}\omega_L & \hat{\boldsymbol{\mu}}\tilde{f}(t) \\ \hat{\boldsymbol{\mu}}\tilde{f}(t)^* & \hat{\mathbf{H}}_1 + \frac{1}{2}\omega_L \end{pmatrix}, \tag{1.42}$$

The rotating wave Hamiltonian eliminates the rapid oscillation of the field. It also reduces the energy difference between the subsystems to $\delta \equiv \Delta E - \omega_L$.

1.3 Open quantum systems: Reduced description

The concept of isolated quantum systems is a useful idealization. However, real systems are coupled to the surroundings. A generic model starts with describing the system under study as a part of a composition of the system and the environment. The Hamiltonian of such a construction is

$$\hat{\mathbf{H}} = \hat{\mathbf{H}}_S \otimes \hat{\mathbf{I}}_E + \hat{\mathbf{I}}_S \otimes \hat{\mathbf{H}}_E + \hat{\mathbf{V}}_{S-E}. \tag{1.43}$$

Here, the operators $\hat{\mathbf{H}}$ and $\hat{\mathbf{I}}$ denote the Hamiltonians and the Identity operator, respectively, and the subscripts S and E represent the system and the environment,

respectively. The operator $\hat{\mathbf{V}}_{S-E}$ is the interaction between the system and the environment.

A full description has to account for all the degrees of freedom of the system and the environment. However, only the system degrees of freedom are of interest. Therefore, we attempt to describe only the system explicitly, and to integrate out the environment degrees of freedom, so they will affect the description only implicitly. The goal is to reduce the description to a small number of variables and obtain a practical way to treat the system. Such a description is called a *reduced description*.

There are several ways to derive the reduced description of the dynamics. They all involve partial tracing on the environmental degrees of freedom:

$$\hat{\rho}_S \equiv \mathrm{Tr}_E \left\{ \hat{\boldsymbol{\rho}} \right\}, \tag{1.44}$$

but can use different approximations. The resulting dynamics has to conserve the properties of the density operator:

1. $\mathrm{Tr}\left\{\rho_S(t)\right\} = 1$.
2. $\rho_S(t)$ is positive semi definite.
3. $\rho_S(t)$ is hermitian.

The dynamics is not limited to hermitian generators and generally it is not unitary. This reflects the non uniform character of the dynamics, caused by the flow of information from the system to the environment and back. An immediate result of the non unitary dynamics is that the purity is not conserved with such dynamics and it can increase or decrease during the evolution.

1.3.1 The Kraus map

A very general description of the time evolution is the Kraus map [Kraus 1971, Kraus 1983, Alicki 2007]. This map requires that the dynamics will be linear and trace preserving. Additionally, the density operator of the entire composition of the system and the environment should be initially a separable state:

$$\rho(0) = \rho_S(0) \otimes \rho_E(0), \tag{1.45}$$

where $\hat{\rho}_S$ and $\hat{\rho}_E$ are the density operators of the system and the environment, respectively. Under such conditions, the system dynamics can be represented in the Kraus form:

$$\rho_S(t) = \Phi\left[\rho_S(0)\right] = \sum_i \hat{\mathbf{K}}_i \rho_S(0) \hat{\mathbf{K}}_i^\dagger. \tag{1.46}$$

The operators $\{\hat{\mathbf{K}}_i\}$ are the Kraus operators, which should satisfy the condition:

$$\sum_i \hat{\mathbf{K}}_i \hat{\mathbf{K}}_i^\dagger = \hat{\mathbf{I}}. \tag{1.47}$$

Every map that can be represented in the Kraus form is a completely positive map [Alicki 2001]. The time evolution of the quantum system is required to be completely positive. The complete positivity requirement is a strengthening of the positivity property: The tensor product of two completely positive maps is always completely positive. This is contrary to positive maps, since the tensor product of two positive maps may be non positive. The complete positivity of the dynamics ensures that the density operator preserves its properties.

1.3.2 Markovian dynamics

For Markovian dynamics further simplifications can be applied. The physical interpretation of the Markovian assumption is that the dynamics of the environment is much quicker than that of the system. Therefore, any information that transfers from the system to the environment is lost, leading to a "no-memory" effect. Davies rigorously derived the weak coupling limit, resulting in a quantum Master equation which leads to a completely positive dynamical *semigroup* with negligible memory effects [Davies 1974]. The term *semigroup* implies that the time evolution forms a family of maps which does not form a full group. It lacks the negative range of the parameter t, which implies that the inverse property required from a group is missing. Physically, this property is the manifestation of irreversible dynamics which allows us to distinguish the future from the past. To summarize, the quantum dynamical semigroup is a continuous one parameter family of maps $\{\Lambda_t, t \geq 0\}$, that satisfies [Alicki 2001]:

1. Λ_t is complete positive.

2. Λ_t is trace preserving.

3. $\Lambda_{t+s} = \Lambda_t \Lambda_s \quad t, s \geq 0$, semigroup Markov property.

4. Λ_t is strongly continuous.

The total density operator in such dynamics remains a tensor product at all times:

$$\rho(t) = \rho_S(t) \otimes \rho_E(t). \tag{1.48}$$

1.3.3 The L-GKS equation

Based on a mathematical construction, Lindblad, as well as Gorini, Kossakowski and Sudarshan, (L-GKS) obtained the most general structure of the generator $\mathcal{L}$ of a completely positive dynamical semigroup [Lindblad 1976, Gorini 1976]. The equation of motion is the L-GKS equation, known also as the Lindblad equation:

$$\begin{array}{rcccc} \frac{\partial}{\partial t}\rho_S = \mathcal{L}(\rho_S) & \equiv & -i\left[\hat{\mathbf{H}},\rho_S\right] & + & \sum_i \gamma_i\left(\hat{\mathbf{A}}_i\rho_S\hat{\mathbf{A}}_i^\dagger - \frac{1}{2}\left\{\hat{\mathbf{A}}_i^\dagger\hat{\mathbf{A}}_i,\rho_S\right\}\right), \\ & \equiv & \mathcal{L}_H(\rho_S) & + & \mathcal{L}_D(\rho_S) \end{array} \tag{1.49}$$

with $\{\hat{\mathbf{A}}_i\}$ a set of orthonormal traceless operators, and $\{\hat{\mathbf{B}},\hat{\mathbf{C}}\}$ is the anti commutator of the operators $\hat{\mathbf{B}}$ and $\hat{\mathbf{C}}$. The super-operator $\mathcal{L}$ is the L-GKS generator, known also as the Lindbladian. $\mathcal{L}_H$ and $\mathcal{L}_D$ are the Hamiltonian and the dissipative parts of the Lindbladian, respectively.

In the absence of the dissipator $\mathcal{L}_D$, the equation resembles the von-Neumann equation, and generates unitary evolution. Under the presence of dissipator $\mathcal{L}_D$ the evolution is not unitary. Using the definition of an adjoint super-operator, the adjoint of the dissipator $\mathcal{L}_D$ can be shown to have the form:

$$\mathcal{L}_D^\dagger\hat{\mathbf{X}} = \sum_i \gamma_i\left(\hat{\mathbf{A}}_i^\dagger\hat{\mathbf{X}}\hat{\mathbf{A}}_i - \frac{1}{2}\left\{\hat{\mathbf{A}}_i^\dagger\hat{\mathbf{A}}_i,\hat{\mathbf{X}}\right\}\right). \tag{1.50}$$

The dissipator is neither hermitian nor anti-hermitian. Therefore the purity is not conserved in such dynamics. The purity change is only due to the dissipator $\mathcal{L}_D$. Therefore, if an external field acts only on the system, the purity cannot be altered by the field. This leads to 'contraction' of the reachable space under the driving of external fields [Altafini 2004].

For a time-independent L-GKS generator, the evolution is given formally by:

$$\hat{\boldsymbol{\rho}}_S(t) = e^{\mathcal{L}t}\hat{\boldsymbol{\rho}}_S(0). \tag{1.51}$$

When the open system interacts with external fields, the dissipator may have to be modified. For example, in a strong periodic driving, one has to use Floquet analysis to derive the quantum master equation [Alicki 2006, Levy 2012]. Another regime is the adiabatic limit, where the Hamiltonian can be instantaneously diagonalized and the master equation is derived accordingly [Geva 1994]. However, if the fields are weak the dissipator can be described as field-independent. The dynamics for such a time-dependent L-GKS equation will involve the time ordering operator $\mathcal{T}$, as in Eq. (1.27).

Outline

The distinct nature of Markovian open quantum systems is peculiar and fascinating. The goal of this work is to unravel a few aspects of the emerging dynamics. We investigated the effect of the environment on the dynamics of the system under the influence of external driving fields.

- Chapter 2, *Numerical methods for the analysis of the L-GKS dynamics*, discusses the numerical methods we used at this work. The particular properties of the Markovian dynamics require employing different numerical tools for the analysis of the L-GKS equation.

- Chapter 3, *Population transfer induced by weak fields*, studies the weak-field phase-only control of open quantum systems. We employed the time dependent perturbation theory of the L-GKS equation to investigate laser-driven population transfer in molecules. We compared the effect of the phase of the weak driving field on the open and isolated system dynamics, and examined the consequences of the coupling of the system to the environment.

- Chapter 4, *Exceptional points in the dynamics of Markovian open quantum systems*, studies exceptional points of the L-GKS equation.
  Non-hermitian degeneracies are known as exceptional points. They gives rise to a subtle unique time evolution, which can be revealed using harmonic inversion methods. We studied the implications of such points in the open system dynamics of two system classes:

  - The two-level system described by the Bloch equations. We calculated the map of exceptional points for this system, and suggested to employ the exceptional points for the estimation of the system parameters.
  - The spontaneous emission of atomic systems. The additional complexity of these systems leads to a more complex map of exceptional points. We calculated the map of exceptional points and suggested to employ them for accurate parameter estimation.

- Chapter 5, *Conclusions and outlook*, discusses the thesis and presents concluding remarks.

Chapter 2

Numerical methods for the analysis of the L-GKS dynamics

2.1 Introduction

The coupling of a quantum system to the external environment incorporates relaxation and dephasing processes into the dynamics. The L-GKS equation describes the dynamics of such Markovian open quantum systems [Breuer 2002, Alicki 2007]. There is an essential difference between the characteristics of the dynamics of open and isolated systems. This difference is manifested in the properties of the generating equations. Therefore, the numerical tools needed for the analysis of the L-GKS dynamics are different from the common tools used in quantum mechanics.

The L-GKS equation, Eq. (1.49), is a first order linear differential equation, described by the operation of the super-operator $\mathcal{L}$ on the density operator $\hat{\boldsymbol{\rho}}$:

$$\frac{d\hat{\boldsymbol{\rho}}}{dt} = \mathcal{L}\hat{\boldsymbol{\rho}}. \tag{2.1}$$

When the super-operator $\mathcal{L}$ is time independent, the formal solution is:

$$\hat{\boldsymbol{\rho}}(t) = e^{\mathcal{L}t}\hat{\boldsymbol{\rho}}(0). \tag{2.2}$$

Typically, the resulting dynamics of the system observables (expectation values and other correlation functions) $C(t)$ will have the analytical form of sum of decaying oscillations[‡]:

$$C(t) = \sum_m d_m e^{\lambda_m t}, \tag{2.3}$$

[‡]There are special cases where the super-operator is not diagonalizable. In such cases, known as exceptional points, the exponential $e^{\lambda t}$ is multiplied by a polynomial of t. A study of exceptional points in L-GKS systems can be found in Chapter 4 of this thesis.

where λ_m are the exponential coefficients and d_m are the associated amplitudes, both can be complex. We may divide λ_m into its real and imaginary parts, $\lambda_m = -\alpha_m + i\omega_m$, with $\alpha_m \geq 0 \in \mathbb{R}$ as the decay rates and $\omega_m \in \mathbb{R}$ as the oscillation frequencies. The coefficients λ_m are the eigenvalues of the super-operator $\mathcal{L}$, obtained by the eigenvalue equation:

$$\mathcal{L}\hat{\boldsymbol{\sigma}}_m = \lambda_m \hat{\boldsymbol{\sigma}}_m. \tag{2.4}$$

These eigenvalues can be used for the analysis of the L-GKS dynamics.

Below we describe the numerical tools we used for the analysis of the L-GKS dynamics. The main numerical methods we used in this work are:

- Numerical simulations of the dynamics generated by the L-GKS equation.
- Characterizing the L-GKS generator by means of its eigenvalues.
- Analysis of the generated dynamics.

Section 2.2 describes the formulation of the L-GKS equation as a matrix-vector equation. Such a formulation eases the use of common numerical methods for simulations of the dynamics and eigenvalue calculations. Section 2.3 describes the harmonic inversion method we used for analysis of the dynamics.

2.2 Matrix-vector representations

As noted above, the dynamics can be investigated by exponentiation of the super-operator $\mathcal{L}$, Eq. (2.2), or by its eigenvalues, Eq. (2.4). The exponential and the eigenvalue problem of the (linear) super-operator $\mathcal{L}$ are well defined. However, the standard formulation of the L-GKS equation defines the operation of the L-GKS generator as sum of left and right matrix multiplications with the density operator. This formulation challenges the use of common numerical techniques for the exponentiation and for the eigenvalues calculation. Calculations of the exponentiation and the eigenvalue equation of linear operators can be done by common numerical techniques if the linear operator is represented by a matrix. Therefore, it is advantageous to represent the L-GKS equation, Eq. (2.1), as a matrix-vector differential equation. This means that we are looking for a matrix L and a vector $\vec{r}_s$ such that the dynamics are expressed as

$$\frac{d}{dt}\vec{r}_s = L\vec{r}_s. \tag{2.5}$$

In this representation, the vector $\vec{r}_s$ represents the state of the system, or some information about it, e.g. a set of expectation values.

Suppose the density operator $\hat{\boldsymbol{\rho}}$ is an $n \times n$ matrix (if $\hat{\boldsymbol{\rho}}$ is a function of continuous variables, e.g. $\hat{\boldsymbol{\rho}}(r, r')$, these variables have to be discretized). The set of all $n \times n$

density operators forms a Liouville space of dimension n^2. In this Liouville space, we consider the density operator $\hat{\boldsymbol{\rho}}$ as an n^2 vector. Similarly, we consider the super-operator $\mathcal{L}$, which is an operator operating on elements in this linear space, as an $n^2 \times n^2$ matrix.

The above observation is the first step towards the representation we seek. In the following, we describe three approaches that use this concept to introduce such a representation:

1. *Vec-ing the density operator* is the most natural way to construct an n^2 vector for the density operator, and a suitable $n^2 \times n^2$ matrix for the super-operator.

2. The *Arnoldi method* approximates a large matrix in smaller dimensions, enabling simpler numerical calculations.

3. With the *Heisenberg picture* of the L-GKS equation we can search for a representation with a dimension smaller than n^2.

These three approaches are described below.

2.2.1 Vec-ing the density operator

In this method, known as vec-ing [Machnes 2014, Roger 1994, Chapter 4], the $n \times n$ density operator $\hat{\boldsymbol{\rho}}$ is flattened into an n^2 vector $\vec{r}$. This flattening is done by ordering the columns of $\hat{\boldsymbol{\rho}}$ one below the other, so the (a, b) entry of the matrix $\hat{\boldsymbol{\rho}}$ is the $(b-1)n+a$ entry of the vector $\vec{r}$. This is equivalent to choosing the representation basis as the set of matrices with all-zero entries, except one.

The next task is to find the suitable matrix that will represent the operation of the super-operator $\mathcal{L}$ on the density operator. We make the following observations [Machnes 2014, Roger 1994]:

1. A left multiplication of the matrix $\hat{\boldsymbol{\rho}}$ by an $n \times n$ matrix A, i.e. $A\hat{\boldsymbol{\rho}}$, is equivalent to an operation on the vector $\vec{r}$ by the $n^2 \times n^2$ matrix $I \otimes A$, where I is the $n \times n$ identity matrix, and $\otimes$ is the Kronecker direct product.

2. Similarly, a right multiplication of the matrix $\hat{\boldsymbol{\rho}}$ by an $n \times n$ matrix B, i.e. $\hat{\boldsymbol{\rho}}B$, is equivalent to an operation on the vector $\vec{r}$ by the $n^2 \times n^2$ matrix $B^T \otimes I$. Here T denotes the transpose of the matrix.

3. Finally, a combination of left and right matrices multiplication, $A\hat{\boldsymbol{\rho}}B$, is equivalent to an operation on the vector $\vec{r}$ by the $n^2 \times n^2$ matrix $B^T \otimes A$.

The L-GKS super-operator is a sum of such right and left multiplications. Therefore, the construction of the $n^2 \times n^2$ matrix representation for the L-GKS generator has

the parts as follows. For the commutator:

$$\left[\hat{\mathbf{H}}, \hat{\boldsymbol{\rho}}\right] \rightarrow \left(I \otimes \hat{\mathbf{H}} - \hat{\mathbf{H}}^T \otimes I\right) \vec{r}.$$

For the dissipative part:

$$\begin{aligned}
\hat{\mathbf{A}}_i \hat{\boldsymbol{\rho}} \hat{\mathbf{A}}_i^\dagger &\rightarrow \left(\left(\hat{\mathbf{A}}_i^\dagger\right)^T \otimes \hat{\mathbf{A}}_i\right) \vec{r} \\
\hat{\mathbf{A}}_i^\dagger \hat{\mathbf{A}}_i \hat{\boldsymbol{\rho}} &\rightarrow \left(I \otimes \hat{\mathbf{A}}_i^\dagger \hat{\mathbf{A}}_i\right) \vec{r} \\
\hat{\boldsymbol{\rho}} \hat{\mathbf{A}}_i^\dagger \hat{\mathbf{A}}_i &\rightarrow \left(\left(\hat{\mathbf{A}}_i^\dagger \hat{\mathbf{A}}_i\right)^T \otimes I\right) \vec{r}.
\end{aligned}$$

Then we write

$$\begin{aligned}
L = &- i \left(I \otimes \hat{\mathbf{H}} - \hat{\mathbf{H}}^T \otimes I\right) \\
&+ \sum_i \gamma_i \left(\left(\hat{\mathbf{A}}_i^\dagger\right)^T \otimes \hat{\mathbf{A}}_i - \frac{1}{2}\left(I \otimes \hat{\mathbf{A}}_i^\dagger \hat{\mathbf{A}}_i + \left(\hat{\mathbf{A}}_i^\dagger \hat{\mathbf{A}}_i\right)^T \otimes I\right)\right),
\end{aligned} \tag{2.6}$$

and represent Eq. (2.1) as

$$\frac{d}{dt}\vec{r} = L\vec{r}$$

as desired.

The mapping of the density operator into a density vector yields in a dramatic increment in the dimension of the problem, which becomes n^2 instead of n [‡]. This yields unfavorable scaling of the desired computations with n:

- *Eigenvalue approach.* Computation of the complete eigenvalue spectrum of L is performed via the diagonalization of L. Diagonalization of a matrix scales as the cube of its dimension. Hence, the diagonalization of L scales as n^6.

- *Exponentiation methods.* The exponentiation of the matrix for time propagation, e^{Lt}, can be computed via various ways [Moler 2003]. Remarkably, two branches are of interest:

  1. Directly employing the diagonalization of L.
  2. Numerical approximations, which usually involve matrix-matrix multiplications.

  Both diagonalization and matrix-matrix multiplications scale as the cube of the matrix dimension. Therefore, the overall scaling of the exponentiation is also n^6.

[‡]The density operator $\hat{\boldsymbol{\rho}}$ is hermitian. Therefore there are only $n(n+1)/2$ unique entries and not n^2. This fact can be used to reduce the size of the vectors and matrices, known as a half-vectorization [Abadir 2005, Chapter 11]. However, we will not discuss this here.

The calculation cost of the operation of the exponential e^{Lt} on an initial vector $\vec{r}_0$, i.e. $e^{Lt}\vec{r}_0$, can be reduced by employing matrix-vector multiplications, and therefore scales as n^4 [Al-Mohy 2011].

For systems larger than a few degrees of freedom, such computations are expensive, and become practically impossible for systems larger than a few hundreds DOF.

The scaling problem suggests that we have to look for approaches that use a smaller number of dimensions. The following two approaches address this issue. The Arnoldi method uses a small-dimension approximation of a large matrix. The operator representation seeks for a small subset of variables that are sufficient to describe the quantities of interest. These two approaches are described in the next two sections.

2.2.2 Arnoldi method

The Arnoldi method is a method to approximate a large matrix A in a smaller dimension [Trefethen 1997]. This is done by choosing an appropriate set of a small number of vectors, which should be representative of the relevant subspace for a specific problem. Then the desired matrix is represented in the reduced subspace which is spanned by the chosen vectors. The method starts with an initial vector $\vec{v}$ and creates set of $K+1$ vectors by the repetitive operation of the matrix A: $\{\vec{v}, A\vec{v}, A^2\vec{v}, \ldots, A^K\vec{v}\}$. Then an orthonormal set is generated from this set by the Gram-Schmidt process. This orthonormal vectors set spans a subspace with dimension $K+1$, and the matrix A is represented in this subspace by a $(K+1)\times(K+1)$ matrix. This smaller matrix can be used for the efficient evaluation of functions of the matrix A, e.g. the exponential [Saad 1992] or the eigenvalues [Arnoldi 1951].

In our case we try to approximate the linear super-operator $\mathcal{L}$ by a matrix which is smaller than $n^2 \times n^2$. Conceptually, we start with the initial density operator $\hat{\boldsymbol{\rho}}_0 \equiv \hat{\boldsymbol{\rho}}_s(0)$, and operate K times with $\mathcal{L}$ to get the set $\{\hat{\boldsymbol{\rho}}_0, \mathcal{L}\hat{\boldsymbol{\rho}}_0, \mathcal{L}^2\hat{\boldsymbol{\rho}}_0, \ldots, \mathcal{L}^K\hat{\boldsymbol{\rho}}_0\}$ which is the starting point for orthogonalization and $(K+1)\times(K+1)$-dimension matrix representation of $\mathcal{L}$. We note that the operation of $\mathcal{L}$ involves $n \times n$ matrix-matrix multiplications, which scales as n^3. Therefore, it is more efficient to use the operation of $\mathcal{L}$ for the procedure than to use the vec-ing matrix L (Eq. (2.6)) described in Sec. 2.2.1 above.

The actual procedure follows, adapted to the notation of a super-operator and density operators:

1. Begin with the normalized density operator $\hat{\boldsymbol{\rho}}_0$.

2. for $j = 0$ to K

(a) Compute a non-orthonormalized new density operator by setting: $\hat{\boldsymbol{\rho}}_{j+1} := \mathcal{L}\hat{\boldsymbol{\rho}}_j$

(b) for $i = 0$ to j

i. Set: $L_{i,j} := \left(\hat{\boldsymbol{\rho}}_i^\dagger, \hat{\boldsymbol{\rho}}_{j+1}\right) = \mathrm{Tr}\left\{\hat{\boldsymbol{\rho}}_i^\dagger \hat{\boldsymbol{\rho}}_{j+1}\right\}$

ii. Subtract the projection on $\hat{\boldsymbol{\rho}}_i$: $\hat{\boldsymbol{\rho}}_{j+1} := \hat{\boldsymbol{\rho}}_{j+1} - L_{i,j}\hat{\boldsymbol{\rho}}_i$

end for

(c) Set: $L_{j+1,j} := \left\|\hat{\boldsymbol{\rho}}_{j+1}\right\| \equiv \sqrt{\mathrm{Tr}\left\{\hat{\boldsymbol{\rho}}_{j+1}^\dagger \hat{\boldsymbol{\rho}}_{j+1}\right\}}$

(d) Normalize $\hat{\boldsymbol{\rho}}_{j+1}$ by setting $\hat{\boldsymbol{\rho}}_{j+1} := \frac{\hat{\boldsymbol{\rho}}_{j+1}}{L_{j+1,j}}$

end for

The procedure yields

$$L_{i,j} = \mathrm{Tr}\left\{\hat{\boldsymbol{\rho}}_i^\dagger \mathcal{L}\hat{\boldsymbol{\rho}}_j\right\} \qquad i \leq j+1$$

For $i > j+1$, the expression in the right-hand side vanishes. Thus, we can define a $(K+1)\times(K+1)$ matrix which its general element is given by a matrix element of $\mathcal{L}$ in the Liouville space:

$$L_{i,j} = \mathrm{Tr}\left\{\hat{\boldsymbol{\rho}}_i^\dagger \mathcal{L}\hat{\boldsymbol{\rho}}_j\right\}$$

(Note that the procedure also yields $\hat{\boldsymbol{\rho}}_{K+1}$ and $L_{K+1,K}$ which are not necessary for our purposes). L represents the operation of the super-operator $\mathcal{L}$ on the subspace that is spanned by the density operators $\{\hat{\boldsymbol{\rho}}_0, \hat{\boldsymbol{\rho}}_1, \hat{\boldsymbol{\rho}}_2, \ldots, \hat{\boldsymbol{\rho}}_K\}$. The matrix L is referred to as the *Hessenberg matrix of* $\mathcal{L}$. The density operator has to be approximated by its projection on the subspace: $\hat{\boldsymbol{\rho}} \approx r_0\hat{\boldsymbol{\rho}}_0 + r_1\hat{\boldsymbol{\rho}}_1 + r_2\hat{\boldsymbol{\rho}}_2 + \ldots + r_K\hat{\boldsymbol{\rho}}_K$. The vector

$$\vec{r} \equiv (r_0, r_1, r_2, \ldots, r_K)^T \tag{2.7}$$

is the representation of the density operator in this subspace. The dynamics of the vector $\vec{r}$ is generated by the matrix L that was constructed in step (2) of the above procedure:

$$\frac{d}{dt}\vec{r} = L\vec{r}.$$

Exponentiation and eigenvalue calculations of the matrix L can be done by common numerical techniques [Arnoldi 1951, Saad 1992].

The Arnoldi algorithm usually becomes problematic when a large dimension approximation is required, i.e. when K is large. In such a case, a *restarted Arnoldi algorithm* should be used instead (see, for example, [Tal-Ezer 2007]). This topic is beyond the scope of this thesis.

2.2.3 The Heisenberg representation

Not always the full state of the system will be of concern. In most cases we will be interested only in the expectation values of some measured quantities. This fact can reduce significantly the dimensions of the problem. For example, in the standard thermalizing master equation the population and the coherences are decoupled, and the population of a certain level is given by solving a single differential equation [Breuer 2002]. The full state of the system can be reconstructed by calculating all the expectation values of the Lie algebra of the system. Generally, a full reconstruction of the state will scale as the Vec-ing of the density operator introduced in Sec. 2.2.1. Nevertheless, in many cases we can use symmetries to reduce the dimensions of the problem. For example, if the initial state of harmonic oscillator is a Gaussian state, then it will stay Gaussian along the dynamics and only the first two moments are necessary to retrieve the full state [Rezek 2006]. Another example is coupled two qubits in which the full dimension of the system is 16, but only 3 operators are sufficient to define the energy and coherence of the system [Kosloff 2002].

To describe the dynamics of the expectation values, it is common to use the master equation in the Heisenberg representation. The operator $\hat{\mathbf{X}}$ belonging to dual Hilbert space of the system follows the dynamics [Alicki 2001, Breuer 2002]:

$$\hat{\mathbf{X}}(t) = e^{\mathcal{L}^\dagger t}\hat{\mathbf{X}}(0), \tag{2.8}$$

which in its differential form is written explicitly as

$$\frac{d}{dt}\hat{\mathbf{X}} = \mathcal{L}^\dagger\hat{\mathbf{X}} \equiv \frac{i}{\hbar}\left[\hat{\mathbf{H}}, \hat{\mathbf{X}}\right] + \sum_i \gamma_i \left(\hat{\mathbf{A}}_i^\dagger \hat{\mathbf{X}} \hat{\mathbf{A}}_i - \frac{1}{2}\left\{\hat{\mathbf{A}}_i^\dagger \hat{\mathbf{A}}_i, \hat{\mathbf{X}}\right\}\right). \tag{2.9}$$

If there is a a set of operators $\{\hat{\mathbf{X}}_k\}_{k=1}^M$, $M < n^2$, that forms a closed set under the operation of $\mathcal{L}^\dagger$, meaning

$$\mathcal{L}^\dagger\hat{\mathbf{X}}_k = \sum_{j=1}^{M} l_{kj}\hat{\mathbf{X}}_j \tag{2.10}$$

then we can write a closed linear system of coupled differential equations. The expectation values $x_k \equiv \left\langle \hat{\mathbf{X}}_k \right\rangle$ will have the corresponding set of coupled differential equations. The analytical form of their dynamics will follow the form of Eq. (2.3). We define the vector of expectation values $\vec{R} \equiv (x_1, x_2, \ldots)^T$. This system can be represented in a matrix-vector notation,

$$\frac{d}{dt}\vec{R} = L^\dagger\vec{R},$$

where the matrix $L^\dagger$ is defined by the equation set Eq. (2.10), $\left(L^\dagger\right)_{kj} = l_{kj}$. The dimension of this matrix is M^2. Note that eigenvalues of the matrix $L^\dagger$ are complex conjugates of a subset of the eigenvalues of the super-operator $\mathcal{L}$ of Eq. (2.4).

2.3 Harmonic inversion of time signals

The analytical form of a time signal that emerge from a system of coupled linear differential equations is generally a sum of decaying exponents:

$$C(t) = \sum_k d_k \exp\left[\lambda_k t\right] \ , \tag{2.11}$$

where the complex coefficients λ_k are composed from real and imaginary parts: $\lambda_k = -\alpha_k + i\omega_k$, with $\alpha_k \geq 0 \in \mathbb{R}$ as the decay rates and $\omega_k \in \mathbb{R}$ as the oscillation frequencies. d_k are the associated amplitudes, which also can be complex.

Such time signals can be the results of an experiment or a simulation. For studying the L-GKS dynamics, we have to analyze this time series end extract the underlying model, which is characterized by the eigenvalues $\{\lambda_k\}$ and the amplitudes $\{d_k\}$. The time signal $C(t)$, $0 \leq t \leq T$, is sampled at some discretized time points $\{t_n\}$, usually at equal time intervals:

$$c[n] \equiv C(t_n) = C(n\delta t), \ 0 \leq n \leq N = \lfloor T/\delta t \rfloor. \tag{2.12}$$

The immediate candidate for such a task is the discretized Fourier transform. The location of the spectrum peaks are the frequencies of the time series, the widths of the peaks are the decay rates, and the magnitudes of the peaks are the amplitudes. However, the Fourier transform enables extracting the frequencies and decay rates only to a limited resolution: $\Delta\omega \geq \frac{1}{T}$. We need a long duration of time signals to reproduce the eigenvalues.

To overcome this limitation, the procedure for extracting the eigenvalues from the time series has to assume a specific model. *Harmonic inversion* methods assume an analytical form of sum of decaying oscillations for the time series, Eq. (2.11), and use this form for extracting the eigenvalues in high resolution. An overview of harmonic inversion methods can be found at [Belkić 2000].

The Filter Diagonalization (FD) method [Wall 1995, Mandelshtam 2001] assumes that the dynamics is generated by a complex matrix H,

$$C(t) = \left\langle \psi_0 \left| e^{-iHt} \right| \psi_0 \right\rangle . \tag{2.13}$$

Based on this model the FD method builds an eigenvalue problem. The parameters

of the time signal are extracted from the solutions for this problem. This method is widely used for analysis of NMR experiments [Hu 1998] and Fourier transform mass spectrometry [Martini 2014]. It was also used in the field of ultrafast pump-probe molecular spectroscopy [Gershgoren 2001].

In this work we used the Padé approximant (PA) method. This method assumes the analytical form of Eq. (2.11) and uses the time series to introduce two polynomials, which are employed to determine the time signal parameters. This algorithm was used for extracting the frequencies and the amplitudes from the simulated time signals. The algorithm is summarized in Refs. [Fuchs 2014, Belkić 2000]. It is presented here for the sake of completeness. The Matlab code we used is presented in Appendix 2.4.

Given:

1. A time signal $c[n] = C(n\tau)$, $0 \leq n < N$, sampled at time interval τ
2. The lower edge of the frequency window ω_-
3. The total number of resonances of the signal K

Output: The frequencies ω_k and the amplitudes d_k of the expansion:

$$c_n \equiv C(n\tau) = -i \sum_k d_k \exp[-i(w_k - w_-)n\tau] \tag{2.14}$$

Steps:

1. Define the polynomial $Q_k(z)$: $Q_k(z) = \sum_{k=1}^{K} a_k z^k - 1$.

   Find the coefficients a_k by solving the linear set of equations:

$$c_n = \sum_{k=1}^{K} a_k c_{n+k}, \quad n = 0, ..., K-1 \tag{2.15}$$

2. Find the roots z_k of the polynomial $Q_k(z)$.
3. Obtain the frequencies ω_k by

$$\omega_k = \omega_- + \frac{i}{\tau} \ln(z_k) \tag{2.16}$$

4. Define the polynomial $P_k(z)$: $P_k(z) = \sum_{k=1}^{K} b_k z^k$

   Find the coefficients b_k by the explicit formula:

$$b_k = \sum_{m=0}^{K-k} a_k c_{n+k}, \quad n = 0, ..., K-1 \tag{2.17}$$

5. Obtain the amplitudes d_k (We use the notation $Q^{(1)}(x) = \frac{d}{dz}Q(z)\big|_{z=x}$):

$$d_k = \frac{P(z_k)}{z_k\, Q^{(1)}(z_k)} \tag{2.18}$$

2.4 Appendix: Matlab code for the Padé approximant harmonic inversion

The Matlab code that we used for the Padé approximant harmonic inversion is presented below.

```
function [d, w] = PadeHarmonicInversion(Cn, K, tau, w_minus)
% [d, w] = PadeHarmonicInversionExtended(Cn, K, tau, w_minus, tol)
% Finds the decomposition of a time signal Cn(t), which is sampled
 with
% equals intervals, into sum of exponentials Sum_k d_k *
 exp(-1i*w_k*t)
% This is done by the Pade approximant harmonic inversion method.
%
% Inputs
% Cn - the time signal
% K - the number of exponent terms in the sum
% tau - the time interval for the sampling
% [w_minus, w_plus] is the frequency window to look at:
%    w_minus is an input, w_plus = w_minus+2*pi/tau
%    (Use w_minus=0 in case you don't know what it is)
%
% The output is the amplitudes d and frequcies w, both can be complex.
% Both d and w have length of K.
%
% Reference:
% Harmonic inversion analysis of exceptional points in resonance
 spectra
% By J. Fuchs, J. Main, H. Cartarius and G. Wunner
% 2014 J. Phys. A: Math. Theor. 47 125304
% doi:10.1088/1751-8113/47/12/125304
%
% (without the extended part)

N = length(Cn);
assert(N>=2*K,'At least 2K signal points are required.')

% We use only 2K time points.
% We choose them to be dispersed as much as possible
step = floor(N/(2*K));
Cn = Cn(1:step:N);
tau = step*tau;

if size(Cn,2) ~= 1 % row vector
  Cn = Cn.'; % Column
end

% The matrix for Eqn (7) : loop over n and k: Cnk(n+1,k) = Cn(n+1+k)
% (with n+1 to shift to Matlab indices)
% We use Matlab's indices instead of the loop (the bsxfun generates a
 plus table):
Cnk = Cn(bsxfun(@plus,(1:K)',1:K));

% The 2nd polynomial of Eqn (6),  Q_K(z)=(sum_k a_k*z^k) -1,
% should be obtained by solving a = Cnk\Cn,
% but we have to force Matlab to use pseudo-inverse
a = pinv(Cnk)*Cn(1:K);
```

```
% The 1st polynomial of Eqn (6),  P_K(z)=sum_k b_k*z^k,
% is obtained directly, Eqn (8):
b = zeros(K,1);
for k = 1:K;
  b(k) = a(k:K).'*Cn(1:(K-k+1)); % n+1 to shift to Matlab indices
end

% The roots of the polynomial are the frequencies.
% Matlab's built-in ROOTS function uses the matrix A of Eqn. (10)
Q_0 = [flipud(a);-1];
P_0 = [flipud(b);0];
z = roots(Q_0);
logz = log(z);
w = w_minus+1i/tau*logz; % Eqn (9)

% Prepare polynomials
Q_1_z = polyval(polyder(Q_0),z);
P_0_z = polyval(P_0,z);

% Find d_k, Eqn (11)
% Without the (-i) factor, since we start from the time signal
d = P_0_z./z./Q_1_z;

% Sort the results by the amplitudes
[d, ind_sorted] = sort(d,'descend');
w = w(ind_sorted);

end
```

Published with MATLAB® R2015a

Chapter 3

Population transfer induced by weak fields

3.1 Introduction

The main question we ask in this thesis is how the environment affects the dynamics of driven systems. A significant application for such driving is measurements: The principle of measurements is to examine an object by employing a probe which minimizes the perturbation to the examined system. In molecular spectroscopy a weak radiation field achieves this task. The basic assumption is that there is a direct link between the energy loss from the field and the molecular spectrum. Usually, the molecule interacts with a solvent which acts as an environment. We study the effect of this environment.

In the present study we concentrate on phase control of the population excitation processes in molecules. The molecule is described by the Hamiltonian $\hat{\mathbf{H}}_0$, and is coupled by the dipole operator $\hat{\boldsymbol{\mu}}$ to an external light field $\epsilon(t)$. In the dipole limit the resulting control Hamiltonian is of the form:

$$\hat{\mathbf{H}} = \hat{\mathbf{H}}_0 + \hat{\boldsymbol{\mu}} \cdot \epsilon(t). \tag{3.1}$$

The energy loss of the probing field at the transition frequency ω_{if} is proportional to the population transfer [Kosloff 1992, Ashkenazi 1997, Am-Shallem 2014]:

$$\Delta E(\omega_{if}) = \hbar\omega_{if}\Delta N. \tag{3.2}$$

For an isolated molecule the probability of transition from an initial state $|i\rangle$ to a final state $|f\rangle$ can be calculated by the first order of the time dependent perturbation theory, to get:

$$P_{i\to f}(t) = \frac{1}{\hbar^2}|\langle f|\hat{\boldsymbol{\mu}}|i\rangle|^2| \int_0^t e^{-i\omega_{if}t'}\epsilon(t')dt'|^2 \tag{3.3}$$

For large t we get the Fourier transform of the field, $\tilde{\epsilon}(\omega)$, at the transition frequency ω_{if}. Therefore, the probability depends only on the magnitude of the field $|\epsilon(\omega)|$ at this frequency. It is clear from this description that the state to state transition probability is independent of the phase of the excitation field $\tilde{\epsilon}(\omega)$, and thus it is phase insensitive.

During the last years, a series of experiments challenged this assertion: They showed a phase-dependence of the branching ratio of the cis and trans isomers of the retinal molecule [Prokhorenko 2005, Prokhorenko 2006]. Other experiments showed that the phase-dependence is induced by the environment of the molecule [van der Walle 2009]. These experiments showed phase sensitivity even in weak fields. Other experiments examined the population transfer under chirped weak fields, and showed dependence on the chirp of the field, therefore phase sensitivity [Prokhorenko 2011]. These experiments were supported by numerical simulations which showed that the phase dependence is induced by the environment [Katz 2011].

In order to examine this phenomena there is a need for a formulation in open quantum system. Therefore we will work with the L-GKS equation. In addition, the terminology of weak versus strong fields, as well as the terms of existence versus non-existence of the phase sensitivity, are not well-defined. Thus we will examine the phenomena of population transfer and phase sensitivity by the scaling of these phenomena with the field strength.

3.2 The scaling of weak field phase-only control in Markovian dynamics

The scaling of weak field phase-only control in Markovian dynamics
Morag Am-Shallem and Ronnie Kosloff
Published on *J. Chem. Phys.* 141, 044121 (2014)

THE JOURNAL OF CHEMICAL PHYSICS **141**, 044121 (2014)

The scaling of weak field phase-only control in Markovian dynamics

Morag Am-Shallem and Ronnie Kosloff
Fritz Haber Research Center and the Institute of Chemistry, The Hebrew University, Jerusalem 91904, Israel

(Received 9 June 2014; accepted 10 July 2014; published online 28 July 2014)

We consider population transfer in open quantum systems, which are described by quantum dynamical semigroups (QDS). Using second order perturbation theory of the Lindblad equation, we show that it depends on a weak external field only through the field's autocorrelation function, which is phase independent. Therefore, for leading order in perturbation, QDS cannot support dependence of the population transfer on the phase properties of weak fields. We examine an example of weak-field phase-dependent population transfer, and show that the phase-dependence comes from the next order in the perturbation. © *2014 AIP Publishing LLC*. [http://dx.doi.org/10.1063/1.4890822]

I. INTRODUCTION

Quantum control is devoted to steering a quantum system toward a desired objective. Coherent control achieves this goal by manipulating interfering pathways via external fields, typically a shaped light field.[1] Early in the development of quantum control, Brumer and Shapiro proved that for weak fields in an isolated system, phase only control is impossible for an objective which commutes with the free Hamiltonian.[2] A qualitative explanation is that under such conditions there are no interfering pathways leading from the initial to the final stationary states.

More formally, the control electromagnetic field in the time domain is $\epsilon(t)$, and its spectrum is given by

$$\tilde{\epsilon}(\omega) = \tilde{A}(\omega)e^{i\tilde{\varphi}(\omega)}, \tag{1}$$

where $\tilde{A}(\omega)$ is the amplitude and $\tilde{\varphi}(\omega)$ is the phase. Any target operator that commutes with the field independent Hamiltonian $\hat{\mathbf{H}}$ is uncontrollable by the phase $\tilde{\varphi}(\omega)$.[3]

Experimental evidence has challenged this assertion. Prokhorenko *et al.* claimed to demonstrate weak-field phase-only (WFPO) control,[4,5] and raised a controversy.[6,7] The target of control was an excited state branching ratio. The phenomena were attributed to the influence of the environment. A subsequent study by van der Walle *et al.* showed that such controllability is solvent dependent.[8]

A careful examination of the assumptions can resolve the discrepancy between theory and experiment, considering that the experiments were carried out for an open quantum system. It has been suggested that the coupling to the environment changes the conditions under which the statement of impossibility holds. A new relaxation timescale emerges which interferes with the timescale influence by the pulses phase. Numerical evidence that WFPO control becomes possible for an open quantum system was shown by Katz *et al.*[9] In line with the original proof, Spanner *et al.*[3] argued that if the coupling between the system and the environment does not commute with the measured observable, then the conditions for phase insensitivity do not hold. Nevertheless, open quantum systems have additional features which are not covered by the Hamiltonian time dependent perturbation theory employed to prove the WFPO no go result. A possible opportunity for WFPO for control of observables commuting with the Hamiltonian can emerge from the continuous nature of the spectrum of the evolution operator and/or the inability to separate the system from its environment.

To clarify this issue we will explore the conditions which enable or disable WFPO control in an open quantum system. We restrict this study to the axiomatic approach of open systems based on quantum dynamical semigroups (QDS). The theory aims to find the propagator of the reduced dynamics of the primary system under the assumption that it is generated by a larger system-bath Hamiltonian scenario. The generator in this case belongs to the class of completely positive maps.[10] An important consequence is that the system and bath are initially uncorrelated or, formally, are in a tensor product state at $t = 0$. An additional assumption is the Markovian dynamics. Under completely positive conditions, Lindblad and Gorini-Kossakowski-Sudarshan (L-GKS) proved that the Markovian generator of the dynamics $\hat{\hat{\mathcal{L}}}$ has a unique structure.[11,12] This generator extends the system-bath separability assumption to all times. The WFPO controllability issue can be related now to observables which are invariant to the field free dynamics.

To shed light on the existence/nonexistence of weak field phase only control for L-GKS dynamics we examine the control of population transfer which is an invariant of the field free dynamics. The population transfer ΔN can be directly observed experimentally for fluorescent dyes with a unit quantum yield. A complementary experiment is the weak field spectrum of a photo absorber in solution. For both types of experiments WFPO control of population will lead to phase sensitivity of weak field spectroscopy.

The main result of the present study is that population transfer and energy absorption spectroscopy in L-GKS dynamics depends, in the leading order, only on the autocorrelation function (ACF) of the field, defined by

$$C(\tau) = \int_{-\infty}^{\infty} dt \epsilon(t+\tau)\epsilon^*(t). \tag{2}$$

The ACF does not depend on the phase of the field $\tilde{\varphi}(\omega)$ (cf. Appendix A). Therefore, phase-dependent control of

population transfer will take place only in the next order of the field strength.

II. THE MODEL

Consider a molecule with two potential electronic surfaces, $\hat{\mathbf{H}}_g$ and $\hat{\mathbf{H}}_e$, coupled with a weak laser field $\epsilon(t)$ through the field operator $\hat{\mathbf{V}}(t)$. Starting with an initial state in the ground electronic surface $|\psi_0\rangle$, the control objective is the population transfer to the excited surface. The system Hamiltonian and the field operators are, respectively,

$$\hat{\mathbf{H}}_0 = \begin{pmatrix} \hat{\mathbf{H}}_e & 0 \\ 0 & \hat{\mathbf{H}}_g \end{pmatrix}, \quad \hat{\mathbf{V}}(t) = \begin{pmatrix} 0 & \hat{\mu}\epsilon(t) \\ \hat{\mu}\epsilon(t)^* & 0 \end{pmatrix}. \tag{3}$$

The control objective is the projection on the excited electronic surface

$$\hat{\mathbf{P}}_e = \begin{pmatrix} \hat{\mathbf{1}}_e & 0 \\ 0 & 0 \end{pmatrix}. \tag{4}$$

This objective commutes with the field free Hamiltonian $[\hat{\mathbf{P}}_e, \hat{\mathbf{H}}_0] = 0$.

The population transfer is calculated by solving for the dynamics of the density operator $\hat{\rho}$ in Liouville space. The L-GKS equation generates the dynamics:

$$i\hbar\frac{\partial\hat{\rho}}{\partial t} = \hat{\hat{\mathcal{L}}}\hat{\rho}, \tag{5}$$

where $\hat{\hat{\mathcal{L}}} = \hat{\hat{\mathcal{L}}}_0 + \hat{\hat{\mathcal{V}}}(t)$ is the Lindbladian, and $\hat{\rho} = \sum \rho_{cd}|c\rangle\langle d|$ is the density operator represented here in the Hamiltonian eigenstates basis, $\hat{\mathbf{H}}_0|c\rangle = \hbar\omega_c|c\rangle$. The action of the superoperator $\hat{\hat{\mathcal{V}}}$ on the density matrix $\hat{\rho}$ is defined by

$$\hat{\hat{\mathcal{V}}}\hat{\rho} = [\hat{\mathbf{V}}, \hat{\rho}]. \tag{6}$$

For a specific element of the density operator $|c\rangle\langle d|$ it yields

$$\hat{\hat{\mathcal{V}}}(t)|c\rangle\langle d| = \sum_m (\epsilon(t)\mu_{mc}|m\rangle\langle d| - \epsilon^*(t)\mu_{dm}|c\rangle\langle m|). \tag{7}$$

The action of $\hat{\hat{\mathcal{L}}}_0$ is more involved. Under the complete positivity and the Markovian assumptions, the general L-GKS expression is[11,12]

$$\hat{\hat{\mathcal{L}}}_0\hat{\rho} = [\hat{\mathbf{H}}_0, \hat{\rho}] + i\sum_k \left(\hat{\mathbf{A}}_k\hat{\rho}\hat{\mathbf{A}}_k^\dagger - \frac{1}{2}(\hat{\mathbf{A}}_k^\dagger\hat{\mathbf{A}}_k\hat{\rho} + \hat{\rho}\hat{\mathbf{A}}_k^\dagger\hat{\mathbf{A}}_k)\right), \tag{8}$$

where $\hat{\mathbf{A}}$ is an operator defined in the systems Hilbert space. The commutator with the Hamiltonian governs the unitary part of the dynamics, while the second term on the rhs leads to dissipation and dephasing. Notice that the target operator is invariant to the dissipative dynamics $\hat{\hat{\mathcal{L}}}_0^*\hat{\mathbf{P}}_e = 0$.

The initial state is an equilibrium distribution $P(a)$ on the ground electronic surface

$$\hat{\rho}_0 = \sum_{a\in g.s.} P(a)|a\rangle\langle a|. \tag{9}$$

The population transfer in this case is $\Delta\hat{\mathbf{N}} = \hat{\mathbf{P}}_e$. $\hat{\mathbf{P}}_e$ will be calculated by means of second order time dependent perturbation theory of L-GKS equation. This is the lowest order that yields population transfer. In the case of unitary dynamics, i.e., $\hat{\hat{\mathcal{L}}}_0\hat{\rho} = [\hat{\mathbf{H}}_0, \hat{\rho}]$, it yields the same results as the equivalent calculation by the first order perturbation theory of the Schrödinger equation. In the same manner, the next order in population transfer calculation is the fourth power of the field strength.

III. POPULATION TRANSFER IN LIOUVILLE SPACE

The lowest order of population transfer, starting from the initial condition of Eq. (9), is calculated employing second order time dependent perturbation theory

$$\Delta N(t) = \langle\hat{\mathbf{P}}_e\rangle(t) = \mathrm{Tr}\{\hat{\mathbf{P}}_e\hat{\rho}_I\} \approx \mathrm{Tr}\left\{\hat{\mathbf{P}}_e\hat{\rho}_I{}^{(2)}(t)\right\}, \tag{10}$$

where $\hat{\rho}_I(t_f)$ is the density matrix in the interaction picture, at the final time t_f, and

$$\hat{\rho}_I{}^{(2)}(t_f) = \left(-\frac{i}{\hbar}\right)^2 \int_{t_i}^{t_f} dt_2 \int_{t_i}^{t_2} dt_1 e^{-i\hat{\hat{\mathcal{L}}}_0(t_f-t_2)}\hat{\hat{\mathcal{V}}}(t_2) \times e^{-i\hat{\hat{\mathcal{L}}}_0(t_2-t_1)}\hat{\hat{\mathcal{V}}}(t_1)e^{-i\hat{\hat{\mathcal{L}}}_0(t_1-t_i)}\hat{\rho}_0 \tag{11}$$

is the second order perturbation term in the interaction picture.

Before we evaluate this expression in some representative cases, it can be simplified. First, we note that if initially the system is in equilibrium and invariant to $\hat{\hat{\mathcal{L}}}_0$, then

$$e^{-\frac{i}{\hbar}\hat{\hat{\mathcal{L}}}_0(t_1-t_i)}\hat{\rho}_0 = \hat{\rho}_0. \tag{12}$$

Next, the order of the left operations can be changed leading to

$$\mathrm{Tr}\left\{\hat{\mathbf{P}}_e\int_{t_i}^{t_f} dt_2 \int_{t_i}^{t_2} dt_1 e^{-\frac{i}{\hbar}\hat{\hat{\mathcal{L}}}_0(t_f-t_2)}\hat{\rho}\right\} = \int_{t_i}^{t_f} dt_2 \int_{t_i}^{t_2} dt_1\, \mathrm{Tr}\left\{e^{-\frac{i}{\hbar}\hat{\hat{\mathcal{L}}}_0(t_f-t_2)}\hat{\mathbf{P}}_e\hat{\rho}\right\}, \tag{13}$$

and, since Lindbladian dynamics preserves the trace then

$$\mathrm{Tr}\left\{e^{-\frac{i}{\hbar}\hat{\hat{\mathcal{L}}}_0 t_2}\hat{\mathbf{P}}_e\hat{\rho}\right\} = \mathrm{Tr}\{\hat{\mathbf{P}}_e\hat{\rho}\}, \tag{14}$$

it yields

$$\Delta N(t_f) = -\frac{1}{\hbar^2}\int_{t_i}^{t_f} dt_2 \int_{t_i}^{t_2} dt_1\, \mathrm{Tr}\left\{\hat{\mathbf{P}}_e\hat{\hat{\mathcal{V}}}(t_2)e^{-\frac{i}{\hbar}\hat{\hat{\mathcal{L}}}_0(t_2-t_1)}\hat{\hat{\mathcal{V}}}(t_1)\hat{\rho}_0\right\}. \tag{15}$$

Equation (15) is now evaluated in unitary and non-unitary dynamics. See Appendix B for detailed calculations.

A. Unitary dynamics generated by the Hamiltonian

In this case we get

$$\Delta N = \sum_{\substack{a\in g.s.\\ b\in e.s}} P(a)\frac{|\mu_{ab}|^2}{\hbar^2}\left\{\int_0^\infty d\tau C^*(\tau)e^{-i\omega_{ba}\tau} + c.c.\right\}, \tag{16}$$

where μ_{ab} is a matrix element of the operator $\hat{\mu}$ in the energy basis, $C^*(\tau)$ is the complex conjugate of the ACF of the field $\epsilon(t)$, defined in Eq. (2), and $\omega_{cd} \equiv \omega_c - \omega_d$. *g.s.* and *e.s.* denote the ground and excited surfaces, respectively. *c.c.* denotes the complex conjugate.

The ACF does not depend on the phase of the field. This is shown in Appendix A by means of the vanishing of the functional derivative of the ACF with respect to the phase. Therefore, the population transfer is not affected, to this order in the field strength, by the phase properties of the field. This result is not new.[3] It is presented here in order to demonstrate the perturbative calculation in Liouville space and to emphasize the dependence on the ACF.

B. General L-GKS dynamics

In the present study, the L-GKS generator can only induce dephasing and relaxation within the electronic surfaces. Electronic dephasing or electronic relaxation is not considered. As a result, population transfer is generated only by $\hat{\mathcal{V}}$ (the commutator of $\hat{\mathbf{V}}$).

The notation is simplified using the fact that all states in the perturbation expansion are filtered by $\hat{\mu}$. We define $|\theta_a\rangle \equiv \hat{\mu}|a\rangle$ (or $\langle\theta_a| \equiv \langle a|\hat{\mu}$, respectively), and it should be understood as a state projected on the excited electronic surface. We will also use the notation $\hat{\mathbf{\Theta}}_a \equiv |\theta_a\rangle\langle a|$ for the relevant density matrix element. With this notation, the expression in Eq. (15) becomes

$$\Delta N = \frac{1}{\hbar^2}\sum_{\substack{a\in g.s.\\ b\in e.s}} P(a)\int_0^\infty d\tau\left(C^*(\tau)\langle b|\left[e^{-\frac{i}{\hbar}\hat{\mathcal{L}}_0\tau}\hat{\mathbf{\Theta}}_a\right]|\theta_b\rangle + c.c.\right). \tag{17}$$

To proceed beyond this point additional details on the operation of $\hat{\mu}$ and $\hat{\mathcal{L}}_0$ are required. Nevertheless, the dependence on the control field is only through its ACF.

C. General non unitary dynamics

These results can be extended to a more general propagator $\hat{\mathcal{U}}_0(t_f, t_i)$. The conditions are:

1. The dynamics under weak fields can be described by a second order perturbation theory,

$$\hat{\rho}_I{}^{(2)}(t_f) = \left(-\frac{i}{\hbar}\right)^2\int_{t_i}^{t_f} dt_2\int_{t_i}^{t_2} dt_1\hat{\mathcal{U}}_0(t_f,t_2)\hat{\mathcal{V}}(t_2) \times\hat{\mathcal{U}}_0(t_2,t_1)\hat{\mathcal{V}}(t_1)\hat{\mathcal{U}}_0(t_1,t_i)\hat{\rho}_0. \tag{18}$$

2. The field-free propagation is homogeneous in time, and therefore depends only on the time difference,

$$\hat{\mathcal{U}}_0(t_b,t_a) = \hat{\mathcal{U}}_0(t_b - t_a), \tag{19}$$

for any t_a, t_b.

3. The initial density matrix is invariant under the field-free propagator

$$\hat{\mathcal{U}}_0(t)\rho_0 = \rho_0. \tag{20}$$

4. The field-free propagator does not couple the two electronic surfaces

$$\mathrm{Tr}\{\hat{\mathcal{U}}_0(t)\hat{\mathbf{P}}_e\hat{\rho}\} = \mathrm{Tr}\{\hat{\mathbf{P}}_e\hat{\rho}\}. \tag{21}$$

Under these conditions, we can get the ACF-dependent expression

$$\Delta N = \frac{1}{\hbar^2}\sum_{\substack{a\in g.s.\\ b\in e.s}} P(a)\int_0^\infty d\tau\left(C^*(\tau)\langle b|[\hat{\mathcal{U}}_0(\tau)\hat{\mathbf{\Theta}}_a]|\theta_b\rangle + c.c.\right). \tag{22}$$

IV. THE RELATION BETWEEN POPULATION TRANSFER AND ENERGY ABSORPTION

Spectroscopy is based on using a weak probe to unravel pure molecular properties. Absorption spectroscopy measures the energy absorption from the field. Here, we relate this quantity to the population transfer measured by delayed fluorescence. We show that in a weak field under the L-GKS conditions also the energy absorption is independent of the phase of the field. In the adiabatic limit, i.e., for a slowly varying envelope function, this relation can be deduced directly from the expression for the population transfer. For the non-adiabatic cases, we prove an additional theorem.

A. Adiabatic limit

The power absorption is derived from the Heisenberg equation of motion,

$$\mathcal{P} = \frac{d\langle E\rangle}{dt} = \left\langle\frac{d\hat{\mathbf{H}}}{dt}\right\rangle = \left\langle\frac{d\hat{\mathbf{V}}(t)}{dt}\right\rangle = \left\langle\begin{pmatrix} 0 & \hat{\mu}\frac{\partial\epsilon}{\partial t}\\ \hat{\mu}\frac{\partial\epsilon^*}{\partial t} & 0\end{pmatrix}\right\rangle. \tag{23}$$

The expectation value of an operator $\hat{\mathbf{A}}$ is defined as $\langle\hat{\mathbf{A}}\rangle = \mathrm{tr}(\hat{\mathbf{A}}\hat{\rho})$. We separate the density matrix to the populations on the upper and lower electronic surfaces $\hat{\rho}_e$, $\hat{\rho}_g$, and for coherences $\hat{\rho}_c$, $\hat{\rho}_c^\dagger$,

$$\hat{\rho} = \begin{pmatrix}\hat{\rho}_e & \hat{\rho}_c\\ \hat{\rho}_c^\dagger & \hat{\rho}_g\end{pmatrix}, \tag{24}$$

leading to the power absorption

$$\mathcal{P} = \mathrm{tr}\left(\frac{\partial\epsilon}{\partial t}\hat{\mu}\hat{\rho}_c + \frac{\partial\epsilon^*}{\partial t}\hat{\mu}\hat{\rho}_c^\dagger\right) = 2\mathcal{R}e\left(\frac{\partial\epsilon}{\partial t}\mathrm{tr}(\hat{\mu}\hat{\rho}_c)\right). \tag{25}$$

Total energy absorption is obtained by integrating the power,

$$\Delta E(t_f) = 2\mathcal{R}e \int_{t_i}^{t_f} \frac{\partial \epsilon}{\partial t} \mathrm{tr}(\hat{\mu}\hat{\rho}_c(t))\, dt. \tag{26}$$

Similarly, the total population transfer is given by

$$\Delta N(t_f) = -\frac{2}{\hbar}\mathcal{I}m \int_{t_i}^{t_f} \epsilon(t) \mathrm{tr}(\hat{\mu}\hat{\rho}_c(t))\, dt. \tag{27}$$

The changes in energy and population are related. If we factorize the field to an envelope $\Lambda(t)$ and fast oscillations with the carrier frequency ω_L,

$$\epsilon(t) = \Lambda(t) e^{i\omega_L t}, \tag{28}$$

then we can write

$$\Delta E(t_f) = 2\mathcal{R}e \int_{t_i}^{t_f} \left(i\omega_L \epsilon(t) + \frac{\partial \Lambda}{\partial t} e^{i\omega_L t} \right) \mathrm{tr}(\hat{\mu}\hat{\rho}_c(t))\, dt. \tag{29}$$

In the adiabatic limit, i.e., for a slowly varying envelope function, i.e.,

$$\frac{\partial \Lambda / \partial t}{\Lambda} \ll \omega_L, \tag{30}$$

the second term is negligible. Then we can write[13,14]

$$\Delta E \approx \hbar\omega \Delta N. \tag{31}$$

In such cases we use the expressions derived above for the population transfer (Eqs. (16), (17), and (22)) to obtain the phase independence of the energy spectrum.

B. Non-adiabatic treatment

In the nonadiabatic case, we have to evaluate the second term in Eq. (29) using the second order perturbation theory.

The coherence $\hat{\rho}_c(t)$ is evaluated from the first order expression for the density matrix

$$\hat{\rho}_I^{(1)}(t) = -\frac{i}{\hbar} \int_{t_i}^{t} dt_1 e^{i\hat{\hat{\mathcal{L}}}_0 t_1} \hat{\hat{\mathcal{V}}}(t_1) e^{-i\hat{\hat{\mathcal{L}}}_0 (t_1 - t_i)} \hat{\rho}_0. \tag{32}$$

Next, we substitute $\hat{\rho}_I^{(1)}(t)$ in the expression for energy absorption, Eq. (26), integrate and manipulate as described in Appendix B. The result is that the energy absorption has a functional dependence on the cross-correlation function of the field with its derivative

$$\int_{-\infty}^{\infty} dt \epsilon(t) \left. \frac{\partial \epsilon^*}{\partial t} \right|_{\tau + t}. \tag{33}$$

However, this expression is also phase-independent. This can be shown using the functional derivative with respect to the phase of the field, cf. Appendix A.

V. DISCUSSION

We demonstrated that, in general, the weak-field spectroscopy is functionally dependent only on the autocorrelation function of the field. As a result, phase sensitivity is absent. This remains true even when the dynamics is generated by the Markovian L-GKS equation. Moreover, this is also true for non-Markovian dynamics, generated by the time independent Hierarchical Equations of Motion approach (HEOM).[15–17] In such dynamics the propagator has the form of Eq. (19).

We note here that the above analysis cannot include the influence of the field on the environment, since the L-GKS open system dynamics does not include such a mechanism.

When a weak-field phase-only control is encountered, we have to examine how this effect scales with the field coupling strength. According to the above analysis, while the total population transfer is the leading order in the perturbation, i.e., second order in the field coupling strength, the phase effect on the population transfer should be the next order, i.e., fourth order in the field coupling strength.

In Sec. VI, we examine such an example and show that the order of the effects are as expected.

VI. ILLUSTRATIVE EXAMPLE: POPULATION TRANSFER IN A FOUR-LEVELS SYSTEM

A numerical evaluation of L-GKS open system dynamics which obeys the four conditions given in Sec. III C was performed. The aim was to examine a case of WFPO control, and check the scaling of the population transfer and phase-dependent phenomena with the field coupling strength.

A. Simulation details

The system under study is driven by a chirped Gaussian field, and coupled to an environment with a L-GKS dissipation. The system is designed such that the final population transfer is affected by the phase of the external field, namely, the chirp. The coupling to the environment induces relaxation which amplifies the chirp effect. The details of the simulations follow. Figure 1 shows a schematic diagram of the simulated system.

The system has four energy levels: Two ground energy levels and two excited ones. The ground levels serve as the ground electronic surface. The two excited levels serve as the

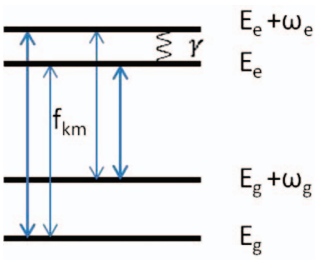

FIG. 1. A schematic diagram of the simulated system: E_e and E_g are the energies of the surfaces. ω_e and ω_g are the vibrational frequencies inside the surfaces. f_{km} are the Franck-Condon coefficients. γ is the relaxation coefficient.

excited electronic surface. These two levels are coupled to each other by a Lindblad-type dissipator. Only the external field couples between the surfaces, and the field-free Hamiltonian does not couple between them. The field-free Hamiltonian is

$$\hat{\mathbf{H}}_0 = \begin{pmatrix} E_e + \omega_e & 0 & 0 & 0 \\ 0 & E_e & 0 & 0 \\ 0 & 0 & E_g + \omega_g & 0 \\ 0 & 0 & 0 & E_g \end{pmatrix}, \tag{34}$$

where E_e and E_g are the energies of the surfaces, while ω_e and ω_g are the vibrational frequencies inside the surfaces. We used the rotating frame for the actual simulations. Therefore, the relevant parameter is the detuning, defined by $\delta \equiv E_e - E_g - \omega_L$, where ω_L is the carrier frequency (see below).

The ground and excited surfaces are coupled with the field operator

$$\mu\hat{\mathbf{V}}(t) = \mu \begin{pmatrix} 0 & 0 & f_{24}\varepsilon(t) & f_{14}\varepsilon(t) \\ 0 & 0 & f_{23}\varepsilon(t) & f_{13}\varepsilon(t) \\ f_{24}^*\varepsilon^*(t) & f_{23}^*\varepsilon^*(t) & 0 & 0 \\ f_{14}^*\varepsilon^*(t) & f_{13}^*\varepsilon^*(t) & 0 & 0 \end{pmatrix}, \tag{35}$$

where μ is the field coupling strength, f_{km} are the Franck-Condon coefficients, and $\varepsilon(t)$ is the external field applied to the system. We set the Franck-Condon coefficients to mimic the case of two displaced harmonic oscillators: f_{14} and f_{23} are large, while f_{24} and f_{13} are small.

The goal of these simulations is to examine the dependence of final population transfer on phase properties of the field. The field we use is a chirped Gaussian pulse. We define the chirp at the frequency domain in such a way that changing the chirp changes the phase properties of the field but not the amplitude, as defined in Sec. I, Eq. (1),

$$\tilde{\epsilon}(\omega) = \frac{1}{\pi^{\frac{1}{4}}\sqrt{\Delta\omega}} \exp\left(-\frac{1}{2}\left(\frac{\omega - \omega_L}{\Delta\omega}\right)^2 + i\chi(\omega - \omega_L)^2\right), \tag{36}$$

with $\Delta\omega$ as the bandwidth, χ as the chirp, and ω_L is the carrier frequency.

Introducing $\sqrt{\Delta\omega}$ in the pre-exponential factor keeps the total energy of the pulse unchanged while changing the bandwidth, such that

$$\int_{-\infty}^{\infty} |\tilde{\epsilon}(\omega)|^2 \, d\omega = 1. \tag{37}$$

The inverse Fourier transform (FT) of the chirped pulse is

$$\epsilon(t) = \frac{1}{\pi^{\frac{1}{4}}\sqrt{\tau_0 - \frac{2i\chi}{\tau_0}}} \exp\left(-\left(\frac{1}{2} + i\frac{\chi}{\tau_0^2}\right)\left(\frac{t}{\tau_{ch}}\right)^2\right) e^{-i\omega_L t}, \tag{38}$$

with $\tau_0 = \frac{1}{\Delta\omega}$ as the duration of the unchirped pulse, and $\tau_{ch} = \omega_{ch}\tau_0$ as the extended pulse duration, caused by the chirp: $\omega_{ch} = \sqrt{1 + 4\frac{\chi^2}{\tau_0^4}}$.

The environment coupling induces a relaxation from the fourth energy level to the third one. The relaxation is described by a L-GKS dissipator, which is induced by an annihilation operator $\hat{\mathbf{s}}_{34} = |3\rangle\langle 4|$. This operator has all-zero entries, except one entry, which transfers population from the fourth level to the third.

This operator induces coupling inside the excited surface, but not between the surfaces. The dissipator is

$$\hat{\hat{\mathcal{L}}}_D[\hat{\rho}] = \hat{\mathbf{s}}_{34}\hat{\rho}\hat{\mathbf{s}}_{34}^\dagger - \frac{1}{2}(\hat{\mathbf{s}}_{34}^\dagger\hat{\mathbf{s}}_{34}\hat{\rho} + \hat{\rho}\hat{\mathbf{s}}_{34}^\dagger\hat{\mathbf{s}}_{34}). \tag{39}$$

1. The dynamics: Equation of motion, initial state, and control target

The equation of motion is

$$i\hbar\frac{\partial\hat{\rho}}{\partial t} = \hat{\hat{\mathcal{L}}}\hat{\rho} = [\hat{\mathbf{H}}_0 + \mu\hat{\mathbf{V}}(t), \hat{\rho}] + i\lambda\hat{\hat{\mathcal{L}}}_D[\hat{\rho}]. \tag{40}$$

Initially, the system is at ground state, i.e., the entire population is on the first level.

Two control targets can be defined and examined:

- The final population on the excited surface, i.e., the sum of populations on the third and fourth levels. In weak fields, we expect it to be the leading order in the perturbation strength μ. The chirp effect is expected to be in the next order in the perturbation.
- The final population on the second level. The population transfer to this level is in essence a second order process. The structure of the system makes this population sensitive to chirp sign, promoting cases when higher frequencies precede lower ones (i.e., negative chirps). In addition, the magnitudes of the Franck-Condon coefficients (large f_{14} f_{23}, small f_{24} f_{13}) create a scenario where the relaxation in the excited surface enhances the negative-chirp-induced population transfer.

The phase-only control effect is examined by performing pairs of simulations in which the only varied parameter is the chirp: positive chirp in one simulation and negative in the other. The difference in the final population on the targets between two simulations in such pairs is defined as the chirp effect.

The values of the parameters used in the simulations are summarized in Table I. The detuning was selected to maximize the final population transfer.

TABLE I. Simulation parameters.

Parameter	Value	Unit
ω_g	0.5	$(\text{time})^{-1}$
ω_e	0.1	$(\text{time})^{-1}$
δ	0.2	$(\text{time})^{-1}$
μ	(several)	$(\text{time})^{-1}$
λ	(several)	$(\text{time})^{-1}$
f_{14}, f_{23}	0.9	(unitless)
f_{24}, f_{13}	0.1	(unitless)
$\Delta\omega$	1	$(\text{time})^{-1}$
χ	± 80	$(\text{time})^2$

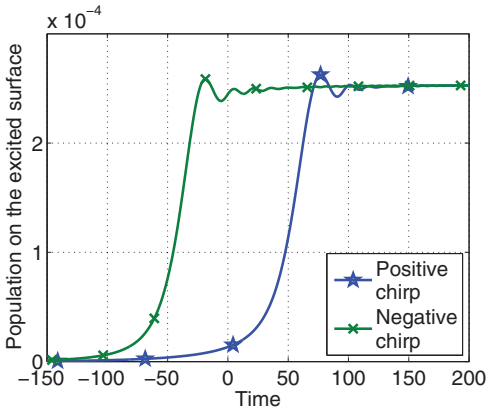

FIG. 2. Population on the excited surface during simulations in which the system is driven by positively (blue line with stars) and negatively (green line with x-marks) chirped fields. The population transfer to this surface is a first order process, and therefore the difference in the final population, which is governed by the next order, cannot be seen on this scale.

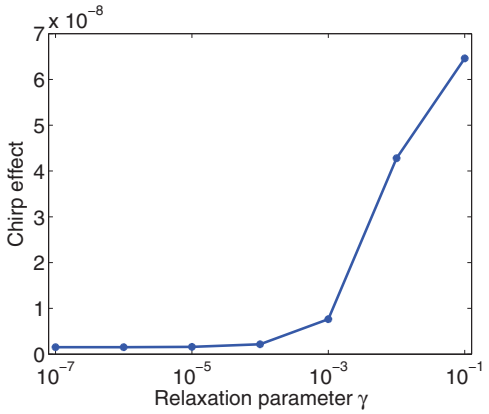

FIG. 4. Chirp effect versus the relaxation coefficient γ. The chirp effect is defined as the difference of the final population transfer between the simulation with positive chirp and the simulation with the negative chirp. X-axis is log-scale. The chirp effect is enhanced by the relaxation process.

B. Simulations results

Simulations were performed with the model described in Eqs. (34), (35), (38), and (40). The phase-only control effect was examined by comparing similar simulations where the only difference is the chirp sign: positive or negative. The difference of the final population transfer between the two cases is defined as the chirp effect. The results are presented below.

1. Simulation dynamics

Figure 2 shows an example of the population of the excited surface during the simulations of the positive and negative chirp. The population transfer to this surface is a first order process, and therefore the difference in the final population, which is governed by the next order, cannot be seen on this scale. The population of the second level is presented in Figure 3. This population is a second order process in essence (note the different scale), and therefore is controlled by the chirp: Positive chirp yields a very small population transfer to the second level, while negative chirp yields population transfer which is by two orders of magnitudes larger.

2. Relaxation-induced chirp effect

Figure 4 presents the chirp effect as a function of the relaxation coupling coefficient γ. The chirp effect is enhanced by the relaxation process. In the following, we will show that despite that enhancement, the chirp effect still scales as the fourth order of the field strength.

3. The scaling of the population transfer and the chirp effect with the field strength

We examined the scaling of the population transfer and the chirp effects with the strength of the external field.

Figure 5 shows the results for the target on the excited surface. As expected, we found that the slope of the

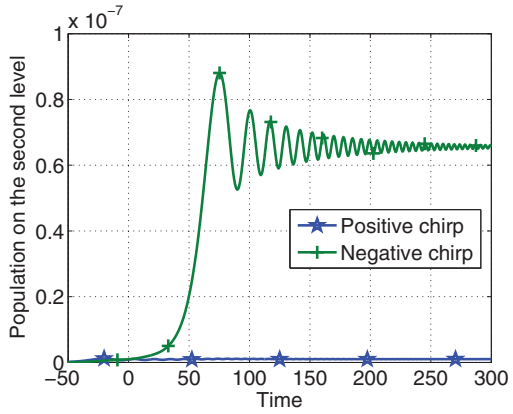

FIG. 3. Population on the second level, during the same simulations as in Figure 2. Note that the scale in this figure is different. This population is a second order process in essence, and therefore is controlled by the chirp: Positive chirp yields a very small population transfer to the second level, while negative chirp yields population transfer which is two order of magnitudes larger (although still small).

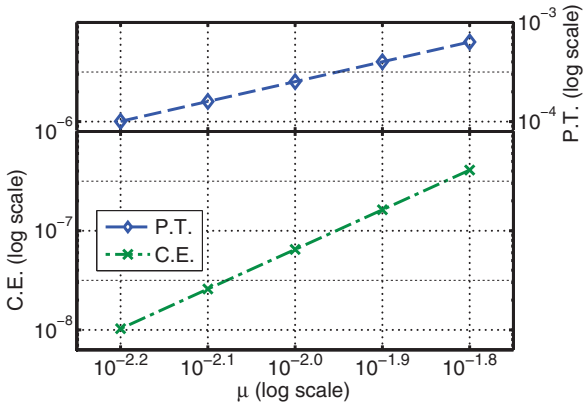

FIG. 5. The final population transfer (P.T., upper panel) to the upper surface and the chirp effect (C.E., lower panel) of this P.T. vs. the field strength μ, on log-log scale. Note that there is a gap in the Y-axis (emphasized by the labels on the right side in the upper panel), although both lines are on the same scale. The slope of the P.T. is 2, i.e., the P.T. scales as μ^2. The slope of the C.E. is 4, i.e., the C.E. scales as μ^4.

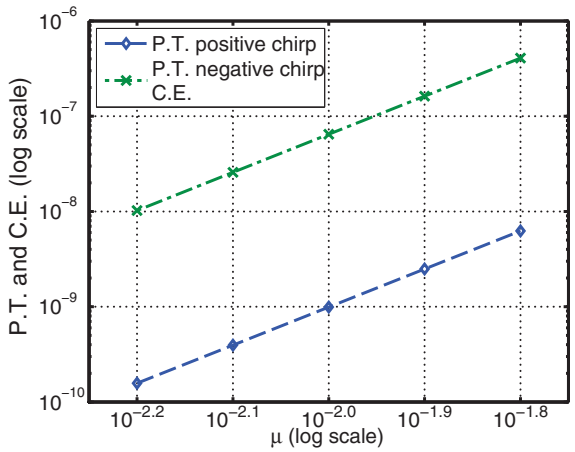

FIG. 6. The final population transfer (P.T.) to the second level: The lower line shows the P.T. for positive chirps. The upper line shows the P.T. for negative chirps, which almost equals the chirp effect (C.E.). Both lines are plotted vs. the field strength μ, on log-log scale. The slope of the both lines is 4, i.e., they scale as μ^4.

population transfer is 2, i.e., the population transfer scales as μ^2, while the slope of the chirp effect is 4, i.e., the chirp effect scales as μ^4.

Figure 6 shows the results for the target on the second level. Essentially, the population transfer to this level is of the next order, which is in the same order of the chirp effect. Therefore, we expect to find the same scaling with field strength for both phenomena. Actually, the population transfer to this level in the case of positive chirps is very small, and almost vanishes, and therefore the chirp effect and the population transfer for negative chirp are almost the same. As expected, we found that the slope of population transfer for both chirp signs, as well as the slope of the chirp effect is four, i.e., they all scale with field strength as μ^4.

VII. CONCLUSIONS

The issue of the weak field phase only control is of fundamental importance. Molecular spectroscopy in condensed phase assumes that the energy absorbed for each frequency component in the linear regime depends only on the molecular properties. At normal temperatures the molecule is in its ground electronic surface. By relating the energy absorbed to the population transfer we find that the validity of molecular spectroscopy in condensed phase relies on the impossibility of WFPO. Brumer and co-workers have studied extensively this phenomenon.[3,18,19] The present study is in line with these findings. For a molecular system modelled by the L-GKS Markovian dynamics WFPO is impossible for observables which are invariant to the field free dynamics.

The method of proof, based on functional derivative (cf. Appendix A), can be extended to other scenarios.

The numerical model is also consistent with the work of Konar, Lozovoy, and Dantus[20] showing fourth order scaling of the chirp effect with the driving field strength. Contrary to their finding that the positive chirp is sensitive to the solvent,[21] our numerical model finds strong sensitivity to negative chirp.

Shapiro and Han[22] argue that apparent linear response experimental phenomena are not necessarily weak-field effects. In the present study, the analysis is based on order by order perturbation theory and addresses this issue. Experimental or numerical tests have to be extremely careful in checking the scaling order of the effect.

Readdressing the theme of the study: Is there a weak field phase only control in open systems? We obtained a partial answer. Under Markovian L-GKS dynamics WFPO is impossible. This still leaves open the possibility of WFPO in non-Markovian scenarios. The main assumption that should be challenged is the tensor product separability of the system and bath in L-GKS dynamics. Preliminary numerical evidence from non separable system-bath models may point to the possibility of WFPO for population transfer with enhancement for positive chirp. More work is required to establish this possibility.

ACKNOWLEDGMENTS

This work was supported by the Israel Science Foundation (ISF). We want to thank Brian Burrows, Gil Katz, Amikam Levy, Ido Schaefer, Dwayne Miller, and Valentyn Prokhorenko for useful discussions.

APPENDIX A: THE PHASE INDEPENDENCE OF THE AUTOCORRELATION FUNCTION

The ACF of the field $\epsilon(t)$ is the inverse FT of the spectral density of the field, $J(\omega) = |\tilde{\epsilon}(\omega)|^2$. In this paper, the population transfer to second order is proportional to the Laplace transform of the ACF (cf. Eq. (16)). Therefore, a careful examination of the phase properties in this case is required. First, we derive the phase independence of the ACF. Similarly, the phase independence of the cross-correlation function of the field with its derivative is obtained. We use the functional derivative of these two correlation functions to prove the phase independence of the absorption spectrum.

The autocorrelation function is defined as

$$C(t) = \int_{-\infty}^{\infty} d\tau \epsilon(\tau + t)\epsilon^*(\tau). \tag{A1}$$

Similarly, the cross-correlation function of the field with its derivative is defined as

$$D(t) = \int_{-\infty}^{\infty} d\tau \left.\frac{\partial \epsilon}{\partial t}\right|_{\tau+t} \epsilon^*(\tau). \tag{A2}$$

We will use the spectral representation of the field

$$\epsilon(t) = \int_{-\infty}^{\infty} d\omega \tilde{\epsilon}(\omega) e^{-i\omega t} = \int_{-\infty}^{\infty} d\omega \tilde{A}(\omega) e^{i\tilde{\varphi}(\omega)} e^{-i\omega t}, \tag{A3}$$

where the real functions $\tilde{A}(\omega)$ and $\tilde{\varphi}(\omega)$ are the amplitude and phase, respectively. The spectral representation of the field derivative equals the spectral representation of the field,

multiplied by $(-i\omega)$,

$$\frac{\partial \epsilon(t)}{\partial t} = \frac{\partial}{\partial t}\int_{-\infty}^{\infty} d\omega \tilde{\epsilon}(\omega) e^{-i\omega t} = \int_{-\infty}^{\infty} d\omega(-i\omega)\tilde{\epsilon}(\omega)e^{-i\omega t}. \tag{A4}$$

The functional derivatives of these correlation functions with respect to the phase are

$$\frac{\delta C(t)}{\delta \tilde{\varphi}(\omega)} = \int_{-\infty}^{\infty} d\tau \left\{ \frac{\delta \epsilon(\tau + t)}{\delta \tilde{\varphi}(\omega)} \epsilon^*(\tau) + \epsilon(\tau + t) \frac{\delta \epsilon^*(\tau)}{\delta \tilde{\varphi}(\omega)} \right\}, \tag{A5}$$

$$\frac{\delta D(t)}{\delta \tilde{\varphi}(\omega)} = \int_{-\infty}^{\infty} d\tau \left\{ \frac{\delta \left(\frac{\partial \epsilon}{\partial \tau}\Big|_{\tau+t} \right)}{\delta \tilde{\varphi}(\omega)} \epsilon^*(\tau) + \frac{\partial \epsilon}{\partial \tau}\Big|_{\tau+t} \frac{\delta \epsilon^*(\tau)}{\delta \tilde{\varphi}(\omega)} \right\}. \tag{A6}$$

We need the following functional derivatives with respect to the phase

$$\begin{aligned}
\frac{\delta \epsilon(t)}{\delta \tilde{\varphi}(\omega)} &= i\tilde{A}(\omega) e^{i\tilde{\varphi}(\omega)} e^{-i\omega t} = i\tilde{\epsilon}(\omega) e^{-i\omega t}, \\
\frac{\delta \epsilon^*(t)}{\delta \tilde{\varphi}(\omega)} &= -i\tilde{A}(\omega) e^{-i\tilde{\varphi}(\omega)} e^{i\omega t} = -i\tilde{\epsilon}^*(\omega) e^{i\omega t}, \\
\frac{\delta \left(\frac{\partial \epsilon(t)}{\partial t} \right)}{\delta \tilde{\varphi}(\omega)} &= i(-i\omega)\tilde{A}(\omega) e^{i\tilde{\varphi}(\omega)} e^{-i\omega t} = i(-i\omega)\tilde{\epsilon}(\omega) e^{-i\omega t}.
\end{aligned} \tag{A7}$$

Substituting in the functional derivative of the correlation functions, we get (changing integration variable in the second line $\tilde{\tau} = \tau + t$)

$$\begin{aligned}
\frac{\delta C(t)}{\delta \tilde{\varphi}(\omega)} &= \int_{-\infty}^{\infty} d\tau [i\tilde{\epsilon}(\omega) e^{-i\omega(\tau+t)} \epsilon^*(\tau) - i\epsilon(\tau + t)\tilde{\epsilon}^*(\omega) e^{i\omega\tau}] \\
&= i\tilde{\epsilon}(\omega) e^{-i\omega t} \left[\int_{-\infty}^{\infty} d\tau e^{i\omega\tau} \epsilon(\tau) \right]^* \\
&\quad - i \left[\int_{-\infty}^{\infty} d\tilde{\tau} \epsilon(\tilde{\tau}) e^{i\omega(\tilde{\tau} - t)} \right] \tilde{\epsilon}^*(\omega) \\
&= i\tilde{\epsilon}(\omega) e^{-i\omega t} \tilde{\epsilon}^*(\omega) - i\tilde{\epsilon}(\omega) e^{-i\omega t} \tilde{\epsilon}^*(\omega) \\
&= 0,
\end{aligned} \tag{A8}$$

and, similarly,

$$\begin{aligned}
\frac{\delta D(t)}{\delta \tilde{\varphi}(\omega)} &= \int_{-\infty}^{\infty} d\tau \left[i(-i\omega)\tilde{\epsilon}(\omega) e^{-i\omega(\tau+t)} \epsilon^*(\tau) \right. \\
&\quad \left. - i \frac{\partial \epsilon}{\partial t}\Big|_{\tau+t} \tilde{\epsilon}^*(\omega) e^{i\omega\tau} \right] \\
&= i(-i\omega)\tilde{\epsilon}(\omega) e^{-i\omega t} \left[\int_{-\infty}^{\infty} d\tau e^{i\omega\tau} \epsilon(\tau) \right]^* \\
&\quad - i \left[\int_{-\infty}^{\infty} d\tilde{\tau} \frac{\partial \epsilon}{\partial t}\Big|_{\tilde{\tau}} e^{i\omega(\tilde{\tau} - t)} \right] \tilde{\epsilon}^*(\omega) \\
&= i(-i\omega)\tilde{\epsilon}(\omega) e^{-i\omega t} \tilde{\epsilon}^*(\omega) - i(-i\omega)\tilde{\epsilon}(\omega) e^{-i\omega t} \tilde{\epsilon}^*(\omega) \\
&= 0.
\end{aligned} \tag{A9}$$

APPENDIX B: DETAILED CALCULATION OF THE POPULATION TRANSFER

We show here the details of the calculations.

1. Unitary dynamics generated by the Hamiltonian

From Eq. (7) we get (the operator $\hat{\mathbf{V}}$ transfers population between the surfaces)

$$\hat{\hat{\mathcal{V}}}(t_1)|a\rangle\langle a| = \sum_{\substack{a\in g.s. \\ b\in e.s}} P(a)(\epsilon(t_1)\mu_{ba}|b\rangle\langle a| - \epsilon^*(t_1)\mu_{ab}|a\rangle\langle b|). \tag{B1}$$

Next, we operate with the propagator $e^{-\frac{i}{\hbar}\hat{\hat{\mathcal{L}}}_0(t_2-t_1)}$. When the dynamics is unitary, the Lindbladian includes only the commutator with the Hamiltonian, and the propagation of an element in the density matrix $|c\rangle\langle d|$ is simply a multiplication by $e^{-i\omega_{cd}t}$, where $\omega_{cd} \equiv \omega_c - \omega_d$, so we get

$$\begin{aligned}
&\sum_{\substack{a\in g.s. \\ b\in e.s}} P(a)\big(\epsilon(t_1)\mu_{ba}|b\rangle\langle a|e^{-i\omega_{ba}(t_2-t_1)} \\
&\quad - \epsilon^*(t_1)\mu_{ab}|a\rangle\langle b|e^{-i\omega_{ab}(t_2-t_1)}\big).
\end{aligned} \tag{B2}$$

Now, we operate with $\hat{\hat{\mathcal{V}}}(t_2)$, to get (using Eq. (7))

$$\begin{aligned}
&\sum_{\substack{a\in g.s. \\ b\in e.s \\ k}} P(a)\big\{\epsilon(t_1)\epsilon^*(t_2)\mu_{ba}(\mu_{kb}|k\rangle\langle a| \\
&\quad - \mu_{ak}|b\rangle\langle k|)e^{-i\omega_{ba}(t_2-t_1)} + h.c.\big\},
\end{aligned} \tag{B3}$$

where $h.c.$ stands for hermitian conjugate.

Now we project on the excited surface (with $\hat{\mathbf{P}}_e$), and perform the trace. For a general element in the density matrix $|c\rangle\langle d|$, we do so by taking the sum of diagonal matrix elements that belong to the excited surface: $\sum_{m\in e.s.} \langle m|c\rangle\langle d|m\rangle$, so we get

$$\begin{aligned}
&- \sum_{\substack{a\in g.s. \\ b\in e.s \\ k \\ m\in e.s.}} P(a)\big\{\epsilon(t_1)\epsilon^*(t_2)\mu_{ba}\mu_{ak}\langle m|b\rangle\langle k|m\rangle \\
&\times e^{-i\omega_{ba}(t_2-t_1)} + c.c.\big\}.
\end{aligned} \tag{B4}$$

$\langle m|b\rangle$ and $\langle k|m\rangle$ are δ_{mb} and δ_{km}, respectively. When we sum over k and m we get

$$-\sum_{\substack{a\in g.s.\\ b\in e.s}} P(a)\{\epsilon(t_1)\epsilon^*(t_2)|\mu_{ab}|^2 e^{-i\omega_{ba}(t_2-t_1)}+c.c.\}. \quad \text{(B5)}$$

Next, we integrate over t_1 and t_2. Since the pulse has a finite duration, we can extend the integration limits to $(-\infty,\infty)$

$$\sum_{\substack{a\in g.s.\\ b\in e.s}} P(a)\frac{|\mu_{ab}|^2}{\hbar^2}\int_{-\infty}^{\infty} dt_2 \int_{-\infty}^{t_2} dt_1 \{\epsilon(t_1)\epsilon^*(t_2)e^{-i\omega_{ba}(t_2-t_1)}+c.c.\}. \quad \text{(B6)}$$

We change variables in the integral, from t_2 to $\tau = t_2 - t_1$, and we get the integral

$$\int_0^{\infty} d\tau \left(\int_{-\infty}^{\infty} dt_1 \epsilon(t_1)\epsilon^*(\tau+t_1)\right) e^{-i\omega_{ba}\tau} = \int_0^{\infty} d\tau C^*(\tau)e^{-i\omega_{ba}\tau}, \quad \text{(B7)}$$

where $C^*(\tau)$ is the complex conjugate of the ACF of the field $\epsilon(t)$ (defined in Appendix A). Finally, we have

$$\Delta N = \sum_{\substack{a\in g.s.\\ b\in e.s}} P(a)\frac{|\mu_{ab}|^2}{\hbar^2}\left\{\int_0^{\infty} d\tau C^*(\tau)e^{-i\omega_{ba}\tau}+c.c.\right\}. \quad \text{(B8)}$$

We see that the population transfer does not depend directly on the field, only through the field's ACF. This result is not new.[3] It is presented here in order to demonstrate the perturbative calculation in Liouville space, and to emphasise the dependence on the ACF.

2. General Lindbladian-generated dynamics

We show here that the population transfer depends on the field only through the ACF also in QDS description of non unitary dynamics.

Consider a Lindbladian that can induce dephasing and relaxation inside the electronic surfaces, but not between them. We do not treat here electronic dephasing or electronic relaxation. Population transfer is done only by $\hat{\hat{\mathcal{V}}}$ (the commutator of $\hat{\mathbf{V}}$).

Here, we use a more formal notation: we do not write explicitly the matrix elements of the operator $\hat{\mu}$. Instead, for a state $|a\rangle$ (or $\langle a|$) in the ground surface, we write $|\theta_a\rangle \equiv \hat{\mu}|a\rangle$ (or $\langle\theta_a| \equiv \langle a|\hat{\mu}$, respectively), and it should be understood as a state in the excited electronic surface. Also, we will use the notation $\hat{\mathbf{\Theta}}_a \equiv |\theta_a\rangle\langle a|$ for the relevant density matrix element. We also do not write explicitly the resulting states of the propagation by $\hat{\hat{\mathcal{L}}}_0$, and write instead expressions like $e^{-i\hat{\hat{\mathcal{L}}}_0 t}\hat{\mathbf{\Theta}}_a$.

Starting with Eq. (15), and the initial state of Eq. (9), we first operate with $\hat{\hat{\mathcal{V}}}(t_1)$ to get

$$\sum_{a\in g.s.} P(a)(\epsilon(t_1)|\theta_a\rangle\langle a| - \epsilon^*(t_1)|a\rangle\langle\theta_a|). \quad \text{(B9)}$$

Since $|a\rangle$ and $\langle a|$ are in the ground surface, and since $|\theta_a\rangle$ and $\langle\theta_a|$ are in the excited surface, $|\theta_a\rangle\langle a| = \hat{\mathbf{\Theta}}_a$ and $|a\rangle\langle\theta_a| = \hat{\mathbf{\Theta}}_a{}^{\dagger}$ are off-diagonal blocks in the density matrix.

Next, we operate with the propagator $e^{-\frac{i}{\hbar}\hat{\hat{\mathcal{L}}}_0(t_2-t_1)}$ to get

$$\sum_{a\in g.s.} P(a)\left(\epsilon(t_1)e^{-\frac{i}{\hbar}\hat{\hat{\mathcal{L}}}_0(t_2-t_1)}\hat{\mathbf{\Theta}}_a - \epsilon^*(t_1)e^{-\frac{i}{\hbar}\hat{\hat{\mathcal{L}}}_0(t_2-t_1)}\hat{\mathbf{\Theta}}_a{}^{\dagger}\right). \quad \text{(B10)}$$

Again, the two terms here are off diagonal blocks.

When we operate with $\hat{\hat{\mathcal{V}}}(t_2)$ we get four terms. Two of them belong to the ground surface, and therefore will be omitted in the projection on the excited surface. The other terms are

$$\sum_{a\in g.s.} P(a)\left(\epsilon(t_1)\epsilon^*(t_2)\left[e^{-\frac{i}{\hbar}\hat{\hat{\mathcal{L}}}_0(t_2-t_1)}\hat{\mathbf{\Theta}}_a\right]\hat{\mu}+c.c.\right) \quad \text{(B11)}$$

Finally, like the previous calculations, we perform the trace, extend the integration limits, change one integration variable and integrate over the other variable, to get the autocorrelation of the field:

$$\Delta N = \frac{1}{\hbar^2}\sum_{\substack{a\in g.s.\\ b\in e.s}} P(a)\int_0^{\infty} d\tau\left(C^*(\tau)\langle b|\left[e^{-\frac{i}{\hbar}\hat{\hat{\mathcal{L}}}_0\tau}\hat{\mathbf{\Theta}}_a\right]|\theta_b\rangle+c.c.\right). \quad \text{(B12)}$$

We have to obtain more details on the operation of $\hat{\mu}$ and $\hat{\hat{\mathcal{L}}}_0$ in order to evaluate this expression further, but we see that also here the dependence on the field is only through its ACF.

[1] S. A. Rice, "New ideas for guiding the evolution of a quantum system," Science **258**(5081), 412–413 (1992).
[2] P. Brumer and M. Shapiro, "One photon mode selective control of reactions by rapid or shaped laser pulses: An emperor without clothes?," Chem. Phys. **139**(1), 221–228 (1989).
[3] M. Spanner, C. A. Arango, and P. Brumer, "Communication: Conditions for one-photon coherent phase control in isolated and open quantum systems," J. Chem. Phys. **133**(15), 151101 (2010).
[4] V. I. Prokhorenko, A. M. Nagy, and R. J. Dwayne Miller, "Coherent control of the population transfer in complex solvated molecules at weak excitation. An experimental study," J. Chem. Phys. **122**(18), 184502 (2005).
[5] V. I. Prokhorenko, A. M. Nagy, S. A. Waschuk, L. S. Brown, R. R. Birge, and R. J. Dwayne Miller, "Coherent control of retinal isomerization in bacteriorhodopsin," Science **313**(5791), 1257–1261 (2006).
[6] M. Joffre, "Comment on "Coherent control of retinal isomerization in bacteriorhodopsin"," Science **317**(5837), 453 (2007).
[7] V. I. Prokhorenko, A. M. Nagy, S. A. Waschuk, L. S. Brown, R. R. Birge, and R. J. Dwayne Miller, "Response to comment on "Coherent control of retinal isomerization in bacteriorhodopsin"," Science **317**(5837), 453 (2007).
[8] P. van der Walle, M. T. W. Milder, L. Kuipers, and J. L. Herek, "Quantum control experiment reveals solvation-induced decoherence," Proc. Natl. Acad. Sci. U.S.A. **106**(19), 7714–7717 (2009).
[9] G. Katz, M. A. Ratner, and R. Kosloff, "Control by decoherence: weak field control of an excited state objective," New J. Phys. **12**(1), 015003 (2010).
[10] K. Kraus, "General state changes in quantum theory," Ann. Phys. **64**(2), 311–335 (1971).
[11] G. Lindblad, "On the generators of quantum dynamical semigroups," Commun. Math. Phys. **48**(2), 119–130 (1976).
[12] V. Gorini, A. Kossakowski, and E. C. G. Sudarshan, "Completely positive dynamical semigroups of n-level systems," J. Math. Phys. **17**(5), 821–825 (1976).
[13] R. Kosloff, A. Dell Hammerich, and D. Tannor, "Excitation without demolition: Radiative excitation of ground-surface vibration by impulsive stimulated Raman scattering with damage control," Phys. Rev. Lett. **69**(15), 2172 (1992).

[14]G. Ashkenazi, U. Banin, A. Bartana, R. Kosloff, and S. Ruhman, "Quantum description of the impulsive photodissociation dynamics of i-3 in solution," Adv. Chem. Phys. **100**, 229–315 (1997).
[15]J. Jin, X. Zheng, and Y. Yan, "Exact dynamics of dissipative electronic systems and quantum transport: Hierarchical equations of motion approach," J. Chem. Phys. **128**(23), 234703 (2008).
[16]A. Ishizaki and Y. Tanimura, "Quantum dynamics of system strongly coupled to low-temperature colored noise bath: Reduced hierarchy equations approach," J. Phys. Soc. Jpn. **74**(12), 3131–3134 (2005).
[17]C. Meier and D. J. Tannor, "Non-Markovian evolution of the density operator in the presence of strong laser fields," J. Chem. Phys. **111**(8), 3365 (1999).
[18]L. A. Pachon, L. Yu, and P. Brumer, "Coherent one-photon phase control in closed and open quantum systems: A general master equation approach," Faraday Discuss. **163**, 485–495 (2013).
[19]L. A. Pachón and P. Brumer, "Mechanisms in environmentally assisted one-photon phase control," J. Chem. Phys. **139**(16), 164123 (2013).
[20]A. Konar, V. V. Lozovoy, and M. Dantus, "Solvation stokes-shift dynamics studied by chirped femtosecond laser pulses," J. Phys. Chem. Lett. **3**(17), 2458–2464 (2012).
[21]A. Konar, V. V. Lozovoy, and M. Dantus, "Solvent environment revealed by positively chirped pulses," J. Phys. Chem. Lett. **5**(5), 924–928 (2014).
[22]A. C. Han and M. Shapiro, "Linear response in the strong field domain," Phys. Rev. Lett. **108**, 183002 (2012).

3.3 Discussion

The experiments and simulations mentioned above challenge the premise of spectroscopy which asserts the direct link between the molecular spectrum and the energy absorbed from the field. They indicate that the interaction with the environment can enable weak-field phase-only control of open quantum systems. The analysis in the paper shows that such control is impossible under Markovian L-GKS dynamics. Therefore, the question is still open and the assumptions should be reconsidered. Further directions have to be explored, but will not be investigated in this thesis.

Chapter 4

Exceptional points in open quantum systems

4.1 Introduction

The irreversibility of open quantum system dynamics is introduced into the L-GKS equation by the dissipative term. The eigenvalues of the L-GKS generator with the dissipator are complex, with a non-positive real part. Therefore, the resulting evolution operator is not unitary. Instead it is a contraction operator having a norm smaller than 1. Generally, the dynamics expressed by such an evolution operator has the analytical form of sum of decaying oscillatory exponentials. For example, the expectation value of an operator $\hat{\mathbf{X}}$ will have the form:

$$\langle X(t) \rangle = \sum_k d_k \exp\left[\lambda_k t\right] \ . \tag{4.1}$$

Here λ_k are the eigenvalues of the generator and d_k are the associated amplitudes, both can be complex. The complex eigenvalues λ_k can be divided into real and imaginary parts: $\lambda_k = -\alpha_k + i\omega_k$, with $\alpha_k \geq 0 \in \mathbb{R}$ as the decay rates and $\omega_k \in \mathbb{R}$ as the oscillation frequencies.

Another aspect of the non-hermitian character is that the generator is not always diagonalizable. The points in the parameter space for which the generator is not diagonalizable are called exceptional points.

4.2 Preliminaries

4.2.1 Diagonalizable matrices

Suppose we have a vector-matrix differential equation:

$$\dot{\vec{Y}} = M\vec{Y}. \tag{4.2}$$

This is a set of *coupled* linear differential equations. We would like to decouple this set into a set of *decoupled* equations. This is done by diagonalization.

Diagonalizing the matrix M is to find a set of eigenvectors $\{\vec{v}_k\}$ and associated eigenvalues $\{\lambda_k\}$ that have

$$(M - \lambda_k I)\,\vec{v}_k = 0. \tag{4.3}$$

This is done by finding the roots of the characteristic polynomial

$$P(\lambda) = \det(M - \lambda I)\,. \tag{4.4}$$

The roots of the characteristic polynomial are the eigenvalues. For an $N \times N$ matrix we have a characteristic polynomial of order N, which can be decomposed as:

$$P(\lambda) = \prod_k (\lambda - \lambda_k)^{r_k}\,,\ \sum_k r_k = N, \tag{4.5}$$

thus each eigenvalue λ_k has multiplicity r_k, and the sum of all multiplicities is N. For each eigenvalue λ_k we can always find a set of r_k vectors such that

$$(M - \lambda_k I)^{r_k}\,\vec{v}_{k,\alpha} = 0. \tag{4.6}$$

However, we would like to find r_k eigenvectors, i.e. r_k distinct vectors that fulfill

$$(M - \lambda_k I)\,\vec{v}_{k,\alpha} = 0. \tag{4.7}$$

If for each eigenvalue λ_k there are r_k such independent associated eigenvectors, then we have a set N independent eigenvectors. This set spans the entire space, and the matrix M is diagonalizable. We write the matrix M as $M = V^{-1}\Lambda V$, with the non-singular matrix V which is composed from the columns vectors $\{\vec{v}_{k,\alpha}\}$, and the diagonal matrix Λ which has the eigenvalues $\{\lambda_k\}$ on its diagonal (each λ_k appears r_k times). Then we can write Eq. (4.2) in a new basis, namely the basis $\{\vec{v}_{k,\alpha}\}$, and write the differential equation for $\tilde{Y} \equiv V\vec{Y}$:

$$\dot{\tilde{Y}} = \Lambda\tilde{Y}. \tag{4.8}$$

The resulting set of equations, Eq. (4.8) is a set of *uncoupled* differential equations. For each of the components $\tilde{y}_m$ we have

$$\dot{\tilde{y}}_m = \lambda_m \tilde{y}_m. \tag{4.9}$$

Therefore,

$$\tilde{y}_m(t) = e^{\lambda_m t}\tilde{y}_m(0). \tag{4.10}$$

This leads to the analytical form of Eq. (4.1).

4.2.2 Non-diagonalizable matrices

However, there are matrices that do not have N independent eigenvectors. This means that there is (at least) one of the eigenvalues, λ_{nd}, with multiplicity $r_{nd} > 1$, but has less than r_{nd} eigenvectors associated with it. Therefore Eq. (4.7) does not have r_{nd} distinct solutions for this eigenvalue. Nevertheless, Eq. (4.6) still holds.

Suppose, for example, that we have an eigenvalue λ_{nd} with multiplicity $r_{nd} = 2$, with the vector $v_{nd,0}$ obeying the eigenvector equation, Eq. (4.7):

$$(M - \lambda_{nd} I)\, \vec{v}_{nd,0} = 0, \tag{4.11}$$

and that we cannot find another such eigenvector for the eigenvalue λ_{nd}. We are still looking for another vector, $v_{nd,1}$ that obey Eq. (4.6):

$$(M - \lambda_{nd} I)^2\, \vec{v}_{nd,1} = (M - \lambda_{nd} I)\, \{(M - \lambda_{nd} I)\, \vec{v}_{nd,1}\} = 0. \tag{4.12}$$

Since the only eigenvector associated with λ_{nd} is $v_{nd,0}$, we conclude that the expression in the curly brackets has to be equal to this eigenvector:

$$(M - \lambda_{nd} I)\, \vec{v}_{nd,1} = \vec{v}_{nd,0}. \tag{4.13}$$

This equation is referred as the *generalized eigenvalue equation*, and $\vec{v}_{nd,1}$ is denoted as a *generalized eigenvector*. The generalized eigenvector cannot be decoupled from the eigenvector under operation of the matrix M. Instead, we can combine Eqs. (4.13) and (4.11) into a set of coupled eigenvalue equations, which can be written as a set of matrix-vector equations:

$$\begin{pmatrix} M\vec{v}_{nd,0} \\ M\vec{v}_{nd,0} \end{pmatrix} = \begin{pmatrix} \lambda_{nd} & 1 \\ 0 & \lambda_{nd} \end{pmatrix} \begin{pmatrix} \vec{v}_{nd,1} \\ \vec{v}_{nd,0} \end{pmatrix}. \tag{4.14}$$

The set of eigenvectors and generalized eigenvectors $\{\vec{v}_{k,\alpha}\}$ spans the entire space. We write the matrix M as $M = V^{-1}JV$, where the matrix V is composed from the

set of columns vectors $\{\vec{v}_{k,\alpha}\}$. The matrix J is not diagonal. Instead it is a block-diagonal matrix. Each eigenvalue has a block J_k of size $r_k \times r_k$. For eigenvalues with r_k distinct eigenvectors, the block J_k is diagonal, with λ_k on the diagonal. For eigenvalues without enough eigenvectors, the block has λ_{nd} on the diagonal, and 1 on the first upper of diagonal. We write $J_{nd} = \lambda_{nd} I_{r_{nd}} + N_{r_{nd}}$, where $I_{r_{nd}}$ is the r_{nd}-dimension identity matrix, and $N_{r_{nd}}$ is an $r_{nd} \times r_{nd}$ matrix with ones on the first upper off diagonal and zeros elsewhere. Such blocks are denoted *Jordan blocks*.

When we phrase Eq. (4.2) in the new basis $\tilde{Y} \equiv V\vec{Y}$, we get the differential equation $\dot{\tilde{Y}} = J\tilde{Y}$ instead of Eq. (4.8). In particular, for λ_{nd}, we get a set of *coupled* differential equations:

$$\begin{aligned} \dot{\tilde{y}}_{nd,0} &= \lambda_{nd}\tilde{y}_{nd,0} \\ \dot{\tilde{y}}_{nd,1} &= \lambda_{nd}\tilde{y}_{nd,1} + \tilde{y}_{nd,0}, \end{aligned} \tag{4.15}$$

and the solution is

$$\begin{aligned} \tilde{y}_{nd,0}(t) &= e^{\lambda_{nd}t}\tilde{y}_{nd,0}(0) \\ \tilde{y}_{nd,1}(t) &= e^{\lambda_{nd}t}\left(\tilde{y}_{nd,1}(0) + t\tilde{y}_{nd,0}(0)\right). \end{aligned} \tag{4.16}$$

The analytical solution involves a polynomial in t. If we have more than one generalized eigenvector for a specific eigenvalue we will have higher order polynomials in t.

The polynomial term in the solution can be also deduced from the matrix form: In matrix-vector notation, the solution of Eq. (4.2) is:

$$\vec{Y}(t) = e^{Mt}\vec{Y}(0). \tag{4.17}$$

We use the decomposition $M = V^{-1}DV$, where for a diagonalizable matrix $D = \Lambda$ and for a non-diagonalizable matrix $D = J$, to express the exponential e^{Mt} as

$$e^{Mt} = V^{-1}e^{Dt}V. \tag{4.18}$$

For a diagonalizable matrix the exponential e^{Dt} is composed from the exponentials of the eigenvalues, $e^{\lambda_k t}$, on the diagonal. For a non-diagonalizable matrix we have the exponential of the block $J_{nd} = \lambda_{nd}I + N$. This exponential is

$$e^{J_{nd}t} = e^{(\lambda_{nd}I+N)t} = e^{\lambda_{nd}t}e^{Nt}. \tag{4.19}$$

The matrix N is nilpotent and therefore the Taylor series for e^{Nt} is finite, resulting in a polynomial in t.

The analytical form of polynomial times exponential will be present also in other dynamical features. For example, the expectation value of an operator $\hat{\mathbf{X}}$ will have

the form:

$$\langle X(t)\rangle = \sum_k \sum_{\alpha=0}^{r_k-1} d_{k,\alpha} t^\alpha \exp\left[\lambda_k t\right] \ , \tag{4.20}$$

instead of the form of Eq. (4.1).

4.2.3 Harmonic inversion at the exceptional points

The analytical form of a time signal that emerge from a system of coupled linear differential equations is generally a sum of decaying exponents (see, for example, Eq. (4.1)). Experimentally, however, the problem is inverted. The result of an experiment can be a time signal $C(t)$, $0 \leq t \leq T$, sampled at some discretized time points $\{t_n\}$. The goal is to analyze this time series end extract the underlying model, which is characterized by the eigenvalues $\{\lambda_k\}$ and the amplitudes $\{d_k\}$. This task is achieved by the harmonic inversion method, as described in a previous chapter (cf. Section 2.3). At exceptional points, the analytical form of the time signal is different (see, for example, Eq. (4.20)). Therefore, the regular harmonic inversion methods will fail in extracting the signal parameters. Generally, these methods will extract the eigenvalues correctly, but the amplitudes will diverge. The divergence of the amplitudes was proposed as a means to identify the exceptional points [Fuchs 2014].

4.3 Exceptional point of the L-GKS generator

Exceptional points were studied in many areas of physics. Some recent reviews can be found at [Müller 2008, Uzdin 2012, Moiseyev 2011, Chapter 9]. However, to the best of our knowledge, the L-GKS equation was not studied in this context. To initiate such a study, we have to define the parameter space for the driven open quantum system. When the system is driven by a CW laser, it can be described in the rotating frame by a time-independent L-GKS generator using the external field parameters: the detuning between the system and the driving field frequency Δ, and the amplitude of the field ϵ. The parameter space for the L-GKS is composed from these parameters. We investigated the exceptional points for an L-GKS generator that is defined in this parameter space. We found a fascinating structure of exceptional points. Generally, there are continuous lines of exceptional points in the Δ-ϵ parameter space. These lines merge into cusps of higher order degeneracy. Examples can be found in the following research papers.

4.4 Exceptional points for parameter estimation in open quantum systems

The special analytical form of the dynamics at the exceptional points leads to a divergence of the amplitudes. This divergence can be used to identify the exceptional points. The sharp divergence enables locating the exceptional points accurately. Another method of locating the exceptional points can employ any function that includes terms of the kind $\frac{1}{\Delta\lambda}$, where $\Delta\lambda$ is the difference between the coalescing eigenvalues.

The accurate location of the exceptional points can be used for parameter estimation: After identifying and locating of the exceptional points, one can invert the algebraic relations between the eigenvalues and the system parameters to obtain accurate estimation of the system parameters. The accuracy stems from the enhanced sensitivity of the dynamics near the exceptional points: Small changes in the parameters lead to different harmonic inversions. Therefore, for parameter estimation the harmonic inversion at the exceptional points is superior to standard inversion methods.

We studied the exceptional points in a few examples for driven open quantum system dynamics and suggested to search for them in the parameter space by varying the driving laser parameters - the detuning Δ and the amplitude ϵ. The accurate location can be used then for determining the intrinsic system parameters with high accuracy.

The following two research papers elaborate our work:

- *Exceptional points for parameter estimation in open quantum systems: analysis of the Bloch equations.* Published at *New J. Phys.* 17 113036 (2015).
- *Parameter estimation in atomic spectroscopy using exceptional points.* This paper was uploaded to arXiv (*arXiv*:1511.07205) and will be submitted soon.

4.5 Exceptional points for parameter estimation in open quantum systems: analysis of the Bloch equations

Exceptional points for parameter estimation in open quantum systems: analysis of the Bloch equations

Morag Am-Shallem, Ronnie Kosloff, and Nimrod Moiseyev

Published at *New J. Phys.* 17 113036 (2015)

IOP Publishing New J. Phys. 17 (2015) 113036 doi:10.1088/1367-2630/17/11/113036

New Journal of Physics
The open access journal at the forefront of physics

Deutsche Physikalische Gesellschaft DPG
IOP Institute of Physics

Published in partnership with: Deutsche Physikalische Gesellschaft and the Institute of Physics

OPEN ACCESS

RECEIVED
3 August 2015

REVISED
10 October 2015

ACCEPTED FOR PUBLICATION
13 October 2015

PUBLISHED
16 November 2015

PAPER

Exceptional points for parameter estimation in open quantum systems: analysis of the Bloch equations

Morag Am-Shallem[1], **Ronnie Kosloff**[1] **and Nimrod Moiseyev**[2]

[1] Fritz Haber Research Center and the Institute of Chemistry, the Hebrew University, Jerusalem 91904, Israel
[2] Schulich Faculty of Chemistry and Faculty of Physics, Technion, Haifa 3200008, Israel

E-mail: ronnie@fh.huji.ac.il

Keywords: exceptional points, Bloch equation, parameter estimation, open quantum systems

Abstract

We suggest to employ the dissipative nature of open quantum systems for the purpose of parameter estimation: the dynamics of open quantum systems is typically described by a quantum dynamical semigroup generator $\mathcal{L}$. The eigenvalues of $\mathcal{L}$ are complex, reflecting unitary as well as dissipative dynamics. For certain values of parameters defining $\mathcal{L}$, non-Hermitian degeneracies emerge, i.e. exceptional points (EP). The dynamical signature of these EPs corresponds to a unique time evolution. This unique feature can be employed experimentally to locate the EPs and thereby to determine the intrinsic system parameters with a high accuracy. This way we turn the disadvantage of the dissipation into an advantage. We demonstrate this method in the open system dynamics of a two-level system described by the Bloch equation, which has become the paradigm of diverse fields in physics, from NMR to quantum information and elementary particles.

1. Introduction

Felix Bloch [1] pioneered the dynamical description of open quantum systems. Originally Bloch's equations describe the relaxation and dephasing of a nuclear spin in a magnetic field. Soon it became apparent that the treatment can be extended to a generic two-level-system (TLS), such as the dynamics of laser driven atoms in the optical regime [2–4]. The open TLS has been used to model many different fields of physics. The TLS or a q-bit is at the foundation of quantum information [5–9]. In particle physics the TLS algebra has been employed in studies of possible deviations from quantum mechanics in the context of neutrino oscillations [10], as well as quantum entanglement [11–15], associated with electron/positron collisions and entangled systems due to EPR-Bell correlations [16].

The TLS is the base for setting the frequency standard for atomic clocks [17]. As a result accurate measurement of frequency is an important issue. Quantum-enhanced measurements based on interferometry have been suggested as means to beat the shot noise limit [18]. In these methods the decoherence rate is the limiting factor [19]. In some cases quantum error correction can increase the coherence time and the accuracy [20]. In the present study we want to suggest an opposite strategy. By employing the non-Hermitian character of the dynamics, the decoherence can be transformed from a bug to a feature.

2. Exceptional points (EPs) in open quantum systems

The Bloch equation is the simplest example of a quantum master equation. Bloch rederived the equation from first principles, employing the assumption of weak coupling between the system and bath [21, 22]. These studies have paved the way for a general theory of quantum open systems. Davies [23] rigorously derived the weak coupling limit, resulting in a quantum master equation which leads to a completely positive dynamical semigroup [24]. Based on a mathematical construction, Lindblad and Gorini, Kossakowski and Sudarshan (L-

GKS) obtained the general structure of the generator $\mathcal{L}$ of a completely positive dynamical semigroup [25, 26]. In the Heisenberg representation the L-GKS generator becomes [27, ch 3]:

$$\frac{\mathrm{d}}{\mathrm{d}t}\hat{\mathbf{X}} = \frac{\partial \hat{\mathbf{X}}}{\partial t} + \mathrm{i}\left[\hat{\mathbf{H}}, \hat{\mathbf{X}}\right] + \sum_k \left(\hat{\mathbf{V}}_k^\dagger \hat{\mathbf{X}} \hat{\mathbf{V}}_k - \frac{1}{2}\left[\hat{\mathbf{V}}_k^\dagger \hat{\mathbf{V}}_k, \hat{\mathbf{X}}\right]_+\right), \tag{1}$$

where $\hat{\mathbf{X}}$ is an arbitrary operator. The Hamiltonian $\hat{\mathbf{H}}$ is Hermitian and operators $\hat{\mathbf{V}}_k$ are defined to operate in the Hilbert space of the system. The $[\,\cdot\,,\cdot\,]_+$ denotes an anti commutator.

The set of operators $\{\hat{\mathbf{X}}\}$ supports a Hilbert space construction using the scalar product: $(\hat{\mathbf{X}}_1, \hat{\mathbf{X}}_2) \equiv \mathrm{tr}\{\hat{\mathbf{X}}_1^\dagger \hat{\mathbf{X}}_2\}$. A crucial simplification to equation (1) is obtained when a set of operator is closed to the generator $\mathcal{L}$. Then we can rephrase the dynamics with a matrix-vector notation [28]:

$$\dot{\vec{Y}} = M\vec{Y} \tag{2}$$

where $\vec{Y}$ is the vector of basis operators and M is the representation of the generator $\mathcal{L}$ in this vector space. The eigenvalues of the matrix M reflect the non-Hermitian dynamics generated by $\mathcal{L}$. In general they are complex with the steady state eigenvector having an eigenvalue of zero. The solution for this equation is:

$$\vec{Y}(t) = \mathrm{e}^{Mt}\vec{Y}(0).$$

When M is diagonalizable, we can write $M = T\Lambda T^{-1}$, for a non-singular matrix T and a diagonal matrix Λ, which has the eigenvalues $\{\lambda_i\}$ on the diagonal. Then we have $\mathrm{e}^{Mt} = T\mathrm{e}^{\Lambda t}T^{-1}$, with the diagonal matrix $\mathrm{e}^{\Lambda t}$, which has the exponential of the eigenvalues, $\mathrm{e}^{\lambda_i t}$, on its diagonal. The resulting dynamics of expectation values of operators, as well as other correlation functions, follows a sum of decaying oscillatory exponentials. The analytical form of such dynamics is:

$$\langle X(t)\rangle = \sum_k d_k \exp\left[-\mathrm{i}\omega_k t\right], \tag{3}$$

where $-\mathrm{i}\,\omega_k$, denoted as complex frequencies, are the eigenvalues of M, d_k are the associated amplitudes, and both ω_k and d_k can be complex. The real part of the complex frequency ω_k represents the oscillation rate, while the imaginary part, $\mathrm{Im}(\omega_k) \leqslant 0$ represents the decaying rate.

For special values of the system parameters the spectrum of the non-Hermitian matrix M is incomplete. This is due to the coalescence of several eigenvectors, referred to as a non-Hermitian degeneracy. The difference between Hermitian degeneracy and non-Hermitian degeneracy is essential: in the Hermitian degeneracy, several different orthogonal eigenvectors are associated with the same eigenvalue. In the case of non-Hermitian degeneracy several eigenvectors coalesce to a single eigenvector [29, ch 9]. As a result, the matrix M is not diagonalizable.

The exponential of a non-diagonalizable matrix M can be expressed using its Jordan normal form: $M = TJT^{-1}$. Here, J is a Jordan-blocks matrix which has (at least) one non-diagonal Jordan block; $J_i = \lambda_i I + N$, where I is the identity and N has ones on its first upper off-diagonal. The exponential of M is expressed as $\mathrm{e}^{Mt} = T\mathrm{e}^{Jt}T^{-1}$, with the block-diagonal matrix e^{Jt}, which is composed from the exponential of the Jordan blocks $\mathrm{e}^{J_i}t$. For non-Hermitian degeneracy of an eigenvalue λ_i, the exponential of the block J_i will have the form: $\mathrm{e}^{J_i t} = \mathrm{e}^{\lambda_i It + Nt} = \mathrm{e}^{\lambda_i t}\mathrm{e}^{Nt}$. The matrix N is nilpotent and therefore the Taylor series of e^{Nt} is finite, resulting in a polynomial in the matrix Nt. This gives rise to a polynomial behaviour of the solution, and the dynamics of expectation values will have the analytical form of

$$\langle X(t)\rangle = \sum_k \sum_{\alpha=0}^{r_k} d_{k,\alpha} t^\alpha \exp\left[-\mathrm{i}\omega_k^{(r_k)} t\right], \tag{4}$$

replacing the form of equation (3). Here, $\omega_k^{(r_k)}$ denotes an eigenvalue with multiplicity of $r_k + 1$. Note that for non-degenerate eigenvalues, i.e. $r_k = 0$, we have $d_{k,0} = d_k$ and $\omega_k^0 = \omega_k$. The difference in the analytic behaviour of the dynamics results in non-Lorentzian line shapes, with higher order poles in the complex spectral domain.

The point in the spectrum where the eigenvectors coalesce is known as an exceptional point (EP). When two eigenvalues of the master equation coalesce into one, a second-order non-Hermitian degeneracy is obtained. We refer to it as EP2, while a third-order non-Hermitian degeneracy is denoted by EP3.

This study addresses the scenario of the dynamics of a system coupled to a bath. The formalism is a reduced description of a tensor product of the system and the bath [27, 30]. The coupling to the bath introduces dissipation and dephasing into the dynamics. The state is represented as a density operator in Liouville space, and the dynamics is governed by the L-GKS equation. The non Hermitian properties of the dynamical generator $\mathcal{L}$ is caused by tracing out the bath degrees of freedom. We employ the Heisenberg picture with a complete operator basis set in Liouville space.

Previous studies of the physics of EPs investigated the scenario of scattering resonances phenomena. In that different scenario, the non Hermitian properties of the effective Hamiltonian are caused by the interaction

between the discrete states via the common continuum of the scattering states [31, 32]. In those studies only coherent dynamics is considered and the dissipation and dephasing phenomena are absent.

Examples for EPs have been described in optics [33, 34], in atomic physics [35–40], in electron–molecule collisions [41], superconductors [42], quantum phase transitions in a system of interacting bosons [43], electric field oscillations in microwave cavities [44], in PT-symmetric waveguides [45], and in mesoscopic physics [46, 47].

Recently, Wiersig suggested a method to enhance the sensitivity of detectors using EPs [48]. Below we suggest to employ the EPs for the purpose of parameter estimation.

3. Identifying the EPs and parameter estimation

The analytical form of decaying exponentials, equation (3), is used in harmonic inversion methods to find the frequencies and amplitudes of the time series signal [49–51]. These frequencies and amplitudes can be employed to estimate the system parameters. If the sensitivity of the estimated frequencies is increased with respect to the system controls, the accuracy of the parameter estimation is enhanced. Such sensitivity increase can be achieved using the special character of the dynamics at EPs.

At EPs the analytical form includes also polynomials (equation (4)). Fuchs *et al* showed that applying the standard harmonic inversion methods to a signal generated by equation (4) leads to divergence of the amplitudes d_k. An extended harmonic inversion method can fix the problem. The divergence of the amplitudes d_k at the vicinity of EP can be used to locate them in the parameter space very accurately [52]. This is a consequence of the special non analytic character close to the EP (see in ch 9 in [29]).

Relying on the ability to accurately locate the EPs in the parameter space, we suggest to use the EPs for parameter estimation. The procedure we suggest follows:

(i) Accurately locate in the parameter space the desired EP by iterating the following steps:

  (a) Perform the experiment to get a time series of an observable for example the polarization as a function of time.

  (b) Obtain the characteristic frequencies and amplitudes of the signal using harmonic inversion methods.

  (c) In the parameter space, estimate the direction and distance to the EP and determine new parameters for the next iteration.

(ii) Invert the relations between the characteristic frequencies and the system parameters at the EP to obtain the system parameters.

The accurate location of the EPs, followed by inverting the relations, will lead to accurate parameter estimation.

4. Determination of the physical parameters in two level systems

4.1. The Bloch equation

The Bloch equation describes the dynamics of the three components of the nuclear spin, S_x, S_y, and S_z, under the influence of an external magnetic field, or a two-level atom in external electromagnetic field. In the rotating frame, we can write the equations in a matrix-vector notation:

$$\frac{\mathrm{d}}{\mathrm{d}t}\begin{pmatrix}\tilde{S}_x\\ \tilde{S}_y\\ S_z\end{pmatrix}=\begin{pmatrix}-\frac{1}{T_2} & \Delta & 0\\ -\Delta & -\frac{1}{T_2} & \epsilon\\ 0 & -\epsilon & -\frac{1}{T_1}\end{pmatrix}\begin{pmatrix}\tilde{S}_x\\ \tilde{S}_y\\ S_z\end{pmatrix}+\begin{pmatrix}0\\ 0\\ \frac{1}{T_1}S_z^0\end{pmatrix}, \tag{5}$$

with T_1 and T_2 as the dissipation and dephasing relaxation parameters, and the detuning from resonance Δ and the amplitude ϵ as the field parameters. See details in appendix A.

The Bloch equations can be derived from the L-GKS equation of the two-level system, with the effective rotating-frame Hamiltonian

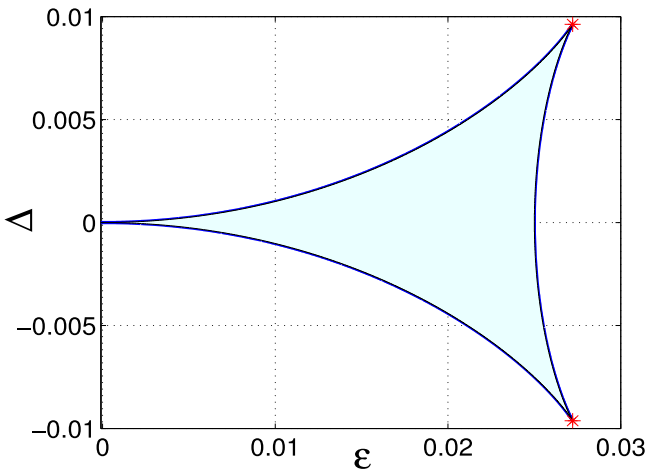

Figure 1. A map of the non-Hermitian degeneracies of the eigenvalues of the matrix M of equation (6), as a function of ϵ and Δ, for fixed $\Gamma = 0.1$. The lines represent second order exceptional points (EP2). The cusps, where $\Delta = \pm\sqrt{1/108}\ \Gamma, \epsilon = \sqrt{8/108}\ \Gamma$ (red asterisks), are third order exceptional point (EP3). In the area inside the 'triangle', marked with pale blue, the eigenvalues of the matrix M are real. The EP2 curve distinguishes between points with real and complex eigenvalues.

$$\hat{\mathbf{H}} = \Delta\hat{\mathbf{S}}_z + \epsilon\hat{\tilde{\mathbf{S}}}_x,$$

along with relaxation and dephasing terms. see appendix B for details.

Reducing the number of parameters, the master equation can be incorporated in the matrix:

$$\mathrm{M} = \begin{pmatrix} -\frac{\Gamma}{2} & \Delta & 0 \\ -\Delta & -\frac{\Gamma}{2} & \epsilon \\ 0 & -\epsilon & -\Gamma \end{pmatrix}, \tag{6}$$

with $\Gamma = \frac{3}{2}\frac{1}{T_1} - \frac{1}{T_2}$ as the general relaxation coefficient (see appendix B).

The dynamics is determined by the exponential e^{Mt}, which typically describes oscillating decaying signal, see equation (3). Nevertheless, for specific parameters leading to EP the dynamics is modified to include polynomials, see equation (4).

4.2. EPs in the Bloch equation

The EPs are non-Hermitian degeneracies in the matrix M of equation (6). The task is to express the EPs using the parameters of this matrix. Explicit derivations are presented in appendix C. Non-Hermitian degeneracies of the eigenvalues [29], EP2, occur when

$$\Gamma^4\Delta^2 + 16\left(\Delta^2 + \epsilon^2\right)^3 + \Gamma^2\left(8\Delta^4 - 20\Delta^2\epsilon^2 - \epsilon^4\right) = 0.$$

Figure 1 shows a map of EP2 curve as a function of ϵ and Δ for fixed $\Gamma = 0.1$. Such figures were obtained in the study of analytical solutions for the Bloch equation [53–55].

A third order EP, EP3, occurs when $\Delta = \pm\sqrt{1/108}\ \Gamma$, $\epsilon = \sqrt{8/108}\ \Gamma$ (red asterisks in figure 1). These triple-degeneracies EP3 occur twice, and have a cusp-like behaviour, emerging from the EP2-curves, identifiable as a section through an elliptic umbilic catastrophe [56]. This topology is also consistent with an analysis of non Hermitian degeneracies in a two-parameters family of 3×3 matrices [57]. In very strong driving fields the matrix M will loose symmetry [58, 59] maintaining the cusps but skewing the topology.

4.3. EP identification and parameter estimation

We now describe the two steps of the method for accurate determination the physical parameters. The first step is to identify the desired EP using a sequence of measured time-dependent signals. The second step is to invert the relations and determine the system parameters.

4.3.1. Identifying the second and third order EPs

To identify the EPs we used time series of the polarization observable $S_z \equiv \langle\hat{\mathbf{S}}_z\rangle$, initially at the ground state. We simulated the dynamics with varying field parameters (ϵ, Δ) generating a time series of polarization $S_z[n] = S_z(n\,\delta t)$. This signals served as the input for the harmonic inversion.

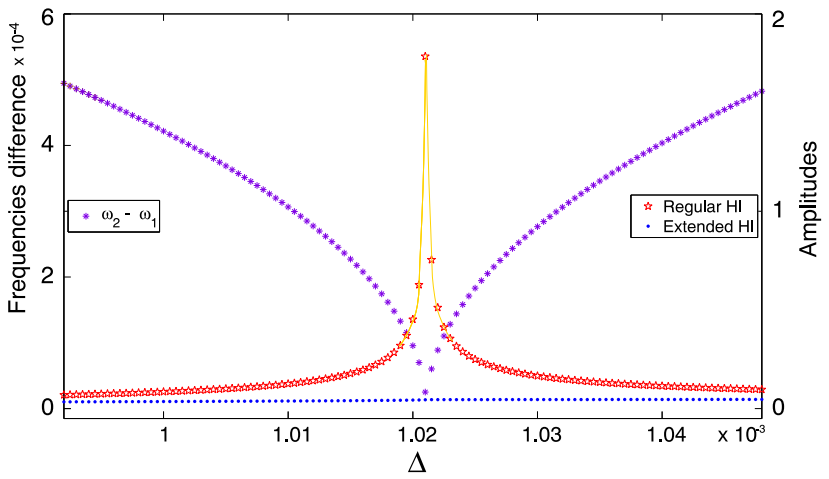

Figure 2. Identifying an EP2 for $\Gamma = 0.1$ and $\epsilon = 0.01$. The left y-axis (purple asterisks) shows the absolute value of the difference between the frequencies, $|\omega_2 - \omega_1|$, versus the detuning Δ. The non-Hermitian degeneracy point is located with high resolution. The right y-axis shows the corresponding amplitude, obtained by the regular harmonic inversion method $|d_1|$ (red stars), and by the extended method $|d_{1,0}|$ (blue points). The diverging behaviour of $|d_1|$ indicates that the degeneracy is an EP.

The parameters Δ and ϵ were tuned close to an EP. Generically we should have

$$S_z(t) = d_1 e^{-i\omega_1 t} + d_2 e^{-i\omega_2 t} + d_3 e^{-i\omega_3 t},$$

but in the EP2 ($r_k = 1$) we get

$$S_z(t) = d_1 e^{-i\omega_1 t} + \left(d_{2,0} + d_{2,1} t\right) e^{-i\omega_2^{(1)} t},$$

and for EP3 ($r_k = 2$)

$$S_z(t) = \left(d_{1,0} + d_{1,1} t + d_{1,2} t^2\right) e^{-i\omega_1^{(2)} t}.$$

(See equations (3) and (4).) We located suspected EPs by identifying possible degeneracies of the assigned frequencies ω_k. As stated earlier, applying standard harmonic inversion methods for the time series generated by a non-diagonalizable matrix, leads to divergence of the amplitudes d_k [52]. This divergence can be used to locate the EPs accurately. A verification can be obtained by using the extended harmonic inversion method.

This procedure was employed to identify an EP2 for fixed $\Gamma = 0.1$ and $\epsilon = 0.01$, with varying Δ. The purple asterisks at figure 2 displays the absolute value of the difference between the frequencies $|\omega_2 - \omega_1|$, obtained by the harmonic inversion for each parameter set. The degeneracy point is clearly observed. The diverging behaviour of the amplitudes is shown in red stars. It is consistent with the degeneracy of the frequencies. The EP2 is located at $\Delta = 1.021 \times 10^{-3}$, consistent with the prediction. Using a finer mesh of sampling points the EP can be identified with a resolution exceeding 0.5×10^{-9}.

The EP3 was identified by a 2D search performed by varying ϵ and Δ, for fixed $\Gamma = 0.1$. We searched for the degeneracies of the three eigenvalues by employing the 2D function

$$F(\Delta, \epsilon, \Gamma) = \log\left(\left|\frac{1}{(\omega_1 - \omega_2)}\frac{1}{(\omega_2 - \omega_3)}\frac{1}{(\omega_3 - \omega_1)}\right|\right), \tag{7}$$

which should diverges at the EP curve. Numerically, we get high values at this curve, with highest values obtained at the EP3. The upper panel of figure 3 shows the sharp curve of peaks following the curve of EPs. The highest point on the merging two ridges is the EP3. The lower panel of figure 3 shows the sum of the absolute values of the amplitudes, calculated by the standard harmonic inversion. The curve of the EPs is clearly identified.

Refining the search leads to very high resolution, and the EP3 can be identified with a high accuracy, approaching the theoretical values of $\Delta = \sqrt{1/108}\ \Gamma, \epsilon = \sqrt{8/108}\ \Gamma$.

An efficient algorithm to identify the EP3 is demonstrated based on a two-dimensional search in the parameter space of Δ and ϵ. This procedure enables the experimentalists to identify accurately the laser parameters for which the EP3 is obtained. We use the maximum of the function equation (7) as the objective leading to EP3.

Evaluating the function at each desired point in the parameter space include the following steps:

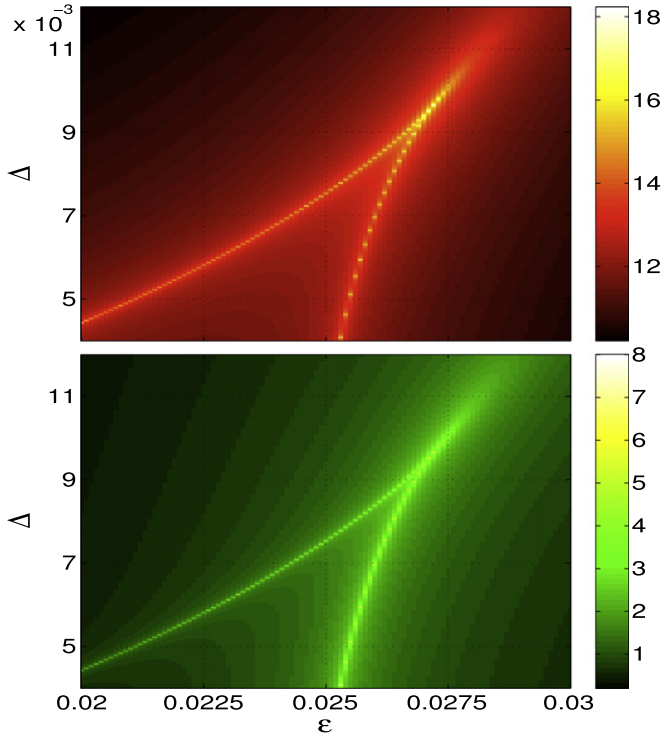

Figure 3. Identifying the triple exceptional point EP3. The upper panel shows the 2D function $F(\Delta, \epsilon, \Gamma)$ presented in the text. The highest point corresponds to the triple-EP point EP3. The lower panel shows the sum of the absolute values of the amplitudes, which were calculated by the regular harmonic inversion method.

(i) *Time series*: obtain a time series of the polarization by performing the experiment or the numerical simulation.

(ii) *Frequencies*: calculate the frequencies from the time series by harmonic inversion.

(iii) *Function evaluation*: evaluate the function $F(\Delta, \epsilon, \Gamma)$ from the calculated frequencies.

Standard search methods can stagnate due to the high values at the EP2 curve. Another difficulty is the cusp behaviour of the EP2 curve close to the EP3. To overcome these diffculties we implemented a 'climbing the valley' procedure: staying on the valley of the local minima ensures the search overcomes the stagnation due to the EP2 curve. The procedure follows:

(i) *Preliminary step—initial point*:

  (a) Locate points inside the triangle-like EP curve (see figure 4). The inner area of the curve is characterized by real-only eigenvalues.

  (b) Perform a 1D search to find a minimum on a straight line.

(ii) *Valley ascend*: each iteration ascends up the valley to a point with higher value of the function F. This is done by finding a minimum on the circular arc that is centred at the current point, enclosed by two radii. The angles of these radii can be predefined or defined on each iteration. We perform the following steps:

  (a) *Determining the angular range*. Predefined or from the previous iterations.

  (b) *Determining the radius*. The radius is the distance from the current point to nearest point on the EP2 curve that is in the angular range.

  (c) *Finding the next point*. Performing a 1D search on the circular arc that is defined by the angular range and the radius (see blue arc in figure 4). The point for the next iteration is the point on the arc with the minimal value of F (see end of green line in figure 4).

These steps converge to the desired EP3 point. Figure 4 demonstrates the progress in the 'valley ascend' method with a few iterations.

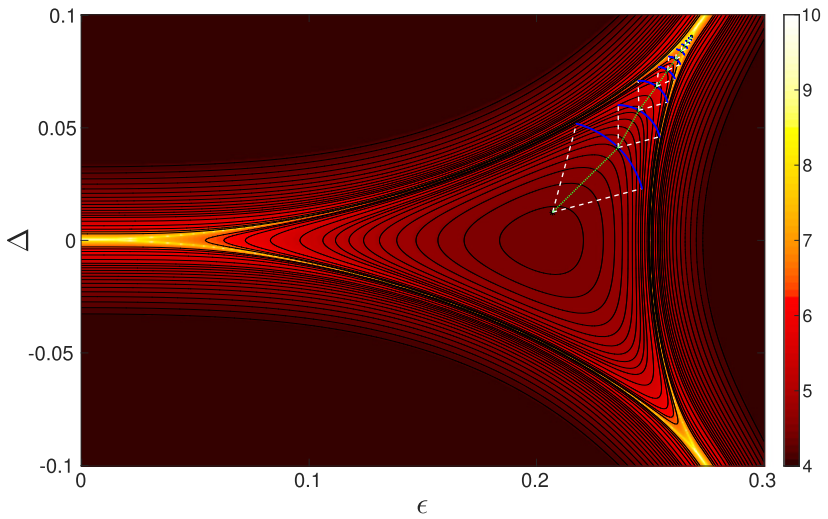

Figure 4. A sketch of the iterations progress in the 'valley ascend' method.The collors on the background and the black contour lines represent the function $F(\Delta, \epsilon, \Gamma)$ of equation (7). In each iteration we plotted with blue line the circular arc on which we searched for the minimum. The black asterisks show these minima, which form the curve, plotted with a dashed light green line, that 'climbs' in the valley of the objective function.

The *Valley ascend* method presented above is a generic method, and can be used also for searching higher order degeneracies in other systems. For the Bloch equation case, where the generating matrix, equation (6), is a 3×3 matrix, the EP3 is the point where the characteristic polynomial

$$P_{\Delta,\epsilon,\Gamma}(\omega) = (\omega - \omega_1)(\omega - \omega_2)(\omega - \omega_3) \tag{8}$$

has roots with multiplicity of 3. Therefore we can use the special properties of the cubic equation and perform a regular root search. We define r, s and t as the coefficient of the polynomial $P_{\Delta,\epsilon,\Gamma}(\omega)$ defined in equation (8):

$$(\omega - \omega_1)(\omega - \omega_2)(\omega - \omega_3) = \omega^3 + r\omega^2 + s\omega + t. \tag{9}$$

We define the functions

$$\begin{aligned} p(\Delta, \epsilon, \Gamma) &= s - \frac{1}{3}r^2 \\ q(\Delta, \epsilon, \Gamma) &= \frac{2}{27}r^3 - \frac{1}{3}rs + t, \end{aligned} \tag{10}$$

and perform a 2D conventional root search. The point in the parameter space where these two functions vanish is point where the three eigenvalues are degenerate. We have applied this method using standard method of 2D root search obtaining high accurate values of the EP3.

4.3.2. Physical parameter estimation from the value at the EP

For the TLS the system parameters are the frequency ω_s associated with the energy gap, the general decay rate Γ and the dipole strength μ. The external experimentally controlled parameters are the driving frequency ν and the power amplitude $\mathcal{E}$. The parameters of equation (6) can be related with $\epsilon = \mu\mathcal{E}$ and $\Delta = \omega_s - \nu$. One would like to estimate the system parameters from experiments. After locating accurately the EP, we can determine the parameters by inverting the relations between the eigenvalues and the system parameters.

To obtain high accuracy, we used the identification the triple-degeneracy point EP3 presented above, so both parameters—Δ and ϵ— are located accurately. The accurate location of Δ and ϵ makes the parameter estimation very robust to uncertainties in the location of the EPs. This is a consequence of the special non analytic character close to the EP3 (see appendix D). Therefore, the system parameters Γ, ω_s and μ can be determined to a high degree of accuracy at this point. From the eigenvalues of the matrix M in equation (6) we get $\Gamma = \frac{\mathrm{i}}{2}(\omega_1 + \omega_2 + \omega_3)$. To obtain ϵ and Δ one has to invert nonlinear relations (see appendix C). At the EP3, the inversion becomes: $\omega_s = \nu + \sqrt{1/108}\ \Gamma, \mu = \sqrt{8/108}\ \Gamma/\mathcal{E}$.

4.3.3. Noise sensitivity

Parameters estimation naturally raises the issue of sensitivity to noisy experimental data. The noise sensitivity will be determined by the method of harmonic inversion. If the sampling periods have high accuracy then the time series can be shown to have an underlying Hamiltonian generator. This is the basis for linear methods, such

as the filter diagonalization (FD) [49, 50]. The noise in these methods results in normally distributed underlying matrices, and the model displays monotonous behaviour with respect to the noise. This was verified analytically and by means of simulations in [60]. As a result sufficient averaging will eliminate the noise. Practical implementations require further analysis with evidence of nonlinear effects of noise. For example, Mandelshtam *et al* analysed the noise-sensitivity of the FD in the context of NMR experiments [61, 62] and Fourier transform mass spectrometry [63]. For some other methods, a noise reduction technique was proposed in [51].

5. Discussion

Bloch's equation has become the template for the dynamics of open quantum systems. Such systems typically decohere with a dynamical signature of decaying oscillatory motion. It is therefore surprising that the existence of non Hermitian degeneracies has been overlooked. Our finding of an intricate manifold of double degeneracies EP2 and triple degeneracies EP3 in the elementary TLS template suggests that any quantum dynamics described by the L-GKS generator [25, 26] will exhibit a manifold of EPs.

Non Hermitian degeneracies of the EP have a subtle influence on the dynamics. The hallmark of EP dynamics is a polynomial component in the decay leading to non-Lorentzian lineshapes. We suggest an experimental procedure to identify the EP in Bloch systems, using harmonic inversion of the polarization time series. The sensitivity of harmonic inversion in the neighbourhood of an EP enables us to accurately locate the EP, and therefore allows us to determine the system parameters: the energy gap ω_s, the dipole transition moment μ, and the decoherence rate Γ.

This study is only the first step in establishing parameter estimation via EPs. A generalization to larger Liouville spaces is under study for atomic spectroscopy. Under the influence of driving fields and due to spontaneous emission, atoms and ions can have a structure of N-level system with relaxation. In these systems we expect non-Hermitian degeneracy of high order. The structure of the EPs in these systems can be used for estimating the energy differences, the lifetimes, and branching ratios. Work in this direction is in progress.

Many quantum systems are open and their dynamics has dissipative nature, which is described well by the L-GKS equation. Therefore we expect to find EPs in many quantum systems. Under the appropriate circumstances these EPs can be used for accurate parameter estimation.

Acknowledgments

We thank Ido Schaefer, Amikam Levy, and Raam Uzdin for fruitful discussions. We thank Jacob Fuchs and Jörg Main for assisting with the extended harmonic inversion method. We thank the referee for proposing the root search for the EP3. Work supported by the Israel Science Foundation Grants No. 2244/14 and No. 298/11 and by I-Core: the Israeli Excellence Center 'Circle of Light'.

Appendix A. Bloch equations

The Bloch equation describes the dynamics of the three components of the nuclear spin, S_x, S_y, and S_z, under the influence of an external magnetic field $\vec{H}$. The equations as appear in Bloch's original paper ([1], equation (38)) are

$$\begin{aligned}\dot{S_x} &= \gamma\left(S_y H_z - S_z H_y\right) - \frac{1}{T_2}S_x \\ \dot{S_y} &= \gamma\left(S_z H_x - S_x H_z\right) - \frac{1}{T_2}S_y \\ \dot{S_z} &= \gamma\left(S_x H_y - S_y H_x\right) - \frac{1}{T_1}\left(S_z - S_z^0\right).\end{aligned} \tag{A.1}$$

T_1 and T_2 are two relaxation parameters (the pure dephasing rate $\frac{1}{T_2^*}$ is related by $\frac{1}{T_2} = \frac{1}{2T_1} + \frac{1}{T_2^*}$), γ is the gyromagnetic ratio, and S_z^0 is the equilibrium value of S_z under the influence of constant external magnetic field $H_z = H_0$. These equations can be recast in a matrix-vector notation:

$$\frac{\mathrm{d}}{\mathrm{d}t}\begin{pmatrix} S_x \\ S_y \\ S_z \end{pmatrix} = \begin{pmatrix} -\frac{1}{T_2} & \gamma H_z & -\gamma H_y \\ -\gamma H_z & -\frac{1}{T_2} & \gamma H_x \\ \gamma H_y & -\gamma H_x & -\frac{1}{T_1} \end{pmatrix}\begin{pmatrix} S_x \\ S_y \\ S_z \end{pmatrix} + \begin{pmatrix} 0 \\ 0 \\ \frac{1}{T_1}S_z^0 \end{pmatrix}. \tag{A.2}$$

For an external field $\vec{H}$ with the components $H_x = H_1 \cos \omega t$, $H_y = -H_1 \sin \omega t$, $H_z = H_0$, we define the rotating frame:

$$\begin{aligned} S_x &= \tilde{S}_x \cos \omega t - \tilde{S}_y \sin \omega t \\ S_y &= -\tilde{S}_x \sin \omega t - \tilde{S}_y \cos \omega t. \end{aligned} \tag{A.3}$$

With the notations $\epsilon = \gamma H_1$ and $\Delta = \gamma H_0 - \omega$ we have (see also [4]):

$$\frac{\mathrm{d}}{\mathrm{d}t}\begin{pmatrix} \tilde{S}_x \\ \tilde{S}_y \\ S_z \end{pmatrix} = \begin{pmatrix} -\frac{1}{T_2} & \Delta & 0 \\ -\Delta & -\frac{1}{T_2} & \epsilon \\ 0 & -\epsilon & -\frac{1}{T_1} \end{pmatrix}\begin{pmatrix} \tilde{S}_x \\ \tilde{S}_y \\ S_z \end{pmatrix} + \begin{pmatrix} 0 \\ 0 \\ \frac{1}{T_1}S_z^0 \end{pmatrix}. \tag{A.4}$$

These equations also describe, in the dipole approximation, a two-level atom in external electromagnetic field. In this case, the system parameters are the the unperturbed frequency of the system ω_s, and the dipole strength μ. The external experimentally controlled parameters are the driving frequency ν and the power amplitude $\mathcal{E}$. The parameters of equation (A.4) are related with $\epsilon = \mu\mathcal{E}$ and $\Delta = \omega_s - \nu$. In the absence of dissipation the eigenvalues of the matrix are pure imaginary, and the dynamics is a free precession of the polarization vector characterized by the Rabi frequency: $\Omega = \sqrt{\epsilon^2 + \Delta^2}$. When dissipation is present the eigenvalues of the homogeneous part of equation (A.4) become complex, reflecting a decaying oscillation dynamics leading asymptotically to a steady state.

Appendix B. Derivation of the Bloch equation from the L-GKS equation

In the Heisenberg representation the L-GKS generator becomes:

$$\frac{\mathrm{d}}{\mathrm{d}t}\hat{\mathbf{X}} = \frac{\partial \hat{\mathbf{X}}}{\partial t} + \mathrm{i}\left[\hat{\mathrm{H}}, \hat{\mathbf{X}}\right] + \sum_k \left(\hat{\mathrm{V}}_k^\dagger \hat{\mathbf{X}} \hat{\mathrm{V}}_k - \frac{1}{2}\left\{\hat{\mathrm{V}}_k^\dagger \hat{\mathrm{V}}_k, \hat{\mathbf{X}}\right\}\right). \tag{B.1}$$

where $\hat{\mathbf{X}}$ is an arbitrary operator. The Hamiltonian $\hat{\mathbf{H}}$ is Hermitian and $\hat{\mathbf{V}}$ is defined to operate in the Hilbert space of the system. The curly brackets denote an anti commutator. The set of operators $\{\hat{\mathbf{X}}\}$ supports a Hilbert space construction, with the scalar product defined as: $(\hat{\mathbf{X}}_1, \hat{\mathbf{X}}_2) \equiv \mathrm{tr}\left\{\hat{\mathbf{X}}_1^\dagger \hat{\mathbf{X}}_2\right\}$.

For two-level system, the effective rotating-frame Hamiltonian under a driving field with detuning Δ and driving frequency ϵ is:

$$\hat{\mathbf{H}} = \Delta \hat{\mathbf{S}}_z + \epsilon \tilde{\mathrm{S}}_x. \tag{B.2}$$

The TLS L-GKS equation for an operator $\hat{\mathbf{X}}$ with relaxation and pure dephasing becomes

$$\begin{aligned} \frac{\mathrm{d}}{\mathrm{d}t}\hat{\mathbf{X}} = \mathrm{i}&\left[\hat{\mathbf{H}}, \hat{\mathbf{X}}\right] \\ &+ \kappa_-\left(\hat{\mathbf{S}}_+ \hat{\mathbf{X}} \hat{\mathbf{S}}_- - \frac{1}{2}\left\{\hat{\mathbf{S}}_+ \hat{\mathbf{S}}_-, \hat{\mathbf{X}}\right\}\right) \\ &+ \kappa_+\left(\hat{\mathbf{S}}_- \hat{\mathbf{X}} \hat{\mathbf{S}}_+ - \frac{1}{2}\left\{\hat{\mathbf{S}}_- \hat{\mathbf{S}}_+, \hat{\mathbf{X}}\right\}\right) \\ &- \gamma\left[\hat{\mathbf{S}}_z, \left[\hat{\mathbf{S}}_z, \hat{\mathbf{X}}\right]\right], \end{aligned} \tag{B.3}$$

where $\kappa_\pm$ are kinetic coefficients, $\kappa_+/\kappa_- = \exp(-\hbar\omega/k_B T)$, and γ is the pure dephasing rate [2, 64].

To rephrase the equation in a matrix-vector notation, We use the polarization operators and the identity matrix to form the vector of basis operators: $\vec{S}' = \left(\tilde{\mathbf{S}}_x, \tilde{\mathbf{S}}_y, \hat{\mathbf{S}}_z, \hat{\mathbf{I}}\right)^T$. Then equation (B.3) can be written as $\dot{\vec{S}}' = M'\vec{S}'$, with an appropriate 4×4 matrix M'. We can reduce the dimensions by writing an inhomogeneous equation for the three-component vector $\vec{S} = \left(\tilde{\mathbf{S}}_x, \tilde{\mathbf{S}}_y, \hat{\mathbf{S}}_z\right)^T$:

$$\dot{\vec{S}} = (M - \gamma I)\left(\vec{S} - \vec{S}_{\rm eq}\right), \tag{B.4}$$

with $\Gamma = \kappa_- + \kappa_+ - \gamma$, I as the 3×3 identity matrix, $\vec{S}_{\rm eq}$ that fulfills $(\gamma I - M)\vec{S}_{\rm eq} = (0,\ 0,\ (\kappa_+ - \kappa_-)\hat{\mathbf{I}})^T$ and the matrix:

$$\mathrm{M} = \begin{pmatrix} -\frac{\Gamma}{2} & \Delta & 0 \\ -\Delta & -\frac{\Gamma}{2} & \epsilon \\ 0 & -\epsilon & -\Gamma \end{pmatrix}. \tag{B.5}$$

Equation (B.4) can be merged with the Bloch's equation (A.4) where $\frac{1}{T_1} = \kappa_+ + \kappa_-$ and $\frac{1}{T_2} = \gamma + \frac{1}{2}(\kappa_+ + \kappa_-)$.

The general solution for this equation is:

$$\vec{S}(t) = \mathrm{e}^{-\gamma t}\mathrm{e}^{Mt}\left(\vec{S}_0 - \vec{S}_{\rm eq}\right) + \vec{S}_{\rm eq}, \tag{B.6}$$

with $\vec{S}_0 = \vec{S}(0)$.

The master equation equation (B.3) is a common form for TLS found in the literature [7, 65, 66]. Equation (B.5) which determines the EP interpolates between two extreme cases. The first is associated with spontaneous emission, then $\Gamma = \kappa_-$. The second is a hot singular bath dominated by pure dephasing, then $\Gamma = -\gamma$.

Appendix C. Eigenvalues of the matrix *M*

The task is to find the eigenvalues of the generator matrix (6).

We first define the variables:

$$\begin{aligned} Y &= 12\Delta^2 + 12\epsilon^2 - \Gamma^2 \\ X &= -36\Delta^2 + 18\epsilon^2 - \Gamma^2. \end{aligned} \tag{C.1}$$

We also define:

$$\begin{aligned} W &= \sqrt{\Gamma^2 X^2 + Y^3} \\ &= \left(\Gamma^4\Delta^2 + 16\left(\Delta^2 + \epsilon^2\right)^3 + \Gamma^2\left(8\Delta^4 - 20\Delta^2\epsilon^2 - \epsilon^4\right)\right)^{1/2}. \end{aligned} \tag{C.2}$$

With these definitions the eigenvalues of equation (6) become:

$$\begin{aligned} m_1 &= -\frac{2}{3}\Gamma + \frac{1}{6}\left((W + \Gamma X)^{1/3} - \frac{Y}{(W + \Gamma X)^{1/3}}\right) \\ m_2 &= -\frac{2}{3}\Gamma + \frac{1}{6}\left(\mathrm{e}^{\mathrm{i}\frac{2}{3}\pi}(W + \Gamma X)^{1/3} + \mathrm{e}^{\mathrm{i}\frac{1}{3}\pi}\frac{Y}{(W + \Gamma X)^{1/3}}\right) \\ m_3 &= -\frac{2}{3}\Gamma + \frac{1}{6}\left(\mathrm{e}^{-\mathrm{i}\frac{2}{3}\pi}(W + \Gamma X)^{1/3} + \mathrm{e}^{-\mathrm{i}\frac{1}{3}\pi}\frac{Y}{(W + \Gamma X)^{1/3}}\right). \end{aligned} \tag{C.3}$$

For real W (i.e. for $\Gamma^2X^2 + Y^3 \geqslant 0$) all eigenvalues are real. For $\Gamma^2X^2 + Y^3 < 0$, W is complex, and two of the eigenvalues are complex (complex conjugate to each other).

Non-Hermitian degeneracies of the eigenvalues occur when W vanishes. In such cases the second and third eigenvalues are degenerated, leading to EP2. A third order EP, EP3, occurs for $X = Y = 0$. This happens when $\Delta = \pm\sqrt{1/108}\ \Gamma$, $\epsilon = \sqrt{8/108}\ \Gamma$. These triple-degeneracies EP3 occur twice, and have a cusp-like behaviour, emerging from the EP2-curves, identifiable as an elliptic umbilic catastrophe [56]. This topology is also consistent with the analysis of non Hermitian degeneracies of a two-parameters family of 3×3 matrices, done by Mailybaev [57]. In very strong driving fields the matrix M will loose symmetry [58, 59] maintaining the cusps but skewing the topology.

Appendix D. Non analytic character close to the EP3

There is a special non analytic character close to the EP3: when $\nu \to \nu^{\rm EP3}$ and $\mathcal{E} \to \mathcal{E}^{\rm EP3}$ then the three frequencies obtained by the standard harmonic inversion coalesce, leading to a branch point (see ch 9 in [29]):

$$\omega_{k=1,2,3} = \omega_1^{(2)} + e^{i\frac{2\pi}{3}}\left[\alpha_k\left(\nu - \nu^{\mathrm{EP3}}\right) + \beta_k\left(\mathcal{E} - \mathcal{E}^{\mathrm{EP3}}\right)\right]^{\frac{1}{3}} \tag{D.1}$$

where α_k and β_k are parameters. At the EP3, i.e. for $\nu \to \nu^{\mathrm{EP3}}$ and $\mathcal{E} \to \mathcal{E}^{\mathrm{EP3}}$, we get $\partial\omega_k/\partial\nu \to \infty$ and $\partial\omega_k/\partial\mathcal{E} \to \infty$, leading to $\partial\Gamma/\partial\nu \to \infty$ and $\partial\Gamma/\partial\mathcal{E} \to \infty$.

References

[1] Bloch F 1946 Nuclear induction *Phys. Rev.* **70** 460
[2] Agarwal G S 1970 Master-equation approach to spontaneous emission *Phys. Rev.* A **2** 2038
[3] Cohen-Tannoudji C, Dupont-Roc J and Grynberg G 2008 Optical Bloch equations *Atom-Photon Interactions: Basic Process and Appilcations* (Paris: Wiley) pp 353–405
[4] DeVoe R G and Brewer R G 1983 Experimental test of the optical Bloch equations for solids *Phys. Rev. Lett.* **50** 1269–72
[5] Lloyd S 1995 Almost any quantum logic gate is universal *Phys. Rev. Lett.* **75** 346
[6] Zrenner A, Beham E, Stufler S, Findeis F, Bichler M and Abstreiter G 2002 Coherent properties of a two-level system based on a quantum-dot photodiode *Nature* **418** 612–4
[7] Gammelmark S and Mølmer K 2014 Fisher information and the quantum Cramér–Rao sensitivity limit of continuous measurements *Phys. Rev. Lett.* **112** 170401
[8] Clarke J and Wilhelm F K 2008 Superconducting quantum bits *Nature* **453** 1031–42
[9] Ladd T D, Jelezko F, Laflamme R, Nakamura Y, Monroe C and OBrien J L 2010 Quantum computers *Nature* **464** 45–53
[10] Lisi E, Marrone A and Montanino D 2000 Probing possible decoherence effects in atmospheric neutrino oscillations *Phys. Rev. Lett.* **85** 1166
[11] Six J 1982 Test of the non separability of the $k^0\bar{K}^0$ system *Phys. Lett.* B **114** 200–2
[12] Selleri F 1983 Einstein locality and the $k^0\bar{K}^0$ 946-1 0 system *Lett. Neovo Cim.* **36** 521
[13] Privitera P and Selleri F 1992 Quantum mechanics versus local realism for neutral kaon pairs *Phys. Lett.* B **296** 261–72
[14] Datta A and Home D 1986 Quantum non-separability versus local realism: a new test using the b0b0 system *Phys. Lett.* A **119** 3–6
[15] Lo Franco R, D'Arrigo A, Falci G, Compagno G and Paladino E 2014 Preserving entanglement and nonlocality in solid-state qubits by dynamical decoupling *Phys. Rev.* B **90** 054304
[16] Bell J S *et al* 2004 Speakable and unspeakable in quantum mechanics *Speakable and Unspeakable in Quantum Mechanics* (*Introduction by Alain Aspect* vol 2004) ed J S Bell (Cambridge: Cambridge University Press) p 1
[17] Essen L and Parry J V L 1955 An atomic standard of frequency and time interval: a cæsium resonator *Nature* **176** 280–2
[18] Giovannetti V, Lloyd S and Maccone L 2004 Quantum-enhanced measurements: beating the standard quantum limit *Science* **306** 1330–6
[19] Huelga S F, Macchiavello C, Pellizzari T, Ekert A K, Plenio M B and Cirac J I 1997 Improvement of frequency standards with quantum entanglement *Phys. Rev. Lett.* **79** 3865–8
[20] Arrad G, Vinkler Y, Aharonov D and Retzker A 2014 Increasing sensing resolution with error correction *Phys. Rev. Lett.* **112** 150801
[21] Wangsness R K and Bloch F 1953 The dynamical theory of nuclear induction *Phys. Rev.* **89** 728
[22] Bloch F 1957 Generalized theory of relaxation *Phys. Rev.* **105** 1206
[23] Brian Davies E 1974 Markovian master equations *Commun. Math. Phys.* **39** 91–110
[24] Kraus K 1983 *States, Effects and Operations* (Berlin: Springer)
[25] Lindblad G 1976 On the generators of quantum dynamical semigroups *Commun. Math. Phys.* **48** 119–30
[26] Gorini V, Kossakowski A and Sudarshan E C G 1976 Completely positive dynamical semigroups of *n*-level systems *J. Math. Phys.* **17** 821–5
[27] Breuer H-P and Petruccione F 2002 *The Theory of Open Quantum Systems* (Oxford: Oxford University Press)
[28] Mukamel S 1999 *Principles of Nonlinear Optical Spectroscopy* (Oxford: Oxford University Press) number 6
[29] Moiseyev N 2011 *Non-Hermitian Quantum Mechanics* (Cambridge: Cambridge University Press)
[30] Alicki R and Lendi K 2007 *Quantum Dynamical Semigroups and Applications* (*Lecture Notes in Physics* vol 717) (Berlin: Springer)
[31] Fano U 1961 Effects of configuration interaction on intensities and phase shifts *Phys. Rev.* **124** 1866–78
[32] Rotter I 2009 A non-Hermitian Hamilton operator and the physics of open quantum systems *J. Phys. A: Math. Theor.* **42** 153001
[33] Berry M V 2004 Physics of nonHermitian degeneracies *Czech. J. Phys.* **54** 1039–47
[34] Uzdin R and Moiseyev N 2012 Scattering from a waveguide by cycling a non-Hermitian degeneracy *Phys. Rev.* A **85** 031804
[35] Latinne O, Kylstra N J, Dörr M, Purvis J, Terao-Dunseath M, Joachain C J, Burke P G and Noble C J 1995 Laser-induced degeneracies involving autoionizing states in complex atoms *Phys. Rev. Lett.* **74** 46
[36] Cartarius H, Jörg Main and Wunner G 2007 Exceptional points in atomic spectra *Phys. Rev. Lett.* **99** 173003
[37] Uzdin R, Torre E G D, Kosloff R and Moiseyev N 2013 Effects of an exceptional point on the dynamics of a single particle in a time-dependent harmonic trap *Phys. Rev.* A **882** 022505
[38] Moiseyev N 2013 Sudden transition from a stable to an unstable harmonic trap as the adiabatic potential parameter is varied in a time-periodic harmonic trap *Phys. Rev.* A **88** 034502
[39] Magunov A I, Rotter I and Strakhova S I 1999 Laser-induced resonance trapping in atoms *J. Phys. B: At. Mol. Opt. Phys.* **32** 1669
[40] Magunov A I, Rotter I and Strakhova S I 2001 Laser-induced continuum structures and double poles of the *s*-matrix *J. Phys. B: At. Mol. Opt. Phys.* **34** 29
[41] Narevicius E and Moiseyev N 2000 Trapping of an electron due to molecular vibrations *Phys. Rev. Lett.* **84** 1681
[42] Rubinstein J, Sternberg P and Ma Q 2007 Bifurcation diagram and pattern formation of phase slip centers in superconducting wires driven with electric currents *Phys. Rev. Lett.* **99** 167003
[43] Cejnar P, Heinze S and Macek M 2007 Coulomb analogy for non-Hermitian degeneracies near quantum phase transitions *Phys. Rev. Lett.* **99** 100601
[44] Dembowski C, Gräf H-D, Harney H L, Heine A, Heiss W D, Rehfeld H and Richter A 2001 Experimental observation of the topological structure of exceptional points *Phys. Rev. Lett.* **86** 787
[45] Klaiman S, Günther U and Moiseyev N 2008 Visualization of branch points in p t-symmetric waveguides *Phys. Rev. Lett.* **101** 080402
[46] Müller M and Rotter I 2008 Exceptional points in open quantum systems *J. Phys. A: Math. Theor.* **41** 244018
[47] Müller M and Rotter I 2009 Phase lapses in open quantum systems and the non-Hermitian Hamilton operator *Phys. Rev.* A **80** 042705
[48] Wiersig J 2014 Enhancing the sensitivity of frequency and energy splitting detection by using exceptional points: application to microcavity sensors for single-particle detection *Phys. Rev. Lett.* **112** 203901

[49] Wall M R and Neuhauser D 1995 Extraction, through filter-diagonalization, of general quantum eigenvalues or classical normal mode frequencies from a small number of residues or a short-time segment of a signal: I. Theory and application to a quantum-dynamics model *J. Chem. Phys.* **102** 8011–22
[50] Mandelshtam V A 2001 Fdm: the filter diagonalization method for data processing in nmr experiments *Prog. Nucl. Magn. Reson. Spectrosc.* **38** 159–96
[51] Belkić D, Dando P A, Main J and Taylor H S 2000 Three novel high-resolution nonlinear methods for fast signal processing *J. Chem. Phys.* **113** 6542–56
[52] Fuchs J, Main J, Cartarius H and Wunner G 2014 Harmonic inversion analysis of exceptional points in resonance spectra *J. Phys. A: Math. Theor.* **47** 125304
[53] Noh H-R and Jhe W 2010 Analytic solutions of the optical Bloch equations *Opt. Commun.* **283** 2353–5
[54] Moroz A 2012 On unorthodox solutions of the Bloch equations (arXiv:1208.5736)
[55] Noh H R 2015 Optical Bloch equations for a two-level atom revisited: analytical solutions *J. Phys. Soc. Japan* **84** 094402
[56] Berry M V, Nye J F and Wright F J 1979 The elliptic umbilic diffraction catastrophen *Phil. Trans. R. Soc.* A **291** 453–84
[57] Mailybaev A A 2006 Computation of multiple eigenvalues and generalized eigenvectors for matrices dependent on parameters *Numer. Linear Algebr. Appl.* **13** 419–36
[58] Geva E, Kosloff R and Skinner J L 1995 On the relaxation of a two-level system driven by a strong electromagnetic field *J. Chem. Phys.* **102** 8541–61
[59] Szczygielski K, Gelbwaser-Klimovsky D and Alicki R 2013 Markovian master equation and thermodynamics of a two-level system in a strong laser field *Phys. Rev.* E **87** 012120
[60] Benko U and Juričić D 2008 Frequency analysis of noisy short-time stationary signals using filter-diagonalization *Signal Process.* **88** 1733–46
[61] Hu H, Van Q N, Mandelshtam V A and Shaka A J 1998 Reference deconvolution, phase correction, and line listing of {NMR} spectra by the 1d filter diagonalization method *J. Magn. Reson.* **134** 76–87
[62] Celik H, Shaka A J and Mandelshtam V A 2010 Sensitivity analysis of solutions of the harmonic inversion problem: are all data points created equal? *J. Magn. Reson.* **206** 120–6
[63] Martini B R, Aizikov K and Mandelshtam V A 2014 The filter diagonalization method and its assessment for Fourier transform mass spectrometry *Int. J. Mass Spectrom.* **373** 1–4
[64] Emch G G and Varilly J C 1979 On the standard form of the Bloch equation *Lett. Math. Phys.* **3** 113–6
[65] Fogli G L, Lisi E, Marrone A, Montanino D and Palazzo A 2007 Probing nonstandard decoherence effects with solar and kamland neutrinos *Phys. Rev.* D **76** 033006
[66] Gammelmark S, Mølmer K, Alt W, Kampschulte T and Meschede D 2014 Hidden markov model of atomic quantum jump dynamics in an optically probed cavity *Phys. Rev.* A **89** 043839

4.6 Parameter estimation in atomic spectroscopy using exceptional points

Parameter estimation in atomic spectroscopy using exceptional points
Morag Am-Shallem, Ronnie Kosloff, and Nimrod Moiseyev
Published at *Phys. Rev. A* 93, 032116 (2016)

Parameter estimation in atomic spectroscopy using exceptional points

Morag Am-Shallem and Ronnie Kosloff

The Fritz Haber Research Center and The Institute of Chemistry, The Hebrew University, Jerusalem 91904, Israel

Nimrod Moiseyev

Schulich Faculty of Chemistry and Faculty of Physics,
Technion, Haifa 3200008, Israel

Abstract. The dynamics of spontaneous emission of an atomic system is studied in the framework of an open quantum system. The resulting quantum master equation for the atomic system is non hermitian. The generator $\mathcal{L}$ can possess non-hermitian degeneracies, i.e. exceptional points (EP), for specific values of the external laser driving amplitude and detuning from the atomic lines. We suggest to employ the special properties of these EPs for accurate parameter estimation. The method is demonstrated for the atomic spectrum of $S \to P$ transitions of ^{85}Rb and ^{40}Ca $^{+}$.

1. Introduction: Electronic transitions and spontaneous emission in atomic systems

Atomic spectroscopy is unique in its experimental accuracy, able to achieve a dynamical range of precision of up to 18 significant digits. High-performance frequency standards is the technological result of this precision leading to applications such as network synchronization and GPS [1]. This technology is enabled by atomic clocks [2, 3]. High accuracy has implications in other fields of physics such as radioastronomy (very-long-baseline interferometry) [4], tests of general relativity [5], and particle physics [6]. Atomic spectroscopy has been a primary source of fundamental constants [7]. For example, a small deviation of the Rydberg constant can indicate the radius of the proton [8].

1.1. Electronic transitions and spontaneous emission

Atomic spectroscopy is the study of electronic transition in atoms. The spectral lines correspond to Bohr frequencies of the transitions between energy levels of the atom. Within this viewpoint the spectral theory involves calculating the eigenvalues of the atomic hermitian Hamiltonian. The observed spectrum is then predicted by

perturbation theory assuming weak excitation and knowledge of the transition dipole matrix elements.

The simple picture of atomic spectroscopy is hampered by the notion that atoms are imbedded in the radiation field. The primary influence is spontaneous emission and Lamb shifts [9]. In principle one can employ quantum field theory and treat the radiation field and the atom using a Hamiltonian description [10].

$$\hat{\mathbf{H}} = \hat{\mathbf{H}}_{atom} + \hat{\mathbf{H}}_{radiation} + \hat{\mathbf{H}}_{interaction}. \tag{1}$$

Our aim is to concentrate on the atomic spectra. We therefore employ a reduced description where we derive effective equations of motion for the atomic system by tracing out the radiation field. This is the approach incorporated in open quantum systems. In this case the reduced dynamics is described by a non-hermitian generator $\mathcal{L}$. We will show that due to non-hermitian degeneracies there is a profound and unexpected influence on the atomic spectrum.

1.2. The L-GKS equation for spontaneous emission

The phenomena of spontaneous emission (SE) cannot be described by a unitary description, such as the Schrödinger equation for the wave function, or the counterpart Liouville-von-Neumann master equation for density matrices. Hamiltonian-based approaches incorporate only coherent dynamics. Dissipation and dephasing phenomena are properly described by the quantum master equation [11, 12]. The general structure of the quantum master equation was introduced by Lindblad [13] and Gorini, Kossakowski and Sudarshan [14] (L-GKS). Based on a mathematical construction they obtained the general structure of the generator $\mathcal{L}$ of a completely positive dynamical semigroup. The L-GKS master equation (known also as the Lindblad equation) adds dissipative terms to the master equation which handles SE:

$$\frac{\partial \hat{\boldsymbol{\rho}}}{\partial t} = \mathcal{L}\hat{\boldsymbol{\rho}} = -\frac{i}{\hbar}\left[\hat{\mathbf{H}}, \hat{\boldsymbol{\rho}}\right] + \sum_{(a,b)} \Gamma_{a\to b}\left(\hat{\mathbf{A}}_{(a,b)}\,\hat{\boldsymbol{\rho}}\,\hat{\mathbf{A}}^{\dagger}_{(a,b)} - \frac{1}{2}\left[\hat{\mathbf{A}}^{\dagger}_{(a,b)}\hat{\mathbf{A}}_{(a,b)}, \hat{\boldsymbol{\rho}}\right]_{+}\right), \tag{2}$$

where the $[\cdot,\cdot]$ denotes a commutator, and the $[\cdot,\cdot]_{+}$ denotes an anti commutator.

The first term is the commutator of the Hamiltonian with the density matrix, which generates the unitary dynamics. The second term is the dissipator, which generates the spontaneous emission. The sum is over the pairs of levels (a, b): Each of the annihilation operators

$$\hat{\mathbf{A}}_{(a,b)} \equiv \hat{\mathbf{A}}_{a\to b} = |b\rangle\langle a| \tag{3}$$

generate a decay from the upper source level $|a\rangle$ to the lower destination level $|b\rangle$. The anti commutator $\left[\hat{\mathbf{A}}^{\dagger}_{(a,b)}\hat{\mathbf{A}}_{(a,b)}, \hat{\boldsymbol{\rho}}\right]_{+}$ expresses the decrease in population of the excited state $|a\rangle$, while the resulting increase of population of the lower state $|b\rangle$ is expressed by the term $\hat{\mathbf{A}}_{(a,b)}\,\hat{\boldsymbol{\rho}}\,\hat{\mathbf{A}}^{\dagger}_{(a,b)}$. Note that the anti commutator contains the term

$$\hat{\mathbf{A}}^{\dagger}_{(a,b)}\hat{\mathbf{A}}_{(a,b)} = (|a\rangle\langle b|)\,(|b\rangle\langle a|) = |a\rangle\langle a| \equiv \hat{\mathbf{P}}_a, \tag{4}$$

where $\hat{\mathbf{P}}_a$ is the projection operator, projecting on the subspace spanned by $|a\rangle$. Therefore, the decrease in population of the excited state is expressed using only the population on this state, and does not require knowledge of other states.

The decay rate for the pair of levels (b, a), $\Gamma_{a\to b}$, can be obtained by a microscopic derivation of the quantum optical master equation from the Hamiltonian of Eq. (1) under the weak coupling limit. The Born-Markov approximation is employed where the perturbation parameter is the dipole interaction between the atom and the radiation at temperature $T = 0$. The rate obtained is equivalent to the golden rule formula [15]:

$$\Gamma_{a\to b} = \frac{4}{3}\frac{\omega_{ab}^3}{\hbar c^3}\left|d_{ab}\right|^2 \tag{5}$$

with ω_{ab} as the transition frequency, c the speed of light, and d_{ab} the transition dipole matrix element. For states with defined angular momentum, the transition dipole matrix element becomes:

$$\Gamma_{a\to b} = \frac{4}{3}\frac{\omega_{ab}^3}{c^2}\alpha\frac{\left|\langle J_a\left|\left|\hat{\mathbf{r}}\right|\right|J_b\rangle\right|^2}{2J_b+1}. \tag{6}$$

Here, α is the fine structure constant, and J_a, J_b are the angular momenta of the states $|a\rangle$ and $|b\rangle$. $\langle J_a\left|\left|\hat{\mathbf{r}}\right|\right|J_b\rangle$ is the reduced dipole matrix element between J_a and J_b.

The total decay rate from a state $|a\rangle$ is the sum $\Gamma_a = \sum_b \Gamma_{a\to b}$. This decay rate defines the lifetime of the excited state: $\tau_a = \Gamma_a^{-1}$.

The spontaneous emission rate is completely determined by the fundamental physical constants: i.e. magnetic moment of the electron and the nuclei, etc. These constants determine the values of the energy levels splitting and lifetime. By inversion, an accurate measurement of the energies and lifetime constitutes an appropriate determination of universal parameters.

1.3. Population leakage

Typically in atomic systems the excitation and de-excitation transitions are not closed. Population can leak to other levels of the atomic system. The population is expressed by the diagonal entries in the density matrix $\hat{\boldsymbol{\rho}}$, and the total population is $\mathrm{Tr}\{\hat{\boldsymbol{\rho}}\}$. The dissipative term in Eq. (2) conserves the total population in the system, i.e. $\partial_t \mathrm{Tr}\{\hat{\boldsymbol{\rho}}(t)\} = 0$. To incorporate population loss we utilize the fact that decrease of population in an excited state is described by the anti commutator terms, which uses only the population on this state and does not require knowledge about other states. Therefore the dissipator $\mathcal{L}$ will include additional terms composed only from the anti commutators. Such terms cause a decrease in the population of the excited state which are not compensated by an increase of population of other states. For each excited state $|a\rangle$ the additional term will have the form:

$$\mathcal{L}_{leak}^{(a)}\hat{\boldsymbol{\rho}} = -\frac{1}{2}\Gamma_{a,leak}\left[\hat{\mathbf{P}}_a, \hat{\boldsymbol{\rho}}\right]_+. \tag{7}$$

The total decay rate from the state $|a\rangle$ is now $\Gamma_a = \Gamma_{a,leak} + \sum_b \Gamma_{a\to b}$. We define $\chi_a = \Gamma_{leak}/\Gamma_a$ as the *branching fraction* that decays from the excited state $|a\rangle$ to states

out of the primary system. Introducing such leaking terms into the dissipator reduces the total population, and therefore $\partial_t \mathrm{Tr}\{\hat{\boldsymbol{\rho}}(t)\} < 0$.

The total spontaneous emission part of the L-GKS equation will have the form:

$$\begin{aligned}\mathcal{L}_{SE}\hat{\boldsymbol{\rho}} &= \sum_a \left(\sum_b \Gamma_{a\to b} \left(\hat{\mathbf{A}}_{(a,b)}\, \hat{\boldsymbol{\rho}}\, \hat{\mathbf{A}}^{\dagger}_{(a,b)} - \tfrac{1}{2} \left[\hat{\mathbf{P}}_a, \hat{\boldsymbol{\rho}} \right]_+ \right) - \tfrac{1}{2} \Gamma_{a,leak} \left[\hat{\mathbf{P}}_a, \hat{\boldsymbol{\rho}} \right]_+ \right) \\ &= \sum_a \sum_b \Gamma_{a\to b} \left(\hat{\mathbf{A}}_{(a,b)}\, \hat{\boldsymbol{\rho}}\, \hat{\mathbf{A}}^{\dagger}_{(a,b)} - \tfrac{1}{2} \Gamma_a \left[\hat{\mathbf{P}}_a, \hat{\boldsymbol{\rho}} \right]_+ \right).\end{aligned} \tag{8}$$

If the excited state $|a\rangle$ decays to a manifold B with N_B states $|b\rangle \in B$ with equal decay rate, then we have $\Gamma_{a\to b} = (1-\chi_a)\Gamma_a / N_B$. The spontaneous emission part will have the form:

$$\mathcal{L}_{SE}\hat{\boldsymbol{\rho}} = \sum_a \Gamma_a \left(\frac{(1-\chi_a)}{N_B} \sum_{b\in B} \hat{\mathbf{A}}_{(a,b)}\, \hat{\boldsymbol{\rho}}\, \hat{\mathbf{A}}^{\dagger}_{(a,b)} - \frac{1}{2} \left[\hat{\mathbf{P}}_a, \hat{\boldsymbol{\rho}} \right]_+ \right). \tag{9}$$

1.4. Pure dephasing

Pure dephasing is the loss of coherence without change in population. Random fluctuations of the energy levels will generate pure dephasing. A possible mechanism is caused by elastic collisions with other atoms in the chamber. An additional mechanism is caused by noise in the monitoring or driving laser. As a result, the pure dephasing rate can be controlled, for example by changing the density of the atomic gas, or by generating fluctuations in the external field. We denote the pure dephasing rate by Γ_{deph}.

Within the L-GKS equation pure dephasing is described by a generator $\mathcal{L}$ which commutes with the Hamiltonian, for example $\mathcal{L} = \Gamma_{deph} \left[\hat{\mathbf{H}}, \left[\hat{\mathbf{H}}, \cdot \right] \right]$

1.5. The Heisenberg form

An alternative description is to describe the dynamics in an operator base. As a result the L-GKS equation is employed in the Heisenberg representation [16, 15, 17], the hermitian conjugate of Eq. (2). The equation of motion for an operator $\hat{\mathbf{X}}$ becomes:

$$\frac{d}{dt}\hat{\mathbf{X}} = \frac{\partial \hat{\mathbf{X}}}{\partial t} + \frac{i}{\hbar} \left[\hat{\mathbf{H}}, \hat{\mathbf{X}} \right] + \sum_{(a,b)} \Gamma_{a\to b} \left(\hat{\mathbf{A}}^{\dagger}_{(a,b)} \hat{\mathbf{X}} \hat{\mathbf{A}}_{(a,b)} - \frac{1}{2} \left[\hat{\mathbf{P}}_a, \hat{\mathbf{X}} \right]_+ \right). \tag{10}$$

For system with population leakage the equation will have additional anti commutator terms as in Eqs. (8) and (9).

2. Dynamics of driven open atomic systems at the exceptional points

The dynamics generated by $\mathcal{L}$ will be represented by an explicit matrix vector notation. The density matrix $\hat{\boldsymbol{\rho}}$, which is an element in Liouville space, is represented as a vector, while $\mathcal{L}$, which is a linear superoperator operating in this space, is represented by a matrix. There are a few methods to generate such a representation cf. a recent

demonstration [17]. In this study we employed the Heisenberg approach for the two-level systems, and the vec-ing approach for larger systems. The vec-ing approach flattens the density matrix into a vector, representing the L-GKS generator by an appropriate matrix. This results in $N^2 \times N^2$ matrices for the L-GKS generator. We denote the vector representation of the density matrix $\hat{\boldsymbol{\rho}}$ as $\vec{\rho}$, and the matrix representation of $\mathcal{L}$ by L. In this notation, Eq. (2), is expressed by a matrix-vector equation:

$$\dot{\vec{\rho}} = L\vec{\rho} \tag{11}$$

The eigenvalues of the matrix L reflect the non-hermitian dynamics generated by $\mathcal{L}$. In general they are complex with the steady state eigenvector having an eigenvalue of zero.

2.1. L-GKS Dynamics and exceptional points

The solution for Eq. (2), given an initial density matrix $\hat{\boldsymbol{\rho}}_0$, and assuming that the generator $\mathcal{L}$ is time-independent, can be formally expressed by:

$$\hat{\boldsymbol{\rho}}(t) = e^{\mathcal{L}t}\hat{\boldsymbol{\rho}}_0. \tag{12}$$

In the matrix-vector representation we have:

$$\vec{\rho}(t) = e^{Lt}\vec{\rho}(0). \tag{13}$$

The dynamics described by Eq. (13) typically is described by a sum of decaying oscillatory exponentials. The dynamics of expectation values of operators, as well as other correlation functions, will have the analytical form (see Appendix A):

$$\langle X(t)\rangle = \sum_k d_k \exp[-i\omega_k t] \,, \tag{14}$$

where $-i\omega_k$ are the eigenvalues of L, d_k are the associated amplitudes, and both ω_k and d_k can be complex.

The spectrum of the non-hermitian matrix L is a function of the external parameters of the system. For specific values the spectrum becomes incomplete. This is due to the coalescence of several eigenvectors, denoted as a non-hermitian degeneracy. For such parameters the matrix L is not diagonalizable. Such points in the parameter space are known as *exceptional points* (*EP*). At the exceptional point the dynamics has a polynomial character. The temporal value of expectation values of operators has the form:

$$\langle X(t)\rangle = \sum_k \sum_{\alpha=0}^{r_k} d_{k,\alpha} t^\alpha \exp[-i\omega_k^{(r_k)} t] \,, \tag{15}$$

which replaces the form of Eq. (14) (see Appendix A).

When two eigenvalues of the master equations coalesce into one, a second-order non-hermitian degeneracy is obtained. We refer to it as a second order exceptional point and denote it with *EP2*. A third-order non-hermitian degeneracy is denoted by *EP3*. There are points in the parameter space in which n pairs of eigenvectors coalesce, each pair into a distinct eigenvector. They will be denoted as $EP2^n$.

2.2. Identification of EP*s using the dynamics*

The analytical form of decaying exponentials, Eq. (14), is used in harmonic inversion methods to find the frequencies and amplitudes of the time series signal [18, 19, 20]. Harmonic inversion methods are widely used for analysis of experiments in diverse fields such as NMR spectroscopy [21], Fourier transform mass spectrometry [22], and ultrafast pump-probe molecular spectroscopy [23].

However, at exceptional points the analytical form is different: Fuchs et al. showed that applying standard harmonic inversion methods, which were designed for Eq. (14), to a signal generated by Eq. (15), leads to divergence of the amplitudes d_k [24]. We used the Padé approximant harmonic inversion algorithm presented in Refs. [20, 24]. The divergence of the amplitudes d_k in the vicinity of exceptional points is employed to accurately locate them in the parameter space [24, 25].

2.3. Parameter estimation using EP*s*

The ability to accurately locate the *EP*s in the parameter space is used for parameter estimation. The procedure is as follows:

(i) Accurately locate in the parameter space the desired exceptional point by iterating the following steps:
   (a) Perform an experiment to obtain a time series of a physical observable.
   (b) Obtain the characteristic frequencies and amplitudes of the signal.
   (c) In the parameter space, estimate the direction and distance to the *EP* and determine new parameters for the next iteration.

(ii) At the *EP*, invert the relations between the characteristic frequencies and the system parameters to obtain the system parameters.

The accurate location of the exceptional points, followed by inverting the relations, will lead to an accurate parameter estimation. This procedure was used to estimate the parameters of the Bloch system from iterations of time series [25]. This parameter estimation is robust to uncertainties in the location of the *EP*s. The noise sensitivity is affected by the harmonic inversion. See a short discussion regarding noise in harmonic inversion methods in Appendix C.

3. Effective two-level systems and Bloch-like *EP*s

3.1. Closed two-level systems

Under the influence of polarized driving fields, some atomic transitions behave as a closed two-level system. An example is the transition between the hyperfine states $\left|5^2\mathbf{S}_{1/2}, F=3, m_F=3\right\rangle$ and $\left|5^2\mathbf{P}_{3/2}, F=4, m_F=4\right\rangle$ of the ^{85}Rb atom, with σ^+ polarization. The selection rules impose that all the transitions - stimulated and spontaneous - occur only between these states. The system parameters are: System

frequency of ω_s=384.229241689 THz (assuming no Zeeman splitting), decay rate of Γ=38.117$\times 10^6 s^{-1}$, and dipole moment of μ=2.98931 ea_0 [26]. We define the detuning between the system frequency ω_s and the electromagnetic field carrier frequency ω_s as $\Delta = \omega_s - \omega_L$. The resonance Rabi frequency is $\Omega_R = -\mu E_0/\hbar$, where E_0 is the amplitude of the electromagnetic field.

We employ the Heisenberg representation to describe the dynamics. We define $|s\rangle$ as the lower state, and $|p\rangle$ as the upper state. The dynamics are described by the set of operators:

$$\begin{array}{rcl} \hat{\mathbf{X}} & \equiv & |s\rangle\langle p| + |p\rangle\langle s| \\ \hat{\mathbf{Y}} & \equiv & |s\rangle\langle p| - |p\rangle\langle s| \\ \hat{\mathbf{Z}} & \equiv & |p\rangle\langle p| - |s\rangle\langle s| \\ \hat{\mathbf{I}} & \equiv & |p\rangle\langle p| + |s\rangle\langle s| \end{array} . \tag{16}$$

We form a four-vector from these operators. We write the Heisenberg equations, Eq. (10), for the operators in this vector, and get a differential equation with a 4×4 matrix [17]. The conservation of population is expressed by $\frac{d}{dt}\hat{\mathbf{I}} = 0$. Therefore we can omit the equation for the operator $\hat{\mathbf{I}}$, and add an inhomogeneous term instead. This results in the Bloch equations [25]. To find the exceptional points we need only the homogeneous part of the equation, which is incorporated in the matrix:

$$\mathrm{M} = \begin{pmatrix} -\frac{\Gamma}{2} & \Delta & 0 \\ -\Delta & -\frac{\Gamma}{2} & \Omega_R \\ 0 & -\Omega_R & \Gamma \end{pmatrix} . \tag{17}$$

The *EP*s of this matrix compose a deltoid-like curve. The curve is demonstrated in Figure 1 (the $\chi = 0$ curve. The other curves in this Figure refer to systems with population leakage and will be described below). The cusps of this *EP*-curve are identified as *EP3*. The accurate location of the *EP*3 can be used to estimate the parameters of such systems, as described on Section 2.3 above and in a previous study [25].

3.2. Two-level systems with population leakage

The Bloch equation can be extended to include SE that leaks into states that are external to the Hamiltonian, resulting in population loss, see Section 1.3 above. Here are two examples for such systems:

- *Rubidium atom.* Consider the TLS composed by the two hyperfine states $\left|5^2\mathbf{S}_{1/2}, F = 3, m_F = 2\right\rangle$ and $\left|5^2\mathbf{P}_{3/2}, F = 4, m_F = 3\right\rangle$ of the ^{85}Rb atom [26], with σ^+ polarization. The selection rules impose stimulated transitions between these states, but the excited state, $\left|5^2\mathbf{P}_{3/2}, F = 4, m_F = 3\right\rangle$, decays spontaneously also to other states in the system. Under σ^+ polarization there are no transitions from these other states back to the TLS. Therefore we can treat this system as a TLS with population loss.

- *Calcium ion.* Consider the TLS composed by the two states $\left|4^2\mathbf{S}_{1/2}, m_J = -1/2\right\rangle$ and $\left|4^2\mathbf{P}_{1/2}, m_J = 1/2\right\rangle$ of the $^{40}Ca^+$ ion, with σ^+ polarization (Cf. Section 4.2 and Figure 2 below). Again, there are stimulated transitions between these states, but the excited states decay also to $\left|3^2\mathbf{D}_{3/2}\right\rangle$ states ($\approx 6.5\%$ of the decay rate) and to the state $\left|4^2\mathbf{S}_{1/2}, m_J = 1/2\right\rangle$ (50% of the remaining decay rate). The population on these states does not revert to the TLS [27].

  The Heisenberg equation in this case is (cf. Eq. (9) with $N_B = 1$ and Eq. (10)):

$$\frac{d}{dt}\hat{\mathbf{O}} = \frac{i}{\hbar}\left[\hat{\mathbf{H}}, \hat{\mathbf{O}}\right] + \Gamma\left((1-\chi)\hat{\mathbf{S}}_+\hat{\mathbf{O}}\hat{\mathbf{S}}_- - \frac{1}{2}\left[\hat{\mathbf{S}}_+\hat{\mathbf{S}}_-, \hat{\mathbf{O}}\right]_+\right). \tag{18}$$

Here Γ is the total decay rate of the excited state. It is the sum of the decay rate into the lower level $|s\rangle$ as in Eq. (10) above, and of the decay rate out of the system as in Eq. (7). χ is the branching fraction that decays to states out of the primary system. $\hat{\mathbf{S}}_+ \equiv |p\rangle\langle s|$ and $\hat{\mathbf{S}}_- \equiv |s\rangle\langle p|$ are the raising and lowering operators. We write the equations for the four operators of Eq. (16). In this case $\frac{d}{dt}\hat{\mathbf{I}} \neq 0$ and we cannot omit the equation for this operator. The resulting set of equations is:

$$\frac{d}{dt}\begin{pmatrix}\hat{\mathbf{X}}\\ \hat{\mathbf{Y}}\\ \hat{\mathbf{Z}}\\ \hat{\mathbf{I}}\end{pmatrix} = \begin{pmatrix} -\frac{1}{2}\Gamma & \Delta & 0 & 0\\ -\Delta & -\frac{1}{2}\Gamma & \Omega_R & 0\\ 0 & -\Omega_R & -\left(1-\frac{\chi}{2}\right)\Gamma & -\left(1-\frac{\chi}{2}\right)\Gamma\\ 0 & 0 & -\frac{\chi}{2}\Gamma & -\frac{\chi}{2}\Gamma \end{pmatrix}\begin{pmatrix}\hat{\mathbf{X}}\\ \hat{\mathbf{Y}}\\ \hat{\mathbf{Z}}\\ \hat{\mathbf{I}}\end{pmatrix}. \tag{19}$$

The rate of population decay out of the system is $\chi\Gamma$, and therefore the lifetime of the population is τ/χ, which is larger than the lifetime without leakage.

When we look at the exceptional points of this matrix, we find that the shape of *EP*-curves is determined by the loss parameter χ. Figure 1 shows *EP*-curves for different values of χ. The total decay rate Γ can be calculated from the eigenvalues of the matrix in Eq. (19): the sum of the eigenvalues is always 2Γ. The branching fraction χ of a given system can be found by fitting the resulting *EP*-curve to the appropriate branching fraction.

4. *EP*s in the H line of the Calcium ion

4.1. The $^{40}Ca^+$ ion

The ^{40}Ca is the most abundant Calcium isotope. The total spin of the ^{40}Ca nucleus vanishes. The ground state of the $^{40}Ca^+$ ion, includes 18 electrons in closed shells, and the remaining single electron occupying the lower orbital of the 4^{th} shell. Therefore $^{40}Ca^+$ ion is isoelectronic to alkali metals. However, since the total spin of the nucleus vanishes, there is no hyperfine structure.

The structure of the energy levels of the $^{40}Ca^+$ ion have been found to be suitable for many applications. In particular, $^{40}Ca^+$ has been used in the field of quantum computing and quantum information [28, 29, 30, 31, 32, 33], for atomic clocks and the frequency standard [34, 35, 3, 2, 1, 36, 37] and recently as a single-atom heat engine

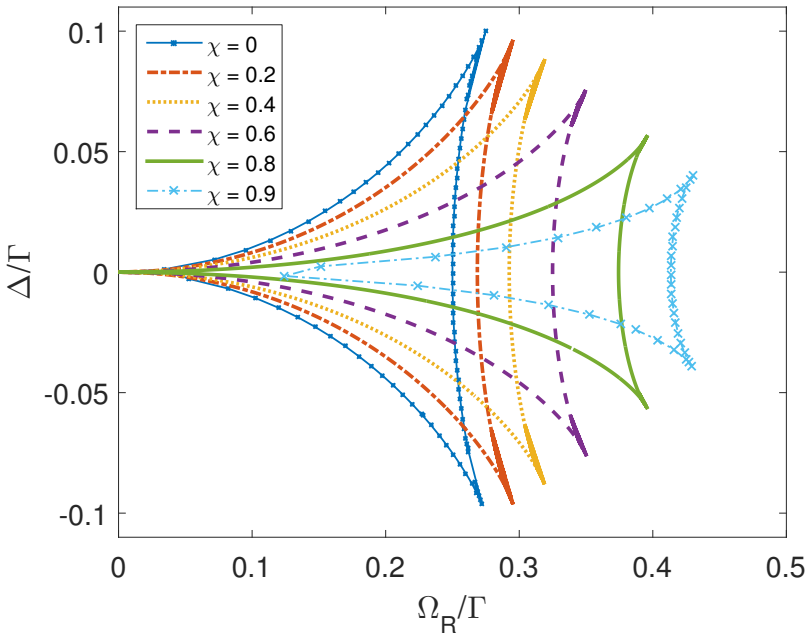

Figure 1. A map of the Bloch-like *EP*-curves of the matrix in Eq. (19), which describes the dynamics of a two-level system with spontaneous emission, when some of the excited population decays out of the system, with χ as the branching fraction. Figure in scaled coordinates could correspond to any leaking TLS such as Rb or Ca^+. The curves are two-fold non-hermitian degeneracy (*EP2*). The curves merge into cusps which are identified as *EP3*. The map of the *EP*-curves can be used for estimation of the system parameters: the system frequency, the decay rate, and the branching fraction.

[38]. The spectrum of $^{40}Ca^+$ has been also employed in the quest for drifts of the fine structure constant over a time span of many billion years [39, 40].

4.2. The H transition of the $^{40}Ca^+$ system

At the ground electronic state the electron occupies the orbital 4s, with an orbital angular momentum $l = 0$. The total angular momentum including the electron spin becomes $j = \frac{1}{2}$. The spectroscopic notation for the ion at this state is $4^2S_{1/2}$. At the first excited electronic state, the electron occupies the orbital 4p, with an orbital angular momentum $l = 1$. This state has a fine structure splitting due to spin-orbit coupling either $j = \frac{1}{2}$ (denoted as $4^2P_{1/2}$), or $j = \frac{3}{2}$ (denoted as $4^2P_{3/2}$).

The transition from $4^2S_{1/2}$ to $4^2P_{1/2}$ is known as the H line. The transition from $4^2S_{1/2}$ to $4^2P_{3/2}$ is known as the K line. These terms stem from the study of the solar spectrum. In the following we concentrate on the H line, i.e. the $4^2S_{1/2} \Leftrightarrow 4^2P_{1/2}$ transition. The frequency of this transition was measured to be 755222766.2(1.7)MHz [39]. The $4^2P_{1/2}$ has a lifetime of $\tau \approx 7ns$, and it spontaneously decays back to the $4^2S_{1/2}$ state, as well as to the $3^2D_{3/2}$ state. The branching between these two decays is $\Gamma_{P\to S} \approx 0.935 \times \Gamma_{total}$. We treat the decay into the $3^2D_{3/2}$ state as leakage out of

the system, with $\chi = 1 - 0.935 = 0.065$. Each of the states $4^2S_{1/2}$ and $4^2P_{1/2}$ is two-fold degenerated, with sub-levels of $m_j = \pm\frac{1}{2}$. When an external magnetic field is applied, the Zeeman effect removes degeneracies. The magnetic-field-dependent shift in the transition frequency is $\pm 19\text{kHz}/\mu\text{T}$ for the $\Delta m = \pm 1$ transitions (i.e., the transitions that is induced by circularly polarized electromagnetic fields) [39]. This shift is the sum of two contributions: The decrease of energy of the lower sub-level of the $S_{1/2}$ ($\approx$75%) and the increase of the upper sub-level of the $P_{1/2}$ ($\approx$25%). The ratio is determined by the appropriate Landé factors. For a linearly polarized electromagnetic field, $\Delta m = 0$ transitions are induced. Therefore, we expect to obtain only half of the above shift, i.e. $\pm 9.5\text{kHz}/\mu\text{T}$. However, in weak magnetic fields this shift is obscured by the natural linewidth in the standard frequency-domain spectroscopy [39, for example]. A scheme of the relevant energy levels is presented in Fig. 2.

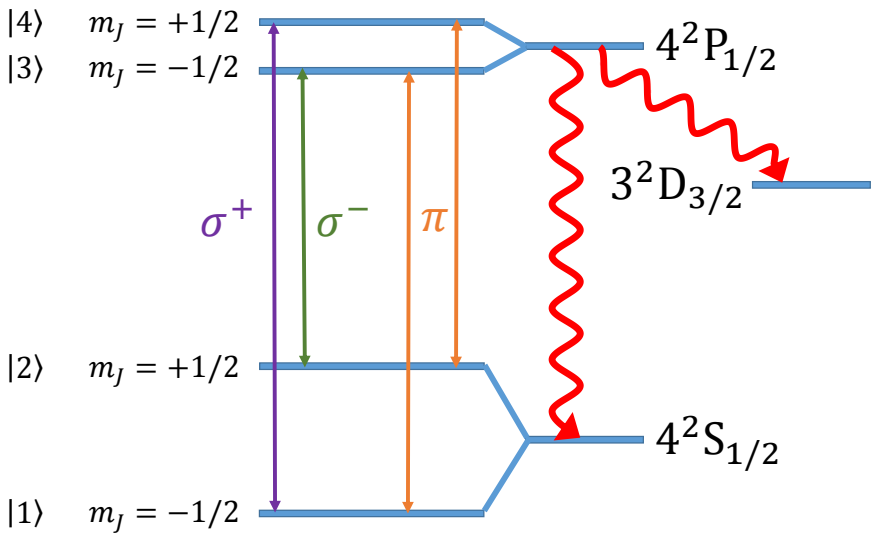

Figure 2. A scheme of the relevant energy levels in $^{40}Ca^+$. The $^2S_{1/2}$ and $^2P_{1/2}$ orbitals have total angular momentum of $j = \frac{1}{2}$. They are split by magnetic field two sub-levels of $m_j \pm \frac{1}{2}$. External electromagnetic fields with σ^+ and σ^- circular polarizations induce $\Delta m = +1$ and $\Delta m = -1$ transitions, respectively. Linearly polarized electromagnetic fields (π polarization) induce $\Delta m = 0$ transitions. The excited population at the $^2P_{1/2}$ state spontaneously decays to the $^2S_{1/2}$ and $^2D_{3/2}$ states. Energy levels are not to scale.

4.3. The system model

The energy levels structure and the spontaneous emission of the $^{40}Ca^+$ ion system allow the use of *EP*s in the task of parameter estimation. The reduced system Hamiltonian includes of 4 levels (see Figure 2 for a sketch of these levels). The $4^2S_{1/2}$ sub levels are denoted as $|1\rangle$ and $|2\rangle$, and the $4^2P_{1/2}$ sub levels are denoted as $|3\rangle$ and $|4\rangle$. The rotating wave Hamiltonian, under the influence of an oscillating electromagnetic field

of detuning Δ and amplitude Ω_R, and under a constant magnetic field which induces a split of ω_{21} between the two $S_{1/2}$ sub-levels, and a split of ω_{43} between the two $P_{1/2}$ sub-levels, is:

$$\hat{\mathbf{H}}_0 = \hbar \begin{pmatrix} \frac{1}{2}(\omega_{43}-\Delta) & 0 & \Omega_R & 0 \\ 0 & \frac{1}{2}(-\omega_{43}-\Delta) & 0 & \Omega_R \\ \Omega_R & 0 & \frac{1}{2}(\omega_{21}+\Delta) & 0 \\ 0 & \Omega_R & 0 & \frac{1}{2}(-\omega_{21}+\Delta) \end{pmatrix}. \quad (20)$$

The spontaneous emission is incorporated into the dynamics by the dissipative part of the L-GKS equation, as described in Section 1.2 above. We used the operators

$$\hat{\mathbf{A}}_{p\to s} \equiv |s\rangle\langle p|, \quad (21)$$

where $|s\rangle$ denotes the states of the two lower levels - $|1\rangle$ and $|2\rangle$, and $|p\rangle$ denotes the states of the upper levels - $|3\rangle$ and $|4\rangle$. This results in four terms in the dissipator, where each of the $P_{1/2}$ sub-levels decays to each of the $S_{1/2}$ sub-levels, with rate of $\Gamma_{P_i\to S_k} = \frac{1}{2}\Gamma_{(P\to S)_{total}} = \frac{1-\chi}{2}\Gamma_{total}$. Another two terms describe the decay from the $P_{1/2}$ sub-levels to the $D_{3/2}$ state, using only the anti-commutator terms as shown in Eq. (7), with the decay rate of $\Gamma_{P\to D} = \chi\Gamma_{total}$. These dynamical terms are incorporated in $\mathcal{L}$ leading to the dynamical equation for the 4×4 density matrix $\hat{\boldsymbol{\rho}}$:

$$\frac{\partial}{\partial t}\hat{\boldsymbol{\rho}} = -\frac{i}{\hbar}\left[\hat{\mathbf{H}}_\mathbf{0}, \hat{\boldsymbol{\rho}}\right] + \sum_{p\in P_{1/2}} \Gamma_{total}\left(\frac{(1-\chi)}{2}\sum_{s\in S_{1/2}} \hat{\mathbf{A}}_{(p,s)}\,\hat{\boldsymbol{\rho}}\,\hat{\mathbf{A}}^\dagger_{(p,s)} - \frac{1}{2}\left[\hat{\mathbf{P}}_p, \hat{\boldsymbol{\rho}}\right]_+\right). \quad (22)$$

4.4. Locations of the EP*s and parameter estimation*

Experimentally, the first step is to obtain a time series from the driven system. As an example, we mimic a possible experiment by simulating the time series of the emission signal by solving Eq. (22). The initial condition is obtained by first setting the laser detuning and amplitude to obtain steady state. To overcome the population leakage, the population from $D_{3/2}$ is repumped to $P_{1/2}$ using an auxiliary laser. After a steady state is reached, the auxiliary laser is turned off, obtaining $\hat{\boldsymbol{\rho}}(0)$. The decay signal is now collected from $\hat{\boldsymbol{\rho}}(t)$ for a particular observable in an ordered time grid. The left panel of Figure 3 shows an example for such time signals. The time series is the input for the harmonic inversion, which extracts the frequencies and amplitudes of the time signal. The frequencies are determined by the system parameters, while the initial state $\hat{\boldsymbol{\rho}}(0)$ determines the amplitudes. The right panel of Figure 3 shows the obtained frequencies in the complex plane. The time interval in this figure is $100ns$, reflecting the population decay life time $\tau_{population} = \tau_{SE}/\chi \approx 108ns$. To map the *EP* at the parameter space, this procedure is repeated for other values of the laser detuning and amplitude.

For any such parameter set defining $\mathcal{L}$, the sum of the 16 eigenvalues of $\mathcal{L}$ can be shown to be: $\sum_{k=1}^{16}\omega_k = 8\Gamma_{total}$. A similar relationship was obtained for the two-level system, where the sum of the 4 eigenvalues is 2Γ.

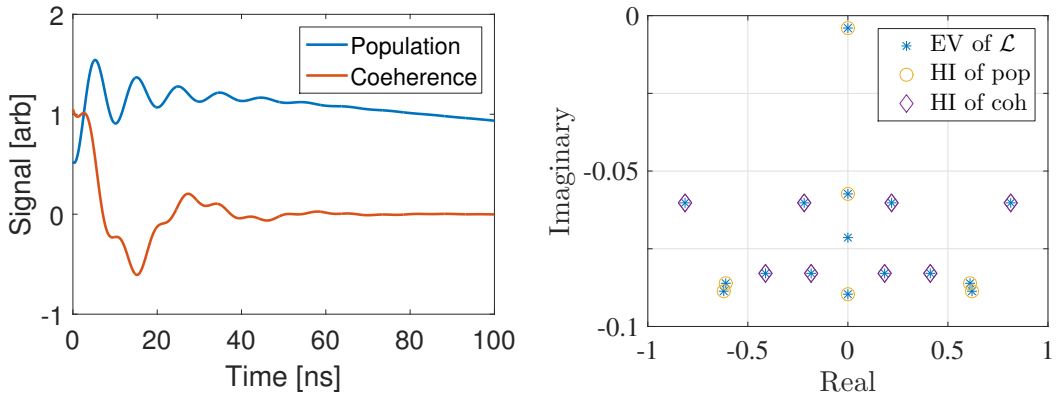

Figure 3. Left panel: An example of two emission time signals of Ca^+, obtained by simulating the dynamics of the populations and the coherences. The initial state is the steady state with re-pumping lasers switched on. The transient dynamics is initiated by turning the pumping laser off. The time interval in this figure, $100ns$, reflects the population decay life time $\tau_{population} \approx 108ns$. Right panel: The locations in the complex plane of the complex frequencies that were obtained from these signals using harmonic inversion (HI). The actual eigenvalues of the generator $\mathcal{L}$ are marked with asterisks. Different subsets of the generator eigenvalues were obtained for different signals. The frequencies of the population signal are marked by circles, while the frequencies of the coherence signal are marked by diamonds.

To calculate the expected locations of the exceptional points in the parameter space of the amplitude and detuning, we used the MFRD and the eigenvalues condition number methods (see Appendix B and Refs. [41, 42]). The map of *EP*-curves is shown in Figure 4 for the $^{40}Ca^+$ ion, with Zeeman splitting of 200MHz. Note the gaps in the Y-axis. The resulting *EP*-curves of the 4-level system are more involved than the 2-level case.

Close to each of the resonances between the upper and lower levels, there is an *EP*-curve which is similar to the deltoid *EP*-curve we got for the Bloch system [25]. The exact frequency of the resonances can be found by locating pairs of *EP*s with detunings above and below the resonance, while maintaining a fixed amplitude. The shape of the curves can be fitted to estimate the branching ratio.

These resonance frequencies can be verified by locating the distinct *EP* on the right of the Bloch-like curves. These two isolated points are classified as $EP2^4$, i.e coalescence of four pairs of eigenvectors with four distinct eigenvalues. Each of these points is located with detuning Δ at the same frequency as the resonance, and amplitude of $\Omega_R = \frac{1}{4}\Gamma_{total}$. These points can be used also to extract the total decay rate Γ.

Between the two Bloch-like *EP*-curves, in the $4^2S_{1/2} \Leftrightarrow 4^2P_{1/2}$ transition frequency, there is a curve of degeneracy points. However, we could not determine whether these degeneracies are exceptional points. Anyway, locating these degeneracies can be employed for determining the transition frequency.

To summarize, the suggested procedure for parameter estimation which include four transition frequencies, laser driving power, spontaneous emission rate and leakage.

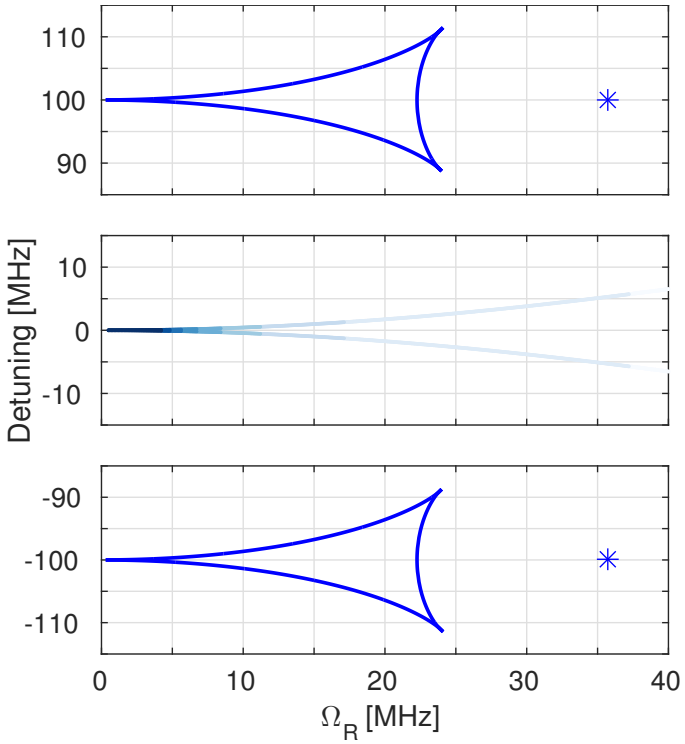

Figure 4. A map of the *EP*-curves of $^{40}Ca^{+}$ ion, with Zeeman splitting of 200MHz, under linearly polarized driving field. Each of the Bloch-like curves (compare to the Bloch curves at Figure 1) is found on a resonance between a pair of sub-levels, one from $4^2S_{1/2}$ and one from $4^2P_{1/2}$. Note the gaps in the Y-axis of the different curves. To the right of each of the Bloch-like *EP*-curves, there is a point of $EP2^4$ (marked with asterisks), in which 4 pairs of eigenvectors coalesce into 4 distinct eigenvectors. The detuning at these points is the splitting of the relevant resonance. The amplitude is $\Omega_R = \frac{1}{4}\Gamma_{total}$.
Between the two Bloch-like *EP*-curves, at the detuning $\Delta = 0$, which is the H-line transition frequency, there is a degeneracy-curve of the L-GKS generator. It is not decisive whether this curve is an *EP*-curve.

(i) The sum of the 16 frequencies obtained by the harmonic inversion of the time signal can be used to estimate the total spontaneous emission rate: $\sum_{k=1}^{16} \omega_k = 8\Gamma_{total}$.

(ii) The locations of the Bloch-like curves are used for the estimation of the frequencies of the resonances between the Zeeman sub-levels.

(iii) The shapes of the Bloch-like curves are used for the estimation of the branching ratio (In particular the EP3 points).

(iv) The locations of the $EP2^4$ points are used to verify the resonances frequencies and the decay rate.

(v) The location of the degeneracy curve between the Bloch-like curve is used to estimate the H line transition frequency.

Repeating this procedure for various magnitudes of the external magnetic field can

be used for tracing the Zeeman and Paschen-Back effects.

For small external magnetic field, the Bloch-like curves approach each other and interfere. The shape of these curves is then skewed. This is demonstrated in Figure 5, which shows the map of *EP*-curves for the $^{40}Ca^{+}$ ion, with Zeeman splitting of 30MHz. However, the resonances frequencies can be estimated using the locations of the *EP*s at small amplitudes, and verified by the location of the isolated $EP2^4$ points. In addition to those *EP*-curves and points, we observed other two isolated $EP2^2$, at larger detuning and slightly larger amplitude. We did not find exact analytical expressions for these points.

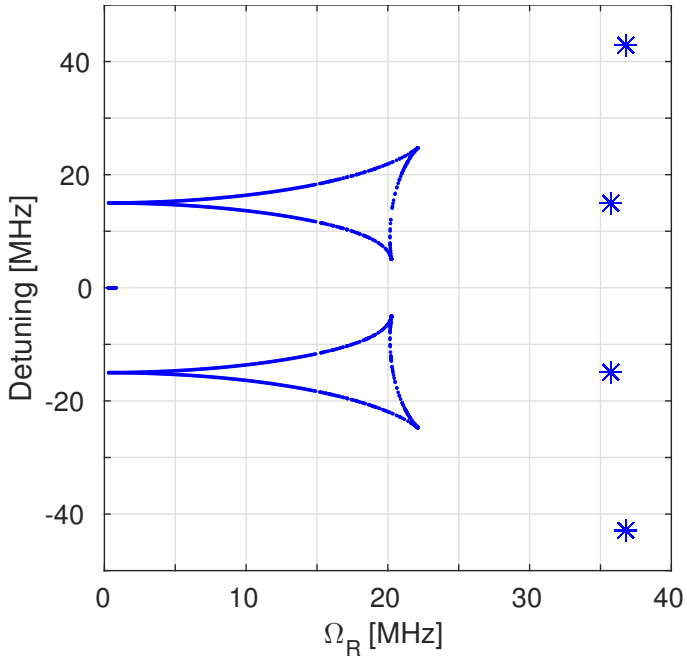

Figure 5. A map of the *EP*-curves of $^{40}Ca^{+}$ ion, with Zeeman splitting of 30MHz. The general structure is similar to the case of 200MHz splitting (Figure 4) but the Bloch-like curves get closer and interfere. The interference leads to skewing of these curves. The $EP2^2$ still can be located and employed for parameter estimation. Another two isolated $EP2^2$ can be seen at the right corners.

4.5. Dependency of the EP*s on other dephasing rates*

Most of the sources for pure dephasing of laser-driven atomic spectroscopy are well controlled experimentally, for example varying the density of the ion gas or the medium gas, or the instrument noise in the laser amplitude and frequency. Care must be taken when analyzing *EP*-curves in atomic spectra to get the relaxation rate Γ, since the rate depends on the various relaxation and dephasing rates in the system. For example, in the Bloch equations, if the spontaneous emission rate is Γ_{SE} and pure dephasing rate Γ_{PD}, then the relaxation rate that appears in the matrix of Eq. (17) is: $\Gamma = \Gamma_{SE} - \Gamma_{PD}$ [25].

Generally, every noise source that can be added to the L-GKS equation, is reflected by the complex eigenvalues of the generator $\mathcal{L}$. These eigenvalues are complex frequencies of the time signal. Therefore the noise source can be traced by the harmonic inversion. The noise will result in changes in the *EP*-curves map. The experimental noise will influence only the harmonic inversion. See Appendix C for a short discussion regarding noise in harmonic inversion methods.

As an example, the influence of noise in the amplitude of the driving laser was analyzed. Such a noise is modeled in the L-GKS equation by a double commutator with the laser amplitude operator $\hat{\mathbf{V}}_{deph}$, which commutes with Ω_R amplitude part of the Hamiltonian:

$$\hat{\mathbf{V}}_{deph} = \sqrt{\frac{1}{2}} \begin{pmatrix} 0 & 0 & 1 & 0 \\ 0 & 0 & 0 & 1 \\ 1 & 0 & 0 & 0 \\ 0 & 1 & 0 & 0 \end{pmatrix}. \tag{23}$$

The dissipation generated by the double commutator with this operator is not pure dephasing since it also generates relaxation.

We calculated the *EP*-map in the parameter space for dissipation rate of $\Gamma_{deph} = 0.01\,ns^{-1}$ with Zeeman splitting of 200MHz. The upper Bloch-like *EP*-curve of the results is presented in Figure 6, along with the associated two $EP2^2$. For comparison, the upper curve of the noiseless case (presented in Figure 4) is also shown. Two prominent differences can be found. The first is that the two branches do not merge at a small amplitude. Instead they are split symmetrically around the resonance. The splitting magnitude is equal to the depahsing rate Γ_{deph}. The second difference is the splitting of the $EP2^4$ into two distinct $EP2^2$s. This splitting is not symmetric, therefore we cannot deduce the system parameters from the locations of these $EP2^2$s.

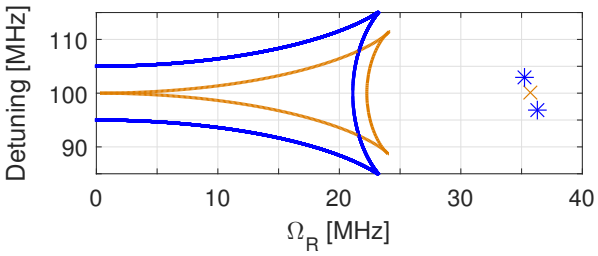

Figure 6. Blue line: The upper Bloch-like *EP*-curve for dissipation rate of $\Gamma_{deph} = 0.01\,ns^{-1}$ and Zeeman splitting of 200MHz, along with the associated two $EP2^2$ (blue asterisks). The orange dashed line and 'x' are the *EP*-curve and the $EP2^4$ obtained for the noiseless case ($\Gamma_{deph} = 0\,ns^{-1}$), shown on Figure 4 above. For the case of $\Gamma_{deph} = 0.01\,ns^{-1}$, the two branches do not merge at a small amplitude. Instead, they are split symmetrically around the resonance. The splitting magnitude is equal to the depahsing rate Γ_{deph}. In addition, the added dephasing splits the $EP2^4$ of the noiseless case into two distinct $EP2^2$s .

5. Discussion

The irreversible character of the L-GKS equation is well known and indicated by the semi-group character of the evolution operator [43, 44, 15, 45]. The generator of the dynamics $\mathcal{L}$ is therefore non hermitian. This means that non-hermitian degeneracies *EP* play an important role in open quantum systems.

So far, *EP* were studied in the coalescence of two resonances. The resonances were metastable states associated with predissociation or autoionization phenomena and with leaking modes in waveguides [46, 47]. A theoretical quest for multiple *EP*s [48], or for high order *EP*s in dissipative physical systems is pursued [49, 50, 51, 52], specifically in the spectra of atoms in external fields [53].

The first study of *EP* in the context of the L-GKS equation, was for the simple two-level-system described by the Bloch equations [25]. In the present study, we generalize to open two-level system where population can leak out. Then we extend to a four-level system where the splitting can be controlled by a magnetic field. We found a rich and fascinating structure of *EP*'s and *EP*-curves, including higher-order *EP*s. Such phenomena is expected for many other open quantum systems described by the L-GKS equation.

The methods developed pave the way for a generic framework of employing *EP*s for parameter estimation of atomic systems. The dynamics near the *EP*s have enhanced sensitivity due to their analytic properties: Small changes in the parameters lead to different harmonic inversion. Therefore, for parameter estimation, the harmonic inversion at the *EP*s is superior to standard inversion methods.

The first stage is to predict the *EP* map of the system: The state of an atom driven by a CW laser can be described in the rotating frame by a time-independent L-GKS equation. The parameter space for such a L-GKS generator contains the field amplitude and the detuning frequency. Such a parameter space can be scanned using the MFRD method to find approximate locations of degeneracies of the generator. The location and character of these degeneracies are then examined using the condition number of the eigenvalues, to identify and locate the *EP*s. The second stage is to search for the predicted *EP*s experimentally: The time signals obtained from the experiments are analyzed using harmonic inversion. The resulting frequencies and amplitudes are then used to find the degeneracies and exceptional points. Finally, we estimate the system parameters by comparing the predicted and the experimental *EP*s.

An interesting different system for an *EP*s search can be two molecular electronic surfaces, with vibrational relaxation. A simple model for such a system can include only four levels [54], or even three - one level from the ground state and two vibrational levels from the excited state. Such systems can have multiple steady states, and therefore can possess richer dynamics.

Aknowledgements

We thank Ido Schaefer, Amikam Levy, and Raam Uzdin for fruitful discussions. We want to thank A. L. Wolf, W. Ubachs, and K. S. E. Eikema for their help on the Ca^+ system. We thank P. Gould for his advice. Work supported by the Israel Science Foundation Grants No. 2244/14 and No. 298/11 and by I-Core: the Israeli Excellence Center "Circle of Light".

Appendix A. Dynamical signature of the *EP*s

The solution for the L-GKS equation in the matrix-vector representation, Eq. (11), is:

$$\vec{\rho}(t) = e^{Lt}\vec{\rho}(0). \tag{A.1}$$

When L is diagonalizable, we can write $L = T\Lambda T^{-1}$, for a non-singular matrix T and a diagonal matrix Λ, which has the eigenvalues $\{\lambda_i\}$ on the diagonal. Then we have

$$e^{Mt} = Te^{\Lambda t}T^{-1}. \tag{A.2}$$

The matrix $e^{\Lambda t}$ is a diagonal matrix, which has the exponential of the eigenvalues, $\exp[\lambda_i t]$, on its diagonal. The resulting dynamics of expectation values of operators, as well as other correlation functions, follows a sum of decaying oscillatory exponentials. The analytical form of such dynamics is:

$$\langle X(t)\rangle = \sum_k d_k \exp[-i\omega_k t] \ , \tag{A.3}$$

where $-i\omega_k$ are the eigenvalues of L, d_k are the associated amplitudes, and both ω_k and d_k can be complex.

For special values of the system parameters the spectrum of the non-hermitian matrix L is incomplete. This is due to the coalescence of several eigenvectors, referred to as a non-hermitian degeneracy. The difference between hermitian degeneracy and non-hermitian degeneracy is essential: In the hermitian degeneracy, several different orthogonal eigenvectors are associated with the same eigenvalue. In the case of non-hermitian degeneracy several orthogonal eigenvectors coalesce to a single eigenvector [47]. As a result, the matrix L is not diagonalizable, and the exponential e^{Lt} cannot be expressed using the eigenvalue decomposition.

The exponential of a non-diagonalizable matrix L can be expressed using its Jordan normal form: $L = TJT^{-1}$. Here, J is a Jordan-blocks matrix which has (at least) one non-diagonal Jordan block; $J_i = \lambda_i I + N$, where I is the identity and N is has ones on its first upper off-diagonal. The exponential of L is expressed as

$$e^{Lt} = Te^{Jt}T^{-1}. \tag{A.4}$$

The exponential of the block J_i in e^{Jt} will have the form:

$$e^{J_i t} = e^{\lambda_i I t + Nt} = e^{\lambda_i t}e^{Nt}. \tag{A.5}$$

The matrix N is nilpotent and therefore the Taylor series of e^{Nt} is finite, resulting in a polynomial in the matrix Nt. This gives rise to a polynomial behaviour of the solution, and the dynamics of expectation values of operators will have the analytical form of

$$\langle X(t)\rangle = \sum_k \sum_{\alpha=0}^{r_k} d_{k,\alpha} t^\alpha \exp[-i\omega_k^{(r_k)} t] \,, \tag{A.6}$$

instead of the form of Eq. (A.3). Here, $\omega_k^{(r_k)}$ denotes a frequency with multiplicity of $r_k + 1$. Note that for non-degenerate frequencies, i.e. $r_k = 0$, we have $d_{k,0} = d_k$ and $\omega_k^{(0)} = \omega_k$. The difference in the analytic behaviour of the dynamics results in non-Lorentzian line shapes, with higher order poles in the complex spectral domain. The point in the spectrum where the eigenvectors coalesce is known as an *exceptional point* (EP).

Appendix B. Searching for *EP*s at the parameter space

Given a parameters-dependent matrix, the task is to find the exceptional points, i.e., to calculate the parameters set for which the matrix is not diagonalizable.

Appendix B.1. Condition number of an eigenvalue

The diagonalization of matrices in the vicinity of a defective matrix is extremely sensitive to perturbations. The sensitivity of the diagonalization can be characterized by the condition numbers of its eigenvalues. Therefore the divergence of the condition number of an eigenvalue can be used to find exceptional points. The condition number of an eigenvalue λ of a matrix A with y and x as the corresponding (normalized) left and right eigenvectors, respectively, is defined by:

$$\kappa(\lambda, A) = \frac{1}{y^H x}, \tag{B.1}$$

where y^H is the hermitian transpose of y [55, 56, 42]. At exceptional points the left and right eigenvectors are perpendicular, and the scalar product $y^H x$ vanishes, leading to divergence of the eigenvalue condition number. The condition number of the eigenvalues is implemented in the Matlab function CONDEIG.

Appendix B.2. Newton methods

There are a few methods that use the special properties of the exceptional points in order to find them iteratively:

- Mailybaev developed a Newton method of finding multiple eigenvalues with one Jordan block and corresponding generalized eigenvectors for matrices dependent on parameters. The method computes the nearest value of a parameter vector with a matrix having a multiple eigenvalue of given multiplicity [57]. This method worked well for us in some cases, but failed to find points in which two different eigenvalues had double multiplicity.

- Akinola and coworkers used an implicit determinant method to obtain a numerical technique for the calculation of a two-dimensional Jordan block in a parameter-dependent matrix [58].

Appendix B.3. The MFRD method for finding a double eigenvalue of a parameter-dependent matrix

Jarlebring and coworkers suggested a method that for a given two $n \times n$ matrices, A and B, computes all pairs (λ,μ) such that λ is a double eigenvalue of $A + \mu B$ [41]. The method they suggest is the method of fixed relative distance (MFRD). It is based on the assumption that in the vicinity of the double eigenvalue (i.e., for close enough μ) there are two close eigenvalues λ and $(1+\epsilon)\lambda$. In order to find such λ and μ we have to solve the following coupled eigenvalue equations:

$$(A + \mu B)\, u = \lambda u \tag{B.2}$$

$$(A + \mu B)\, v = \lambda\,(1 + \epsilon)\, v, \tag{B.3}$$

where I is the $n \times n$ identity matrix. This kind of problem is called "the two-parameter eigenvalue problem". The most common way to solve and analyze two-parameter eigenvalue problems is by means of three so-called matrix determinants

$$\Delta_0 = -I \otimes B + (1+\epsilon) B \otimes I \tag{B.4}$$

$$\Delta_1 = -A \otimes B + B \otimes A \tag{B.5}$$

$$\Delta_2 = I \otimes A - (1+\epsilon) A \otimes I. \tag{B.6}$$

These are $n^2 \times n^2$ matrices. After constructing these matrices, we solve the following generalized eigenvalues problems:

$$\lambda \Delta_0 z = \Delta_1 z \tag{B.7}$$

$$\mu \Delta_0 z = \Delta_2 z, \tag{B.8}$$

to get the approximation for μ and λ and a tensor product $z = u \otimes v$.

The value of ϵ has to be small, in order to reflect the double eigenvalue, but not too small in order to maintain stability. As a rule of thumb, a good choice is

$$\epsilon \sim \epsilon_{mach}^{1/3}, \tag{B.9}$$

where ϵ_{mach} is the machine precision.

To summarize, the steps of the method follows. Given two $n \times n$ matrices A and B:

(i) Choose appropriate ϵ (see Eq. (B.9)). For $\epsilon_{mach} = 2.2 \times 10^{-16}$ (Matlab), we have $\epsilon_{mach}^{1/3} \approx 6 \times 10^{-6}$

(ii) Construct the matrix determinants of Eq. (B.6).

(iii) Solve the generalized eigenvalues Eq. (B.8) problem to get the approximation for μ and λ.

By construction, This method yields only an approximation to the pairs (λ,μ). But this approximation can be an initial guess for an iterative method or an exact one to get an exact pair (λ,μ).

Appendix C. Noise sensitivity of the harmonic inversion

Parameters estimation naturally raises the issue of sensitivity to noisy experimental data. The noise sensitivity will be determined by the method of harmonic inversion. If the sampling periods have high accuracy then the time series can be shown to have an underlying Hamiltonian generator. This is the basis for linear methods, such as the filter diagonalization (FD) [18, 19]. The noise in these methods results in normally distributed underlying matrices, and the model displays monotonous behaviour with respect to the noise. This was verified analytically and by means of simulations In Ref. [59]. As a result sufficient averaging will eliminate the noise. Practical implementations require further analysis with evidence of nonlinear effects of noise. For example, Mandelshtam et. al. analysed the noise-sensitivity of the FD in the context of NMR experiments [21, 60] and Fourier transform mass spectrometry [22]. For some other methods, a noise reduction technique was proposed in Ref. [20].

Bibliography

[1] Hidetoshi Katori. Optical lattice clocks and quantum metrology. *Nature Photonics*, 5(4):203–210, 2011.

[2] Andrew D. Ludlow, Martin M. Boyd, Jun Ye, E. Peik, and P. O. Schmidt. Optical atomic clocks. *Rev. Mod. Phys.*, 87:637–701, Jun 2015.

[3] Kensuke Matsubara, Hidekazu Hachisu, Ying Li, Shigeo Nagano, Clayton Locke, Asahiko Nogami, Masatoshi Kajita, Kazuhiro Hayasaka, Tetsuya Ido, and Mizuhiko Hosokawa. Direct comparison of a ca$^+$ single-ion clock against a sr lattice clock to verify the absolute frequency measurement. *Opt. Express*, 20(20):22034–22041, Sep 2012.

[4] Nitin R Nand, John G Hartnett, Eugene N Ivanov, and Giorgio Santarelli. Ultra-stable very-low phase-noise signal source for very long baseline interferometry using a cryocooled sapphire oscillator. *Microwave Theory and Techniques, IEEE Transactions on*, 59(11):2978–2986, 2011.

[5] Chin-Wen Chou, DB Hume, Till Rosenband, and DJ Wineland. Optical clocks and relativity. *Science*, 329(5999):1630–1633, 2010.

[6] S Blatt, AD Ludlow, GK Campbell, Jan Westenkær Thomsen, T Zelevinsky, MM Boyd, J Ye, X Baillard, M Fouché, R Le Targat, et al. New limits on coupling of fundamental constants to gravity using sr 87 optical lattice clocks. *Physical Review Letters*, 100(14):140801, 2008.

[7] Peter J Mohr, Barry N Taylor, and David B Newell. The 2010 codata recommended values of the fundamental physical constants. *Web version*, 6(2), 2011.

[8] Randolf Pohl, Aldo Antognini, François Nez, Fernando D Amaro, François Biraben, João MR Cardoso, Daniel S Covita, Andreas Dax, Satish Dhawan, Luis MP Fernandes, et al. The size of the proton. *Nature*, 466(7303):213–216, 2010.

[9] Masud Chaichian, MM Sheikh-Jabbari, and A Tureanu. Hydrogen atom spectrum and the lamb shift in noncommutative qed. *Physical Review Letters*, 86(13):2716, 2001.

[10] Claude Itzykson and Jean-Bernard Zuber. *Quantum field theory*. Courier Corporation, 2006.

[11] GS Agarwal. Master-equation approach to spontaneous emission. *Physical Review A*, 2(5):2038, 1970.

[12] Claude Cohen-Tannoudji, Jacques Dupont-Roc, and Gilbert Grynberg. Atom-photon interactions: Basic process and appilcations. pages 353–405, 1998.

[13] Goran Lindblad. On the generators of quantum dynamical semigroups. *Communications in Mathematical Physics*, 48(2):119–130, 1976.

[14] Vittorio Gorini, Andrzej Kossakowski, and Ennackal Chandy George Sudarshan. Completely positive dynamical semigroups of n-level systems. *Journal of Mathematical Physics*, 17(5):821–825, 1976.

[15] Heinz-Peter Breuer and Francesco Petruccione. *The theory of open quantum systems*. Oxford university press, 2002.

[16] Robert Alicki and Mark Fannes. *Quantum dynamical systems*. Oxford university press, 2001.

[17] Morag Am-Shallem, Amikam Levy, Ido Schaefer, and Ronnie Kosloff. Three approaches for representing lindblad dynamics by a matrix-vector notation. http://arxiv.org/abs/1510.08634, 2015.

[18] Michael R. Wall and Daniel Neuhauser. Extraction, through filter-diagonalization, of general quantum eigenvalues or classical normal mode frequencies from a smallï¿œ number of residues or a short-time segment of a signal. i. theory and application to a quantum-dynamics model. *The Journal of Chemical Physics*, 102(20):8011–8022, 1995.

[19] Vladimir A Mandelshtam. Fdm: the filter diagonalization method for data processing in nmr experiments. *Progress in Nuclear Magnetic Resonance Spectroscopy*, 38(2):159–196, 2001.

[20] Dž. Belkić, P. A. Dando, J. Main, and H. S. Taylor. Three novel high-resolution nonlinear methods for fast signal processing. *The Journal of Chemical Physics*, 113(16):6542–6556, 2000.

[21] Haitao Hu, Que N. Van, Vladimir A. Mandelshtam, and A.J. Shaka. Reference deconvolution, phase correction, and line listing of {NMR} spectra by the 1d filter diagonalization method. *Journal of Magnetic Resonance*, 134(1):76 – 87, 1998.

[22] Beau R. Martini, Konstantin Aizikov, and Vladimir A. Mandelshtam. The filter diagonalization method and its assessment for fourier transform mass spectrometry. *International Journal of Mass Spectrometry*, 373(0):1 – 14, 2014.

[23] Erez Gershgoren, Jiri Vala, Ronnie Kosloff, , and Sanford Ruhman. Impulsive control of ground surface dynamics of i_3^- in solution. *The Journal of Physical Chemistry A*, 105(21):5081–5095, 2001.

[24] Jacob Fuchs, Jörg Main, Holger Cartarius, and Günter Wunner. Harmonic inversion analysis of exceptional points in resonance spectra. *Journal of Physics A: Mathematical and Theoretical*, 47(12):125304, 2014.

[25] Morag Am-Shallem, Ronnie Kosloff, and Nimrod Moiseyev. Exceptional points for parameter estimation in open quantum systems: analysis of the bloch equations. *New Journal of Physics*, 17(11):113036, 2015.

[26] Daniel A. Steck. Rubidium 85 d line data, 2010. revision 2.1.6, 20 September 2013.

[27] Michael Ramm, Thaned Pruttivarasin, Mark Kokish, Ishan Talukdar, and Hartmut Häffner. Precision measurement method for branching fractions of excited $P_{1/2}$ states applied to $^{40}Ca^+$. *Phys. Rev. Lett.*, 111:023004, Jul 2013.

[28] Christian Roos. Quantum information processing with trapped ions. In Wolfgang Quint and Manuel Vogel, editors, *Fundamental Physics in Particle Traps*, volume 256 of *Springer Tracts in Modern Physics*, pages 253–291. Springer Berlin Heidelberg, 2014.

[29] Julio T Barreiro, Philipp Schindler, Otfried Gühne, Thomas Monz, Michael Chwalla, Christian F Roos, Markus Hennrich, and Rainer Blatt. Experimental multiparticle entanglement dynamics induced by decoherence. *Nature Physics*, 6(12):943–946, 2010.

[30] Philipp Schindler, Daniel Nigg, Thomas Monz, Julio T Barreiro, Esteban Martinez, Shannon X Wang, Stephan Quint, Matthias F Brandl, Volckmar Nebendahl, Christian F Roos, Michael Chwalla, Markus Hennrich, and Rainer Blatt. A quantum information processor with trapped ions. *New Journal of Physics*, 15(12):123012, 2013.

[31] Maximilian Harlander, Regina Lechner, Michael Brownnutt, Rainer Blatt, and Wolfgang Hänsel.

Trapped-ion antennae for the transmission of quantum information. *Nature*, 471(7337):200–203, 2011.

[32] Stephan A Schulz, Ulrich Poschinger, Frank Ziesel, and Ferdinand Schmidt-Kaler. Sideband cooling and coherent dynamics in a microchip multi-segmented ion trap. *New Journal of Physics*, 10(4):045007, 2008.

[33] U Poschinger, A Walther, M Hettrich, F Ziesel, and F Schmidt-Kaler. Interaction of a laser with a qubit in thermal motion and its application to robust and efficient readout. *Applied Physics B*, 107(4):1159–1165, 2012.

[34] KeLin Gao. Optical frequency standard based on a single 40ca+. *Chinese Science Bulletin*, 58(8):853–863, 2013.

[35] Hua Guan, Yao Huang, Pei-Liang Liu, Wu Bian, Hu Shao, and Ke-Lin Gao. Precision spectroscopy with a single 40 ca + ion in a paul trap. *Chinese Physics B*, 24(5):054213, 2015.

[36] Pei-Liang Liu, Yao Huang, Wu Bian, Hu Shao, Hua Guan, Yong-Bo Tang, Cheng-Bin Li, J. Mitroy, and Ke-Lin Gao. Measurement of magic wavelengths for the ^{40}ca^{+} clock transition. *Phys. Rev. Lett.*, 114:223001, Jun 2015.

[37] Anne Lisa Wolf, Jonas Morgenweg, Jeroen C. J. Koelemeij, Steven A. van den Berg, Wim Ubachs, and Kjeld S. E. Eikema. Direct frequency-comb spectroscopy of a dipole-forbidden clock transition in trapped 40ca+ ions. *Opt. Lett.*, 36(1):49–51, Jan 2011.

[38] Johannes Roßnagel, Samuel Thomas Dawkins, Karl Nicolas Tolazzi, Obinna Abah, Eric Lutz, Ferdinand Schmidt-Kaler, and Kilian Singer. A single-atom heat engine. http://arxiv.org/abs/1510.03681, 2015.

[39] A. L. Wolf, S. A. van den Berg, C. Gohle, E. J. Salumbides, W. Ubachs, and K. S. E. Eikema. Frequency metrology on the $4s\,^2\mathrm{S}_{1/2} - 4p\,^2\mathrm{P}_{1/2}$ transition in ^{40}ca^{+} for a comparison with quasar data. *Phys. Rev. A*, 78:032511, Sep 2008.

[40] A. L. Wolf, S. A. van den Berg, W. Ubachs, and K. S. E. Eikema. Direct frequency comb spectroscopy of trapped ions. *Phys. Rev. Lett.*, 102:223901, Jun 2009.

[41] Elias Jarlebring, Simen Kvaal, and Wim Michiels. Computing all pairs (λ,μ) such that λ is a double eigenvalue of$a + \mu b$. *SIAM Journal on Matrix Analysis and Applications*, 32(3):902–927, 2011.

[42] F. Chatelin. *Spectral Approximation of Linear Operators*, chapter 1, pages 1–65. Society for Industrial and Applied Mathematics, 2011.

[43] R. Alicki. Invitation to quantum dynamical semigroups. In Piotr Garbaczewski and Robert Olkiewicz, editors, *Dynamics of Dissipation*, volume 597 of *Lecture Notes in Physics*, pages 239–264. Springer Berlin Heidelberg, 2002.

[44] Robert Alicki and Karl Lendi. *Quantum Dynamical Semigroups and Applications*, volume 717 of *Lecture Notes in Physics*. Springer Berlin Heidelberg, 2007.

[45] Michael A. Nielsen and Isaac L. Chuang. *Quantum Computation and Quantum Information: 10th Anniversary Edition*. Cambridge University Press, New York, NY, USA, 10th edition, 2011.

[46] Markus Müller and Ingrid Rotter. Exceptional points in open quantum systems. *Journal of Physics A: Mathematical and Theoretical*, 41(24):244018, 2008.

[47] Nimrod Moiseyev. *Non-Hermitian quantum mechanics*. Cambridge University Press Cambridge, 2011.

[48] Jung-Wan Ryu, Soo-Young Lee, and Sang Wook Kim. Analysis of multiple exceptional points related to three interacting eigenmodes in a non-hermitian hamiltonian. *Phys. Rev. A*, 85:042101, Apr 2012.

[49] W D Heiss. Chirality of wavefunctions for three coalescing levels. *Journal of Physics A: Mathematical and Theoretical*, 41(24):244010, 2008.

[50] Gilles Demange and Eva-Maria Graefe. Signatures of three coalescing eigenfunctions. *Journal of Physics A: Mathematical and Theoretical*, 45(2):025303, 2012.

[51] W D Heiss and G Wunner. Resonance scattering at third-order exceptional points. *Journal of Physics A: Mathematical and Theoretical*, 48(34):345203, 2015.

[52] W.D. Heiss. Green's functions at exceptional points. *International Journal of Theoretical Physics*, pages 1–6, 2015.

[53] Holger Cartarius, Jörg Main, and Günter Wunner. Exceptional points in the spectra of atoms in external fields. *Phys. Rev. A*, 79:053408, May 2009.

[54] Morag Am-Shallem and Ronnie Kosloff. The scaling of weak field phase-only control in markovian dynamics. *The Journal of Chemical Physics*, 141(4), 2014.

[55] Gene H Golub and Charles F Van Loan. *Matrix computations. Johns Hopkins series in the mathematical sciences*. Johns Hopkins University Press, Baltimore, MD, 1989.

[56] C. Moler. *Numerical Computing with Matlab*, chapter 10, pages 269–305. Society for Industrial and Applied Mathematics, 2004.

[57] Alexei A. Mailybaev. Computation of multiple eigenvalues and generalized eigenvectors for matrices dependent on parameters. *Numerical Linear Algebra with Applications*, 13(5):419–436, 2006.

[58] Richard O. Akinola, Melina A. Freitag, and Alastair Spence. The computation of jordan blocks in parameter-dependent matrices. *IMA Journal of Numerical Analysis*, 34(3):955–976, 2014.

[59] Uroš Benko and Đani Juričić. Frequency analysis of noisy short-time stationary signals using filter-diagonalization. *Signal Processing*, 88(7):1733 – 1746, 2008.

[60] Hasan Celik, A.J. Shaka, and V.A. Mandelshtam. Sensitivity analysis of solutions of the harmonic inversion problem: Are all data points created equal? *Journal of Magnetic Resonance*, 206(1):120 – 126, 2010.

4.7 Discussion

Exceptional points have gained growing interest in recent years [Müller 2008, Moiseyev 2011]. In particular, the search for multiple *EP*s [Ryu 2012], or for high order *EP*s in dissipative physical systems [Heiss 2008, Demange 2012, Heiss 2015a, Heiss 2015b]. However, most previous studies of the EP phenomenon have been based on non hermitian Hamiltonians caused by the interaction of the discrete states via the common continuum of scattering states. Such Hamiltonian-based approaches incorporate only coherent dynamics, while the dissipation and dephasing phenomena are absent.

The study of exceptional points in this thesis utilizes this concept to a new field: Markovian open quantum systems. The L-GKS formalism is a reduced description of a system and bath scenario, and the non hermitian properties of the dynamical generator are caused by tracing out the bath degrees of freedom. The dissipation and dephasing phenomena are properly described by this formalism. The exceptional points here are non-hermitian degeneracies of the L-GKS quantum dynamical semigroup generator. They represent dynamical properties of the system, where few decay modes of the system coalesce. The studies reported here initiate a new perspective on the dynamics of open quantum systems which invites further research.

Chapter 5

Conclusions and outlook

The studies presented in this thesis investigated the dynamics of driven Markovian open quantum systems. The main objective of the research was to examine the impact of the surrounding environment on the interaction of quantum systems with external driving fields. A subsequent question is the limits of validity of the Markovian assumptions.

We studied the weak-laser-driven population transfer between electronic surfaces in molecules. Such a scenario frequently takes place in spectroscopy. The framework for this study was the weak-field phase-only (WFPO) control of quantum systems. For an objective which commutes with the free Hamiltonian, WFPO control of an isolated system is impossible [Brumer 1989, Spanner 2010]. A series of experiments and simulations questioned this premise, and suggested that WFPO control can be achieved by the environment of the system [Prokhorenko 2005, Prokhorenko 2006, van der Walle 2009, Prokhorenko 2011, Katz 2011].

We formulated the question of WFPO control of an open quantum system within the L-GKS framework. We showed that under an additional certain set of assumptions, the scaling with the field strength of phase-dependent phenomena is not altered. This set of assumption (Eq. (18)-(20) in the research paper [Am-Shallem 2014]) can be used to analyze the dynamics of other systems, which have different dissipators, or even systems that are not described by the L-GKS framework. In particular, we extended these results to systems with a field-free propagator which depends only on the time difference (time-homogeneous field-free propagation, see Eq. (19) of the research paper). Such time-homogeneity is a character of dynamics which is generated by a linear differential equation (as oppose to an integro-differential equation) with time-independent field-free part. Therefore these results can be extended to a broad set of systems, including a larger set of non-Markovian systems, generated by the time independent Hierarchical Equations of Motion approach [Meier 1999, Ishizaki 2005, Jin 2008], in which the propagator

has a similar form.

The evidences for WFPO control still need a theory. We pointed out that the WFPO control can originate from non-Markovian dynamics. The non-Markovian character can be manifested by non-separability of the system+environment structure. It can also arise by memory effects. However, extra care must be taken when attributing the WFPO control to non-Markovian effects, since the set of assumption we used in our study comprises more than only Markovian dynamics.

An additional direction for such a theory is to examine the influence of the external fields on the environment. The analysis of the WFPO control that we carried out cannot include the influence of the field on the environment, since the L-GKS open system dynamics does not include such a mechanism. Nevertheless, a non-direct influence can be presented, through the system dynamics. A careful derivation of the master equation can lead to field-induced dissipation [Levy 2014, for example]. We have indications that the field-induced dissipation can lead to WFPO control. We performed numerical simulations of a simple model driven by a pulse of a chirped Gaussian external field. In addition to the standard hermitian coupling between field and the system, we added a small non-hermitian coupling term. We assigned different phases to different pulses by altering the chirp rate. Comparing the final population transfer among several values of the chirp of the field, we found a prominent dependence on the chirp rate.

In the non-Markovian formalism the influence of the external fields on the environment can be described explicitly. If the environment can be controlled or measured, the space available for the system can be expanded. Therefore there could be more ways to drive an initial given state to a target state. This can lead to enhanced controllability [Wu 2007, Lloyd 2001]. In particular, WFPO control might emerge from the impact of the fields on the environment.

Lastly, these observations may challenge the time-dependent perturbation theory we used. The common time-dependent perturbation theory relies on the time reversibility of the evolution. The contraction of the available space in Markovian dynamics [Altafini 2004] leads to non-reversibility on long times. In addition, in the vicinity of exceptional points there is a subtle difference in the dynamics which can lead to time-irreversibility. Moreover, the non-analytical properties of the eigenvalues in the vicinity of exceptional points suggests that the standard time-dependent perturbation theory has to be revised to handle such cases.

The irreversibility of Markovian dynamics is reflected by the contracting non unitary evolution propagator. The eigenvectors of non unitary operators are not orthogonal. The emergence of exceptional points in the dynamics of open quantum systems is the extreme manifestation of non orthogonality. The subtle difference

of the dynamics at exceptional points is therefore an indication for the essential different character of the dynamics.

We investigated the exceptional points of the L-GKS generator in the parameter space of laser amplitude and detuning. We suggested to estimate the system parameters by employing the ability to locate accurately the exceptional points. The method can be employed for precision spectroscopy of atoms and molecules which is related to the measurement of the fundamental constants. High accuracy has implications also in other fields of physics, such as radioastronomy, tests of general relativity, and particle physics. We believe that this method can be developed and incorporated as a standard tool for precise measurements.

Other types of systems can be accounted for in this context. For example, the vibrational relaxation inside molecular electronic surfaces can be described by the L-GKS equation with dissipative terms for relaxation, excitation and dephasing. Another example is a series of laser-coupled quantum dots where each quantum dot is relaxed due to the interaction with the external environment. The exceptional points in such systems can indicate circumstances where the time reversal symmetry is broken. The breaking of time-reversal symmetry makes the dynamics essentially different and new effects and phenomena can arise. An example discussed above is that the time dependent perturbation theory may have a different analytical form in the vicinity of an exceptional point. This kind of research is still being explored.

Exceptional points can emerge also in non-Markovian dynamics. On such dynamics the non unitary evolution propagator is not limited to contractions, reflecting the ability of the information to flow back and forth between the system and the environment. The change of purity of the system is not monotonic and it can increase and decrease alternately. The richer possibilities of the dynamics suggest that the concept of exceptional points in non-Markovian systems does appeal as a further research objective.

Bibliography

[Abadir 2005] Karim M Abadir and Jan R Magnus. Matrix algebra, volume 1. Cambridge University Press, 2005. (Cited on page 20.)

[Al-Mohy 2011] Awad H. Al-Mohy and Nicholas J. Higham. *Computing the Action of the Matrix Exponential, with an Application to Exponential Integrators.* SIAM Journal on Scientific Computing, vol. 33, no. 2, pages 488–511, 2011. (Cited on page 21.)

[Alicki 2001] Robert Alicki and Mark Fannes. Quantum dynamical systems. Oxford university press, 2001. (Cited on pages 13, 23.)

[Alicki 2002] R. Alicki. *Invitation to Quantum Dynamical Semigroups.* In Piotr Garbaczewski and Robert Olkiewicz, editors, Dynamics of Dissipation, volume 597 of *Lecture Notes in Physics*, pages 239–264. Springer Berlin Heidelberg, 2002. (Cited on page 3.)

[Alicki 2006] Robert Alicki, Daniel A. Lidar and Paolo Zanardi. *Internal consistency of fault-tolerant quantum error correction in light of rigorous derivations of the quantum Markovian limit.* Phys. Rev. A, vol. 73, page 052311, May 2006. (Cited on page 14.)

[Alicki 2007] Robert Alicki and Karl Lendi. Quantum dynamical semigroups and applications, volume 717 of *Lecture Notes in Physics*. Springer Berlin Heidelberg, 2007. (Cited on pages 3, 12, 17.)

[Altafini 2004] Claudio Altafini. *Coherent control of open quantum dynamical systems.* Physical Review A, vol. 70, no. 6, page 062321, December 2004. (Cited on pages 14, 88.)

[Am-Shallem 2014] Morag Am-Shallem and Ronnie Kosloff. *The scaling of weak field phase-only control in Markovian dynamics.* The Journal of Chemical Physics, vol. 141, no. 4, 2014. (Cited on pages 29, 87.)

[Arnoldi 1951] Walter Edwin Arnoldi. *The principle of minimized iterations in the solution of the matrix eigenvalue problem.* Quarterly of Applied Mathematics, vol. 9, no. 1, pages 17–29, 1951. (Cited on pages 21, 22.)

[Ashkenazi 1997] Guy Ashkenazi, Uri Banin, Allon Bartana, Ronnie Kosloff and Sanford Ruhman. *Quantum Description of the Impulsive Photodissociation Dynamics of I- 3 in Solution.* Advances in Chemical Physics, Volume 100, pages 229–315, 1997. (Cited on page 29.)

[Belkić 2000] Dž. Belkić, P. A. Dando, J. Main and H. S. Taylor. *Three novel high-resolution nonlinear methods for fast signal processing.* The Journal of Chemical Physics, vol. 113, no. 16, pages 6542–6556, 2000. (Cited on pages 24, 25.)

[Bird 1983] R.E. Bird, R.L. Hulstrom and L.J. Lewis. *Terrestrial solar spectral data sets.* Solar Energy, vol. 30, no. 6, pages 563 – 573, 1983. (Cited on page 8.)

[Bird 1984] Richard E. Bird. *A simple, solar spectral model for direct-normal and diffuse horizontal irradiance.* Solar Energy, vol. 32, no. 4, pages 461 – 471, 1984. (Cited on page 8.)

[Blanes 2009] S. Blanes, F. Casas, J.A. Oteo and J. Ros. *The Magnus expansion and some of its applications.* Physics Reports, vol. 470, no. 5–6, pages 151 – 238, 2009. (Cited on page 9.)

[Breuer 2002] Heinz-Peter Breuer and Francesco Petruccione. The theory of open quantum systems. Oxford university press, 2002. (Cited on pages 3, 17, 23.)

[Brumer 1989] Paul Brumer and Moshe Shapiro. *One photon mode selective control of reactions by rapid or shaped laser pulses: An emperor without clothes?* Chemical Physics, vol. 139, no. 1, pages 221–228, December 1989. (Cited on page 87.)

[Davies 1974] E Brian Davies. *Markovian master equations.* Communications in mathematical Physics, vol. 39, no. 2, pages 91–110, 1974. (Cited on page 13.)

[Demange 2012] Gilles Demange and Eva-Maria Graefe. *Signatures of three coalescing eigenfunctions.* Journal of Physics A: Mathematical and Theoretical, vol. 45, no. 2, page 025303, 2012. (Cited on page 86.)

[Fuchs 2014] Jacob Fuchs, Jörg Main, Holger Cartarius and Günter Wunner. *Harmonic inversion analysis of exceptional points in resonance spectra.* Journal of Physics A: Mathematical and Theoretical, vol. 47, no. 12, page 125304, 2014. (Cited on pages 25, 47.)

[Gershgoren 2001] Erez Gershgoren, Jiri Vala, Ronnie Kosloff, and Sanford Ruhman. *Impulsive Control of Ground Surface Dynamics of I_3^- in Solution*. The Journal of Physical Chemistry A, vol. 105, no. 21, pages 5081–5095, 2001. (Cited on page 25.)

[Geva 1994] Eitan Geva and Ronnie Kosloff. *Three-level quantum amplifier as a heat engine: A study in finite-time thermodynamics*. Phys. Rev. E, vol. 49, pages 3903–3918, May 1994. (Cited on page 14.)

[Gorini 1976] Vittorio Gorini, Andrzej Kossakowski and Ennackal Chandy George Sudarshan. *Completely positive dynamical semigroups of N-level systems*. Journal of Mathematical Physics, vol. 17, no. 5, pages 821–825, 1976. (Cited on page 14.)

[Heiss 2008] W D Heiss. *Chirality of wavefunctions for three coalescing levels*. Journal of Physics A: Mathematical and Theoretical, vol. 41, no. 24, page 244010, 2008. (Cited on page 86.)

[Heiss 2015a] W D Heiss and G Wunner. *Resonance scattering at third-order exceptional points*. Journal of Physics A: Mathematical and Theoretical, vol. 48, no. 34, page 345203, 2015. (Cited on page 86.)

[Heiss 2015b] W.D. Heiss. *Green's Functions at Exceptional Points*. International Journal of Theoretical Physics, pages 1–6, 2015. (Cited on page 86.)

[Hu 1998] Haitao Hu, Que N. Van, Vladimir A. Mandelshtam and A.J. Shaka. *Reference Deconvolution, Phase Correction, and Line Listing of NMR Spectra by the 1D Filter Diagonalization Method*. Journal of Magnetic Resonance, vol. 134, no. 1, pages 76 – 87, 1998. (Cited on page 25.)

[Ishizaki 2005] Akihito Ishizaki and Yoshitaka Tanimura. *Quantum Dynamics of System Strongly Coupled to Low-Temperature Colored Noise Bath: Reduced Hierarchy Equations Approach*. Journal of the Physical Society of Japan, vol. 74, no. 12, pages 3131–3134, 2005. (Cited on page 87.)

[Jin 2008] Jinshuang Jin, Xiao Zheng and YiJing Yan. *Exact dynamics of dissipative electronic systems and quantum transport: Hierarchical equations of motion approach*. The Journal of Chemical Physics, vol. 128, no. 23, pages –, 2008. (Cited on page 87.)

[Katz 2011] Gil Katz and Ronnie Kosloff, 2011. private communication. (Cited on pages 30, 87.)

[Kosloff 1992] Ronnie Kosloff, Audrey Dell Hammerich and David Tannor. *Excitation without demolition: Radiative excitation of ground-surface vibration by impulsive stimulated Raman scattering with damage control.* Physical review letters, vol. 69, no. 15, page 2172, 1992. (Cited on page 29.)

[Kosloff 2002] Ronnie Kosloff and Tova Feldmann. *Discrete four-stroke quantum heat engine exploring the origin of friction.* Phys. Rev. E, vol. 65, page 055102, May 2002. (Cited on page 23.)

[Kraus 1971] Karl Kraus. *General state changes in quantum theory.* Annals of Physics, vol. 64, no. 2, pages 311–335, 1971. (Cited on page 12.)

[Kraus 1983] Karl Kraus, A. Böhm, J. D. Dollard and W. H. Wootters, editors. States, effects, and operations fundamental notions of quantum theory, volume 190. Springer Berlin Heidelberg, Berlin, Heidelberg, 1983. (Cited on page 12.)

[Levy 2012] Amikam Levy, Robert Alicki and Ronnie Kosloff. *Quantum refrigerators and the third law of thermodynamics.* Phys. Rev. E, vol. 85, page 061126, Jun 2012. (Cited on page 14.)

[Levy 2014] Amikam Levy and Ronnie Kosloff. *The local approach to quantum transport may violate the second law of thermodynamics.* EPL (Europhysics Letters), vol. 107, no. 2, page 20004, 2014. (Cited on page 88.)

[Lindblad 1976] Goran Lindblad. *On the generators of quantum dynamical semigroups.* Communications in Mathematical Physics, vol. 48, no. 2, pages 119–130, 1976. (Cited on page 14.)

[Lloyd 2001] Seth Lloyd and Lorenza Viola. *Engineering quantum dynamics.* Physical Review A, vol. 65, no. 1, page 010101, December 2001. (Cited on page 88.)

[Machnes 2014] Shai Machnes and Martin B. Penio. *Surprising Interactions of Markovian noise and Coherent Driving.* arXiv:1408.3056v1, 2014. (Cited on page 19.)

[Mandelshtam 2001] Vladimir A Mandelshtam. *FDM: the filter diagonalization method for data processing in NMR experiments.* Progress in Nuclear Magnetic Resonance Spectroscopy, vol. 38, no. 2, pages 159–196, 2001. (Cited on page 24.)

[Martini 2014] Beau R. Martini, Konstantin Aizikov and Vladimir A. Mandelshtam. *The filter diagonalization method and its assessment for Fourier transform*

mass spectrometry. International Journal of Mass Spectrometry, vol. 373, no. 0, pages 1 – 14, 2014. (Cited on page 25.)

[Meier 1999] Christoph Meier and David J. Tannor. *Non-Markovian evolution of the density operator in the presence of strong laser fields*. The Journal of Chemical Physics, vol. 111, no. 8, pages 3365–3376, 1999. (Cited on page 87.)

[Moiseyev 2011] Nimrod Moiseyev. Non-hermitian quantum mechanics. Cambridge University Press, 2011. (Cited on pages 47, 86.)

[Moler 2003] Cleve Moler and Charles Van Loan. *Nineteen Dubious Ways to Compute the Exponential of a Matrix, Twenty-Five Years Later*. SIAM Review, vol. 45, no. 1, pages 3–49, 2003. (Cited on page 20.)

[Müller 2008] Markus Müller and Ingrid Rotter. *Exceptional points in open quantum systems*. Journal of Physics A: Mathematical and Theoretical, vol. 41, no. 24, page 244018, 2008. (Cited on pages 47, 86.)

[Nielsen 2011] Michael A. Nielsen and Isaac L. Chuang. Quantum computation and quantum information: 10th anniversary edition. Cambridge University Press, New York, NY, USA, 10th édition, 2011. (Cited on page 3.)

[Prokhorenko 2005] Valentyn I. Prokhorenko, Andrea M. Nagy and R. J. Dwayne Miller. *Coherent control of the population transfer in complex solvated molecules at weak excitation. An experimental study*. Journal of Chemical Physics, vol. 122, no. 18, pages 184502–184502–11, May 2005. (Cited on pages 30, 87.)

[Prokhorenko 2006] Valentyn I. Prokhorenko, Andrea M. Nagy, Stephen A. Waschuk, Leonid S. Brown, Robert R. Birge and R. J. Dwayne Miller. *Coherent Control of Retinal Isomerization in Bacteriorhodopsin*. Science, vol. 313, no. 5791, pages 1257 –1261, 2006. (Cited on pages 30, 87.)

[Prokhorenko 2011] Valentyn I. Prokhorenko and R. J. Dwayne Miller, 2011. private communication. (Cited on pages 30, 87.)

[Rezek 2006] Yair Rezek and Ronnie Kosloff. *Irreversible performance of a quantum harmonic heat engine*. New Journal of Physics, vol. 8, no. 5, page 83, 2006. (Cited on page 23.)

[Rice 2000] S.A. Rice and M. Zhao. Optical control of molecular dynamics. Baker Lecture Series. Wiley, 2000. (Cited on page 8.)

[Riordan 1986] C.J. Riordan. *Spectral solar irradiance models and data sets*. Solar Cells, vol. 18, no. 3–4, pages 223 – 232, 1986. (Cited on page 8.)

[Roger 1994] Horn Roger and R Johnson Charles. Topics in matrix analysis. Cambridge University Press, 1994. (Cited on page 19.)

[Ryu 2012] Jung-Wan Ryu, Soo-Young Lee and Sang Wook Kim. *Analysis of multiple exceptional points related to three interacting eigenmodes in a non-Hermitian Hamiltonian.* Phys. Rev. A, vol. 85, page 042101, Apr 2012. (Cited on page 86.)

[Saad 1992] Y. Saad. *Analysis of Some Krylov Subspace Approximations to the Matrix Exponential Operator.* SIAM Journal on Numerical Analysis, vol. 29, no. 1, pages 209–228, 1992. (Cited on pages 21, 22.)

[Shapiro 2003] Moshe Shapiro and Paul Brumer. Principles of the quantum control of molecular processes. Wiley-Interscience, 2003. (Cited on page 8.)

[Spanner 2010] Michael Spanner, Carlos A Arango and Paul Brumer. *Communication: Conditions for one-photon coherent phase control in isolated and open quantum systems.* Journal of Chemical Physics, vol. 133, no. 15, page 151101, October 2010. (Cited on page 87.)

[Tal-Ezer 2007] Hillel Tal-Ezer. *On Restart and Error Estimation for Krylov Approximation of $w = f(A)v$.* SIAM Journal on Scientific Computing, vol. 29, no. 6, pages 2426–2441, 2007. (Cited on page 22.)

[Tannor 2007] D.J. Tannor. Introduction to quantum mechanics: A time-dependent perspective. University Science Books, 2007. (Cited on page 8.)

[Trefethen 1997] Lloyd N Trefethen and David Bau III. Numerical linear algebra, volume 50. Siam, 1997. (Cited on page 21.)

[Uzdin 2012] Raam Uzdin. *The Effects of Non-Hermitian Degeneracies on Light and Matter Interactions.* PhD thesis, Technion - Israel Institute of Technology, 2012. (Cited on page 47.)

[van der Walle 2009] P. van der Walle, M. T. W. Milder, L. Kuipers and J. L. Herek. *Quantum control experiment reveals solvation-induced decoherence.* Proceedings of the National Academy of Sciences, vol. 106, no. 19, pages 7714 –7717, May 2009. (Cited on pages 30, 87.)

[Wall 1995] Michael R. Wall and Daniel Neuhauser. *Extraction, through filter-diagonalization, of general quantum eigenvalues or classical normal mode frequencies from a small number of residues or a short-time segment of a*

signal. I. Theory and application to a quantum-dynamics model. The Journal of Chemical Physics, vol. 102, no. 20, pages 8011–8022, 1995. (Cited on page 24.)

[Wu 2007] Rong Wu, Alexander Pechen, Constantin Brif and Herschel Rabitz. *Controllability of open quantum systems with Kraus-map dynamics.* Journal of Physics A: Mathematical and Theoretical, vol. 40, no. 21, pages 5681–5693, 2007. (Cited on page 88.)

על מנת לתאר את המחקר שלנו בנושא *הנקודות הייחודיות בדינמיקה של מערכות קוונטיות פתוחות* נדרש רקע מתמטי: הערכים העצמיים של היוצר של משוואת L-GKS הם מרוכבים. תכונה זו משקפת את האופי הדיסיפטיבי של הדינמיקה. עבור ערכים מסוימים של הפרמטרים המגדירים יוצר זה, מתקבלים ניוונים לא הרמיטיים, הידועים בכינוי נקודות ייחודיות (exceptional points). בנקודות אלה המטריצה המייצגת את היוצר אינה לכסינה. בדינמיקה הנוצרת במקרה זה מעורבת התנהגות פונקציונלית של פולינום. ניתן לזהות את האופי הייחודי של הדינמיקה על ידי שימוש בשיטות של אינוורסיה הרמונית. האופי הייחודי יכול לשמש כאמצעי לאיתור של הנקודות הייחודיות באופן מדויק. הצענו להשתמש בתכונה זו על מנת להעריך באופן מדויק את הפרמטרים הפנימיים של המערכת.

האמפליטודה והתדירות של השדה החיצוני ניתנים לשליטה. פרמטרים אלה מגדירים את מרחב הפרמטרים של היוצר של משוואת L-GKS. חקרנו את הנקודות הייחודיות של היוצר המוגדר במרחב פרמטרים זה. מצאנו שבאופן טיפוסי הנקודות הייחודיות במרחב זה יוצרות עקומות רציפות. עקומות אלה מתמזגות לנקודות חדות בהן יש ניוון מסדר יותר גבוה. חקרנו את ההשלכות של נקודות אלה על הדינמיקה של משוואות בלוך ושל פליטה ספונטנית של אטומים תחת השפעת לייזר.

משוואת בלוך היא הדוגמא הפשוטה ביותר למשוואת L-GKS, ומשמשת כהמחשה לדינמיקה קוונטית דיסיפטיבית בהרבה תחומים בפיסיקה – מתהודה מגנטית גרעינית לאינפורמציה קוונטית ופיסיקת החלקיקים. למרות זאת, הנקודות הייחודיות של משוואה זו לא נחקרו. חישבנו את העקומות של הנקודות הייחודיות במערכת זו, והצענו פרוצדורה להערכה מדויקת הפרמטרים של המערכת – התדירות העצמית, מומנט הדיפול וקבוע השיכוך.

ניתן להשתמש במשוואת L-GKS על מנת לתאר באופן מהימן את הפליטה הספונטנית של אטומים מעוררים. הפרמטרים של מערכות אטומיות כאלה נקבעים על ידי הקבועים הפיסיקליים היסודיים, ולכן יש עניין בהערכה מדויקת של הפרמטרים. איבוד הפאזה המלווה את הפליטה הספונטנית מגביל את הדיוק של טכניקות מדידה מקובלות. השיטה הצענו - שיטת הערכת הפרמטרים באמצעות הנקודות הייחודיות – הופכת את החיסרון של הדיסיפציה ליתרון. הדגמנו את השיטה הזו בספקטרום האטומי של המעברים בין רמות S לרמות P באטום ^{85}Rb וביון $^{40}Ca^{+}$.

תקציר

מערכות קוונטיות פתוחות מאופיינות על ידי הצימוד לסביבה חיצונית. הדינמיקה של המערכת מושפעת מהצימוד. באופן טיפוסי מתרחשים תהליכי שיכוך ואיבוד פאזה. אנחנו משתמשים בשיטה של תיאור מצומצם כדי לתאר את המערכת העיקרית באופן מפורש ואת הסביבה באופן עקיף, דרך ההשפעה שלה על המערכת. התיאור המצומצם של מערכות קוונטיות פתוחות מרקוביות מתאר את הדינמיקה על ידי משוואת המאסטר של L-GKS, הידועה גם בשם משוואת לינדבלד.

האינטראקציה של מערכות קוונטיות עם שדות חיצונים מאלצים ממלאת תפקיד מרכזי בהרבה תחומים בפיסיקה וכימיה. שתי דוגמאות כלליות הן ספקטרוסקופיה – בה השדה החיצוני משמש כדי לבחון את המערכת, ובקרה קוהרנטית – שמשתמשת בשדה חיצוני על מנת להביא את המערכת למצב הרצוי.

בעבודת גמר זו חקרנו את ההשפעה של הסביבה על הדינמיקה של מערכות תחת אילוץ של שדות חיצוניים. התמקדנו בשתי תופעות:

- הקינום (scaling) של בקרה של מערכות מרקוביות המשתמשת רק בתכונות הפאזה של שדה חלש.
- הנקודות הייחודיות (exceptional points) בדינמיקה של מערכות קוונטיות פתוחות.

המחקר בנושא *הקינום של בקרה של מערכות מרקוביות המשתמשת רק בתכונות הפאזה של שדה חלש* עולה מתוך התחום של ספקטרוסקופיה מולקולרית, ומהווה דוגמה בולטת לתרחיש בו יכולה להופיע השפעה של הסביבה של הדינמיקה של מערכת מאולצת. כאשר שדה קרינה חלש מגיב עם מולקולה, אנרגית השדה הנבלעת במולקולה משמשת לבחינת רמות האנרגיה של המולקולה. הנחת היסוד היא שיש קשר ישיר בין איבוד הקרינה של השדה לבין הספקטרום של המולקולה. הנחה זו מאושררת על ידי תורת ההפרעות התלויה בזמן של מערכות מבודדות. תורת ההפרעות מראה שתכונות הפאזה של השדה המאלץ אינן משפיעות על המצב הסופי של המערכת.

סדרה של ניסויים וסימולציות מעלות את ההשערה שבמערכות פתוחות מתקבלת תמונה שונה. לכן מתעורר הצורך לנתח את ההשפעה של תכונות הפאזה של שדות מאלצים חלשים תוך שימוש בפורמליזם של מערכות פתוחות. לשם כך, בחנו את התרחיש של מעבר אוכלוסיה במערכות פתוחות המתוארות על ידי משוואת L-GKS. השתמשנו בתורת ההפרעות מסדר שני של משוואה זו כדי לנתח את הדינמיקה. הראנו שמעבר האוכלוסיה תלוי בשדה החיצוני רק דרך פונקציית האוטו-קורלציה של השדה, שאינה מושפעת מתכונות הפאזה של השדה. לכן, בסדר המוביל של ההפרעה, הדינמיקה לא יכולה לתאר תלות של מעבר האוכלוסיה בתכונות הפאזה של שדה חלש. כתוצאה מכך יש להסביר את הניסויים בפורמליזם חלופי.

הדגמנו את התוצאות על ידי סימולציה של מעבר אוכלוסיה כתוצאה משדה חלש. השתמשנו בשדה חיצוני בעל צורה פונקציונלית של גאוסיאן עם צ׳ירפ, שמבטא את זה שלכל רכיב ספקטרלי יש פאזה שונה, כך שתכונות הפאזה של השדה מתבטאות בקצב הצ׳ירפ. הראנו שמעבר האוכלוסיה הוא מתכונתי לסדר המוביל של ההפרעה, כלומר ריבוע של חוזק השדה החיצוני. לעומת זאת, השפעת הצ׳ירפ על מעבר האוכלוסיה, שמבטאת במקרה זה את השפעת תכונות הפאזה, מופיעה רק בסדר הבא של ההפרעה.

עבודה זו נעשתה בהדרכתו של

פרופסור רוני קוזלוב

השפעת הסביבה על הדינמיקה של מערכות קוונטיות פתוחות מאולצות

חיבור לשם קבלת תואר דוקטור לפילוסופיה

מאת

מורג עם-שלם

הוגש לסנט האוניברסיטה העברית בירושלים

כסלו ה'תשע"ו

דצמבר 2015